INFLUENCE OF GRAIN SIZE AND WIDMANSTÄTTEN COLONIES ON VARIABILITY OF TENSILE PROPERTIES OF FORGED TI-6AL-4V

A Thesis

presented to

the Faculty of California Polytechnic State University,

San Luis Obispo

In Partial Fulfillment

of the Requirements for the Degree

Master of Science in Engineering

by

Blake Thomas Gaspar

May 2014

COMMITTEE MEMBERSHIP

TITLE:	Influence of Grain Size and Widmanstätten Colonies on Variability of Tensile Properties of Forged Ti-6Al-4V
AUTHOR:	Blake Thomas Gaspar
DATE SUBMITTED:	May 19, 2014
COMMITTEE CHAIR:	Trevor Harding, PhD Professor of Materials Engineering
COMMITTEE MEMBER:	Katherine Chen, PhD Professor of Materials Engineering
COMMITTEE MEMBER:	Jim Davlantes Senior Project Metallurgist – Shultz Steel

ABSTRACT

Influence of Grain Size and Widmanstätten Colonies on Variability of Tensile Properties of Forged Ti-6Al-4V

Blake Thomas Gaspar

When testing forgings for specifications, it was found that some parts did not meet the requirements for mechanical properties. This triggered an investigation into two of the parts from the lot that did not meet specification. The ultimate reason for failure was due to lower than necessary yield strength and ultimate tensile strength values, as well as unwanted variability between regions of the part. Therefore, samples of the regions were tensile tested to determine the differences that existed in yield strength, ultimate tensile strength, and elongation. After tensile testing, quantitative metallography and fractography were conducted to identify aspects of the microstructure and fracture surfaces that may have caused the variability. Three aspects of the microstructure that were identified as characteristics that may affect the mechanical properties were: grain size, Widmanstätten colony size, and volume fraction of the β phase. Based on measurements it was determined that a smaller Widmanstätten colony size found to be roughly 120 microns/colony was associated with a larger yield strength and UTS than larger colony sizes of roughly 170 microns/ colony. Grain size also played a role with smaller grain sizes of roughly 1550 microns/grain being associated with a higher yield strength and UTS than the larger grains of roughly 2000 microns/grain. Fractography also suggested that the presence of interlamellar decohesion and trans-lamellar failure may have created sites of further crack initiation, resulting in a lower ultimate tensile strength. These differences were theorized to be caused by a temperature gradient created during the heat treatment that created non-uniform cooling rates, resulting in the differences in microstructural characteristics.

Keywords: Ti-6Al-4V, mechanical properties, metallography, fractography, property variation

ACKNOWLEDGMENTS

I would like to extend a thank you to Shultz Steel for donation of the material, machining of samples, and metallography consumables. Another thank you to Dr. Trevor Harding, the advisor for the project for his help and guidance. Also, a final thank you to Joey Dei Rossi an undergraduate student who helped with preparation of metallographic samples.

TABLE OF CONTENTS

LIST OF TABLES

LIST OF FIGURES

1 INTRODUCTION

1.1 Motivation for this Study

Shultz Steel is a forging company that produces large scale forgings, rolled rings, and other products. Unwanted variability existed in one of the products that Shultz Steel manufactures. Representatives believed this problem was due to variation in microstructure that had caused abnormally low and variable tensile properties. The component in question (Figure 1) is made of the Ti-6Al-4V alloy. Use for this component is in cargo aircraft landing gears and as such the part is subjected to large applied forces. During preliminary investigation by Shultz Steel consisting of tensile testing sampled from another part from the same lot of forgings, the yield strength and ultimate tensile strength (UTS) were lower than specification and exhibited unwanted variability. These lower than required properties were what ultimately prompted the current investigation.

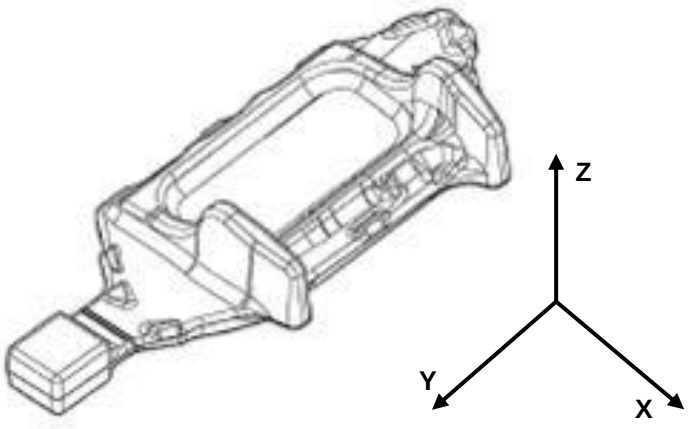

Figure 1. Forged Ti-6Al-4V landing gear. The die parting line was in the x-y plane with crosshead motion in the z-axis.

Tensile properties, both yield strength and UTS, are the properties that were the primary determining factor for destructive testing that determined whether the component met specification. According to Ding, Guo, and Wilson, different characteristics of the microstructure can significantly alter mechanical properties as found in their study, the most notable property being tensile strength. Therefore, relationship of microstructural characteristics to regions of the component that exhibited variations in tensile properties will be examined in this study.

1.2 Goals and Objectives

The ultimate goal of this study was to determine if the samples obtained from the lot of forgings that did not meet specification had any variation in mechanical properties within regions of the part and across the entire part, and whether any variation could be related to one or more microstructural characteristic. Behavior of the samples in tension with regards to yield strength, ultimate tensile strength (UTS), and elongation were of primary interest. It was necessary to see if any differences existed based on sample orientation relative to the die parting line and axis of applied strain as well as region of the part from which the samples were taken. Metallography was conducted, and the microstructure quantitatively analyzed. Results of metallography were then compared with any differences in mechanical properties to identify microstructural causes for variation.

2 BACKGROUND

2.1 Process Utilized for Study

Shultz Steel uses a standard process for creating the part as outlined in Figure 2. The process begins with vacuum arc remelting (VAR) of the material into ingot form. This is where the initial microstructure is achieved which has the ability to alter properties if the incorrect microstructure is used since different microstructures vary in their mechanical properties. After this raw material is obtained it is heated and pre-formed. This preforming step is carried out using hydraulic presses, and utilizes an open die method. During the preforming step concentrations of dislocations form and, if uneven, could create varying tensile properties. Once preforming is completed the part is kept at temperature and a hot deformation process is applied to the workpiece. The temperature of the workpiece and applied strain rate was not disclosed. These processing parameters, as will be seen later, can be influential in the development of microstructure and resulting mechanical properties (Kuhlman 2005). At this point the contours have the ability to influence uneven flow rates and the potential for texturing and elongated grains. Following hot deformation, the workpiece is subjected to two heat treating cycles, called a duplex anneal. Heat treatments were conducted outside of the die after all deformation processes had concluded. The first heat treatment was conducted above the beta transus temperature (β_T) which is between 1800 °F to 1850 °F. The idea behind this is to promote recrystallization and primary grain growth. This is followed by a mill anneal. This mill anneal is conducted at a temperature range between 1200 °F – 1400 °F. When all heat treatments are completed, final machining of excess material is conducted. Heat treatments can ultimately influence the final microstructural characteristics achieved.

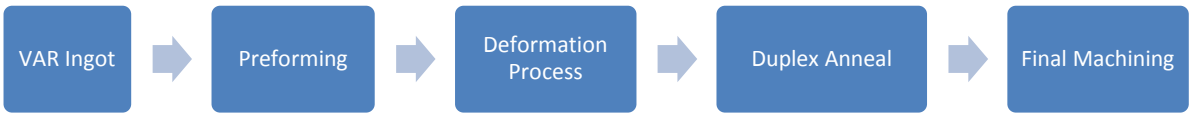

Figure 2. General process used to create part.

2.2 General Forging Practice

2.2.1 Alloy Types

Titanium and titanium alloys consist of two allotropic phases: the α phase, which is hexagonal close-packed (HCP), and the β phase, which is body-centered cubic (BCC). These two phases exist in different proportions based on the chemical composition of the alloy and thermo-mechanical processing history of the workpiece. Alloys are classified as either alpha, beta, or alpha-beta titanium alloys based on the stabilizing elements used and the phases present in the material (Kuhlman 2005).

Of the two phases present in titanium alloys, the α phase is harder to deform and typically exists at lower temperatures. On the other hand, the β phase exists at higher temperatures and is thought to be more ductile than the α phase (Kuhlman 2005). This is contrary to a study conducted by Poondla et. al. (2009) where Ti-6Al-4V, which has β phase, and is harder compared to pure titanium, which is an α alloy used for comparison in the study. Poondla et. al. (2009) found that the microhardness and macrohardness of Ti-6Al-4V was higher due to the presence of more β phase. Samples were characterized by a duplex microstructure consisting of equiaxed α and β phases. Therefore, the volume fraction of phases from the resulting microstructure has the ability to alter the mechanical properties of the part.

The α and β phases may exist in different proportions based on the alloying elements used in the alloy formulation. Alloying elements are classified as either α or β stabilizers. Alpha stabilizing elements raise the temperature at which α transforms to β. In this study,

the α stabilizing element was aluminum. Other α stabilizing elements that can be used in alloy formulations are: oxygen, nitrogen, and carbon. However, nitrogen and carbon are not typically added intentionally. Beta stabilizers lower the α to β transformation temperature and consist of vanadium, manganese, chromium, iron, molybdenum, and niobium. The purpose of β stabilizers is to allow more β phase at room temperature. Alpha-beta alloys are typically utilized because they are the most versatile, allowing manipulation of phase composition and the size and distribution of phases present (Gilbert and Shannon 1991).

2.2.2 Forging Methods

Methods used for forging can influence the final microstructure and all commercially utilized forging methods may be employed to forge titanium and its alloys (Kuhlman 2005). However, the method chosen for the process is dictated by the shape and the desired mechanical properties and microstructure (Kuhlman 2005). Sometimes the process incorporates multiple methods; for example, a preform may be created using open die forging with the final shape achieved through closed die forging. Using a multiple step method allows conservation of material and tighter control of the final microstructure (Kuhlman 2005).

Components of the processing history for forged components that can influence the microstructure and thus mechanical properties include: initial structure, hot working temperature, strain, strain rate, and cooling rate (Ding, Guo and Wilson 2002).

During the forging process, material and die temperature are crucial in microstructural evolution, which ultimately determines the mechanical properties of the finished product (Kuhlman 2005). Process history from ingot to billet to intermediate and eventually final forging can affect the phase composition of the product. The morphology of the phases achieved through die and material temperature during forging and any subsequent heat treatments dictate the final mechanical properties (Kuhlman 2005).

2.2.3 Effect of Forging Temperature

When forging titanium alloys, the forging temperature is found by Kuhlman (2005) to be important to deformation characteristics. The range of temperatures at which the Ti-6Al-4V part is processed is much more restrictive than forged beta alloys, as seen in Figure 3. The beta alloy in the figure, Ti-13V-11Cr-3Al, has a wider range of processing temperatures over which it is typically forged. However, the beta alloys, as compared to alpha-beta alloys, still typically exhibit a higher required forging pressure similar to that of alpha alloys (Kuhlman 2005).

It should be noted that this diagram only shows the required forging pressure to elicit plastic deformation in response to temperature for alloys representative of their classes. While the pressure required for forging for a specific temperature based on alloy type can be seen in Figure 3, the flow stress associated with forging should be looked at within an alloys class. As such, the flow stress as it relates to temperature exhibits a higher sensitivity for alpha-beta alloys than beta alloys but still less than alpha alloys (Kuhlman 2005).

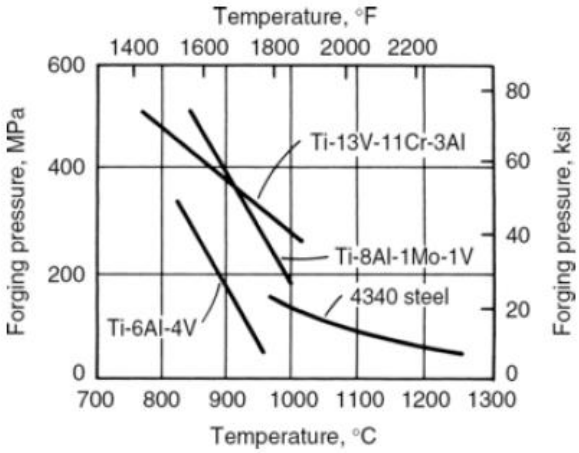

Figure 3. Plot showing the influence of temperature on required forging pressure. It should be noted for Ti-6Al-4V the lower position of the line compared to the other titanium alloys (Kuhlman 2005).

Two different options may be employed when choosing the workpiece temperature during the deformation process depending on the class of alloy being used. The first method utilizes temperatures below the β_T and is known as conventional or α-β forging since both phases are present during the deformation process. This method may be used for alpha or alpha-beta alloys. A second option is to conduct the deformation process with temperatures above the β_T, known as beta forging, and can be utilized for beta and alpha-beta alloys. These practices are sometimes combined in variations to achieve the desired final microstructural properties that dictate the mechanical properties (Kuhlman 2005).

Conventional alpha-beta forging utilizes die temperatures at around 1000 °F or less. This technique works the forging workpiece at temperatures where both the α- and β-phases are present with the composition of each phase dictated by that of the alloy chemistry and the actual working temperature used. Microstructures characteristic of this technique are equiaxed primary α in a transformed β matrix. These structures produced by the alpha-beta forging technique are utilized to create a structure that optimizes strength and ductility while maintaining fatigue properties (Kuhlman 2005).

When beta forging is used, the process is carried out above the β_T. This method is used for α, α+β, and metastable β alloys. Beta forging is characterized in commercial practices by supratransus forging during early and/or intermediate steps in the process. Finishing deformation processes then occur below the β_T and are dependent on the alloy, design of the die, and desired combinations of mechanical properties (Kuhlman 2005).

Unlike conventional forging, influences on microstructure are not completely cumulative in beta forging. Therefore, effects from previous steps upon cooling and reheating are partially lost due to recrystallization when heating above the β_T. This means that desired microstructural characteristics achieved during the process may be lost (Kuhlman 2005). Common microstructures produced by beta forging are Widmanstätten colonies or acicular primary α in a transformed β matrix. This method is utilized to enhance fracture

toughness, fatigue crack propagation resistance, and creep resistance while maintaining strength (Kuhlman 2005).

Benefits of beta forging also include lower forging unit pressure requirements and a reduction in cracking tendency during deformation processes (Kuhlman 2005). However, when conducting forging operations it is important to minimize non-uniform working, excessive prior β grain growth, and poorly worked structures. These result in varying mechanical properties within the final forging (Kuhlman 2005). To reduce non-uniform working, pre-forming is recommended. This may be reduced by introducing a pre-forming step in the process (Kuhlman 2005).

2.2.4 Effect of Strain Rate during Forging

Titanium and its alloys are more difficult to forge than aluminum or steel alloys. This is most true at low to moderate strain rates while a non-isothermal die temperature of 1000°F or less is utilized, alpha-beta forging. Most of this effect has to do with the chemistry of the alloy, highly alloyed titanium alloys prevent the movement of dislocations that facilitate deformation. In the case of Ti-6Al-4V the alloy behaves similarly to commercially pure titanium at temperatures below its β_T because there is more α phase present than β phase which takes the same HCP structure as is found in pure Ti (Kuhlman 2005).

2.2.4.1 Flow Softening

Strain and strain rate can influence the microstructure achieved after processing. If hot deformation occurs in the α+β region, the flow stress decreases with an increase in plastic deformation. This increase in ductility, or flow softening, is a function of strain rate and temperature. Softening is attributed to adiabatic heating, causing increases in the actual temperature of the workpiece (Ding, Guo and Wilson 2002). An increase in workpiece temperature due to adiabatic heating influences the

microstructure in ways that compromises the microstructure of the final part. Another, thing that contributes to flow softening is the proportion of β phase during deformation. Ding, Guo, and Wilson found that hot deformation taking place above the β_T creates a near constant flow stress (Ding, Guo and Wilson 2002).

A near constant flow stress is useful in the deformation process. If a constant flow stress is achieved, a more uniform microstructure is also achieved. More uniform microstructures consist of equiaxed grains and similar volume fractions of phases across samples. As such, with a more uniform microstructure comes more uniform mechanical properties (Ding, Guo and Wilson 2002). This more uniform microstructure has benefits in decreasing orientation dependence when mechanical testing is conducted. It is seen in Figure 4 that an increasing temperature is associated with a decrease in flow stress. Also, as would be expected, an increase in strain rate yields an increase in flow stress. As such, temperature plays a key role during the deformation process in reducing the applied stress. However, depending on the temperature being applied there can be changes to the microstructure depending on if the temperature during deformation is above or below the β_T (Ding, Guo and Wilson 2002).

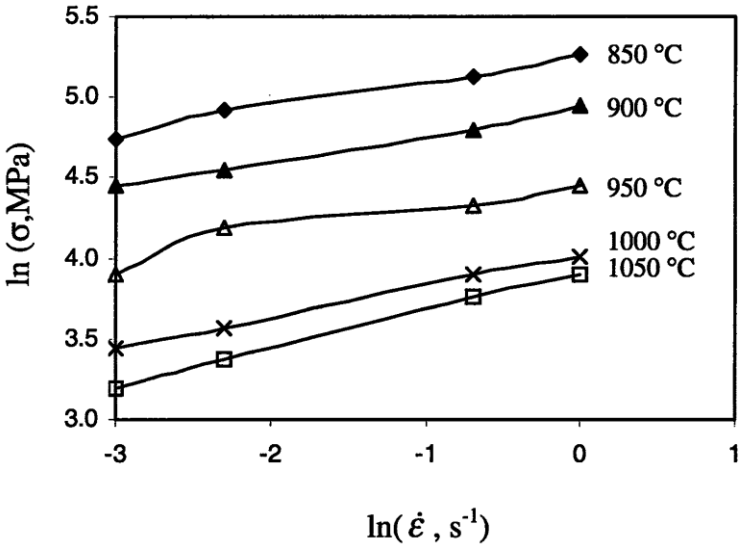

Figure 4. Variation of flow stress as dependent on strain rate at different temperatures for Ti-6Al-4V (Ding, Guo and Wilson 2002).

One phenomena relevant to this study is the flow-softening behavior shown by titanium alloys at strain rates well within those used in commercial forging applications. One problem that results from this flow-softening behavior is decreases in desirable mechanical properties affecting the ability of the final part to pass specifications. However, when forged above the β_T temperature the flow-softening effect is reduced thus reducing its effect on decreasing mechanical properties (Kuhlman 2005). The difference in flow-softening behavior for a given alloy is noticed through the achieved microstructure and is a function of the differences in microstructure before and during deformation. This is independent of whether deformation takes place above or below the β_T. A structure consisting of α-phase in an α-β matrix redistributes strain and promotes the movement of dislocations when compared to acicular α in a transformed β structure and is characterized by increased flow-softening (Kuhlman 2005).

Deformation occurring above the β_T reduces the flow softening effect due to the presence of the β phase and resulting changes in the microstructure (Kuhlman

2005). Process development must consider this to facilitate the required microstructure and decrease flow stress in the workpiece during deformation (Kuhlman 2005).

In a deformation process like forging the strain rate during the process is crucial as titanium alloys are more sensitive to strain rate than other alloys. From Figure 5 it is seen that a decrease in strain rate is associated with a decrease in the flow stress of the material. For example, at 20% strain at a rate of 10/s the flow stress is upwards of 30 ksi, while for the same strain at a rate of 0.1/s the strain rate is around 15 ksi. However, at the strain rate of 0.001/s it is seen that the relationship between lower strain rate and lower flow stress does not decrease uniformly. Therefore, a decrease in strain rate is associated with a decrease in the flow stress (Kuhlman 2005). Due to this non-uniformity there is an ideal value that minimizes flow stress while maintaining strain rate (Kuhlman 2005).

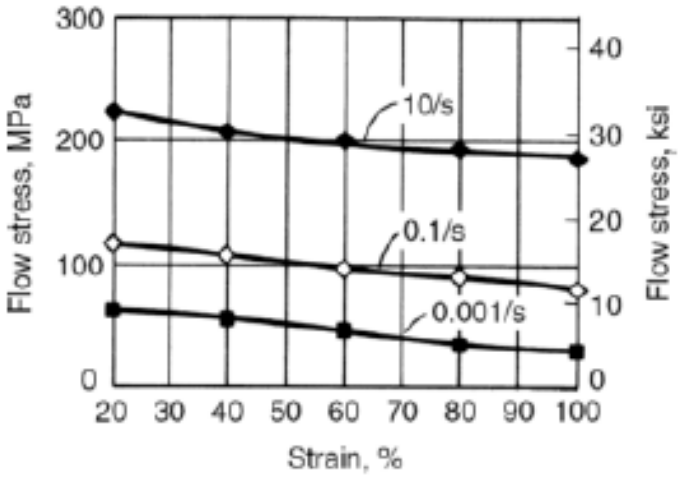

Figure 5. Affect of strain rate on flow stress of Ti-6Al-4V. As the strain rate decreases the flow stress in turn decreases. This plot is shown at 1650°F (Kuhlman 2005).

2.3 Heat Treating

Heat treating titanium and its alloys is primarily dependent on the composition of the alloy and the alloying elements used, which determine the α-β transformation of the titanium alloy. Since different alloys are utilized for different applications, heat treatments vary depending on the alloy and its proposed application (Gilbert and Shannon 1991).

Of the three types of titanium alloys, alpha-beta titanium alloys are the most versatile due to the easy manipulation of phase composition, size, and distribution. With these changes varied properties can be achieved, most notably strengths (Gilbert and Shannon 1991).

2.3.1 Annealing

The primary purpose of annealing titanium and titanium alloys is to improve fracture toughness, ductility at room temperature, dimensional and thermal stability, and creep resistance (Gilbert and Shannon 1991). Gilbert and Shannon explains that it is not uncommon to use forgings directly after annealing for their primary purpose. However, since annealing has the ability to compromise other properties, such as strength, the annealing cycle is chosen based on the desired properties and with the end application in mind. Table 1 contains a list of common heat treatments and the resulting microstructures.

Table 1. Summary of annealing α-β heat treatments for Ti-6Al-4V. The β_T for the alloy is 1830 °F (Gilbert and Shannon 1991).

Heat treatment designation	Heat treatment cycle	Microstructure produced
Duplex Anneal	Solution treat at 90-135°F below β_T, air cool and age for 2-8 hrs at 1000-1250°F	Primary α, plus Widmanstätten α-β regions
Solution treat and age	Solution treat at ~70°F below β_T, water quench and age for 2-8 hrs at 995-1250°F	Primary α, plus tempered α' or a β-α mixture
Beta anneal	Solution treat at ~30°F above β_T, air cool and stabilize at 1200-1400°F for 2 hrs	Widmanstätten α-β colony microstructure
Beta quench	Solution treat at ~30°F above β_T, water quench and temper at 1200-1400°F for 2 hrs	Tempered α'
Recrystallization anneal	1700°F for 4 hrs, cool at 90°F/h to 1400°F, air cool	Equiaxed α with β at grain-boundary triple points
Mill anneal	α-β hot work plus anneal at 1300°F for 30 min to several hrs and air cool	Incompletely recrystallized α with a small volume fraction of β particles

Different cooling practices after the heat treatment: furnace cooling, air cooling, fan cooling, and quenching, produce different cooling rates. Uneven cooling rates have the potential to influence microstructural characteristics (Gilbert and Shannon 1991). An uneven cooling rate also has the potential to jeopardize dimensional tolerances. Therefore, workpieces that have tight dimensional tolerances require a uniform cooling rate down to 600 °F (Gilbert and Shannon 1991).

Different methods may be used for annealing. These consist of: mill, duplex, recrystallization, and beta annealing. A general purpose anneal treatment is mill annealing. With heavily worked products mill annealing leaves remnants of cold or warm working in the microstructure. This is beneficial in increasing strength but detrimental to other mechanical properties (Gilbert and Shannon 1991).

Another method, known as recrystallization annealing, is a method where the workpiece is heated into the upper region of the α-β range, held for a predetermined time, and then cooled slowly. Recently, this process has replaced β annealing in industrial applications and is used to improve fracture toughness (Gilbert and Shannon 1991).

Beta annealing is similar to recrystallization annealing, but is conducted just slightly above the β_T so as to not cause excessive grain growth (Gilbert and Shannon 1991). The time at which the workpiece is held at the temperature depends on the thickness, but should be sufficient to completely transform the entire part. While the holding time and temperature are important, so is the cooling rate. In order to prevent α at the grain boundary, larger parts are typically fan cooled or quenched (Gilbert and Shannon 1991).

Duplex annealing is used to alter the shape, size, and distribution of the phases so as to improve toughness and creep resistance (Gilbert and Shannon 1991). It is often common practice to anneal at two different temperatures. The first temperature is meant to globularize the deformed α-phase. While the purpose of the second, lower temperature anneal, being to precipitate acicular α between the globularized α particles and reduce the volume fraction of α (Gilbert and Shannon 1991).

2.4 Microstructural Development

2.4.1 Structure and Properties

2.4.1.1 Transformation

With titanium-aluminum based alloys such as Ti-6Al-4V the mechanical properties are predominantly affected by their microstructure (Stefanescu and Ruxanda 2004). These microstructures take the form of fully lamellar, martensitic, duplex grains, or equiaxed grains. Fully lamellar microstructures are composed of Widmanstätten colonies, which are intersecting lamellar sub-granular structures. Each microstructure has its benefits for mechanical properties. A fully lamellar structure has benefits of higher strength, creep resistance, and fatigue and fracture toughness when compared to a duplex microstructure. Although, lamellar structures typically have lower ductility. Aluminum content is the most influential factor in alloy strength and

acts by lowering the volume fraction of the hard α phase (Stefanescu and Ruxanda 2004).

2.4.1.2 Ti-6Al-4V Microstructures

Microstructure, as determined by Filip, Kubiak, and Sieniawski, highly influences mechanical properties. Microstructure is controlled by the processing of the workpiece. It is also heavily influenced by the heat treating and thermal history of the workpiece. Therefore, the thermo-mechanical processing of the workpiece dictates the mechanical properties (Filip, Kubiak and Sieniawski 2003).

The amount of stabilizing elements in combination with the heat treatment determines the eventual volume fraction of phases of the workpiece. However, it is the heat treatment that ultimately determines the microstructure. The achieved microstructure is dictated by diffusion or diffusionless transformations and is found to result in different allowable microstructures that include: equiaxed, duplex, martensitic and fully lamellar microstructures (Filip, Kubiak and Sieniawski 2003).

Each of the different microstructures has something to offer in regards to mechanical properties. Duplex structures result in better ductility and strength, both yield and ultimate tensile strengths, as well as a superior fatigue strength (Filip, Kubiak and Sieniawski 2003). On the other hand, fully lamellar structures, produced from slower cooling rates, yield high fatigue crack propagation resistance and high fracture toughness with faster cooling rates creating a martensitic structure (Filip, Kubiak and Sieniawski 2003). The continuous cooling transformation (CCT) diagram for Ti-6Al-4V can be found in Figure 6. This CCT diagram shows that the martensitic transformation occurs at fast cooling rates, characterized by quenching. However, if held longer at the β_T and cooled more slowly, a duplexf, lamellar, or equiaxed structure forms. Which structure forms is dependent on the hold time above the β_T and the cooling rate utilized (Sieniawski, et al. 2013).

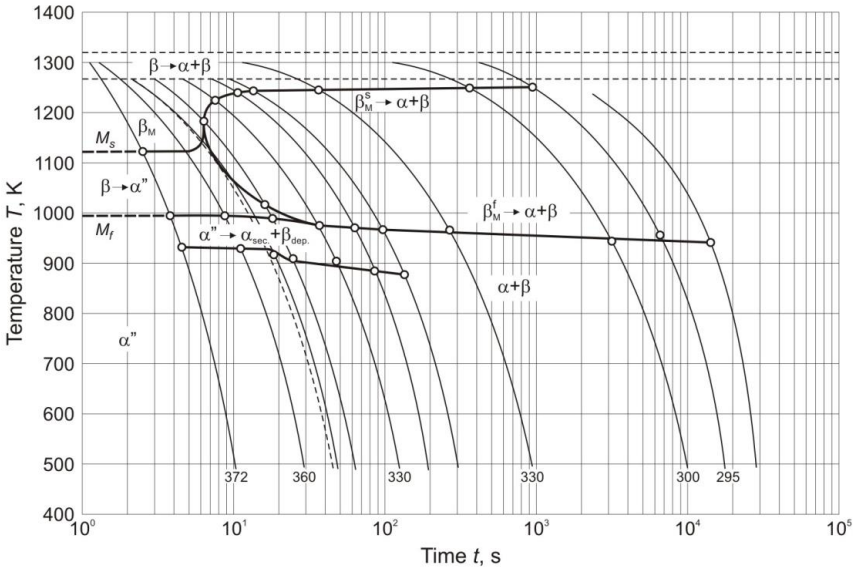

Figure 6. CCT diagram of the Ti-6Al-4V alloy showing time and temperature's effect on structure (Sieniawski, et al. 2013).

A lamellar structure forms at lower to intermediate cooling rates due to a diffusion controlled nucleation and growth of the α lamellae into the β grains (Filip, Kubiak and Sieniawski 2003). Several things are influential in their effect on mechanical properties: β grain size, size of the colonies of α lamellae, thickness of the α lamellae, and the nature of the β-phase interlamellar interface (Filip, Kubiak and Sieniawski 2003).

When achieving a lamellar or martensitic structure, the cooling rate is more important in the heat treating process than that of duplex or equiaxed structures. The primary factor for achieving a duplex or equiaxed structure relies more on the time held at the temperature as compared to the cooling rate. However, based on the heat treating process used for the part in this study a lamellar structure composed of Widmanstätten colonies is what is expected. Therefore, the structures discussed hereafter will be that of lamellar and martensitic structures.

When observing the microstructure of heat treated Ti-6Al-4V there are two primary microstructures that form. The first is an α lamellar structure in a β matrix and the other is an α' (α'') martensitic structure. Figure 7 provides an example of a microstructure of air cooled Ti-6Al-4V producing a clearly defined Widmanstätten structure with colonies of α lamellae within the β matrix. A martensitic structure of the same alloy is found in Figure 8, utilizing water as a quenching medium. As observed by Filip, Kubiak, and Sieniawski (2003), the cooling rate has an intense effect on microstructure, which is seen in a summary of their results in Table 2. As a result, large workpieces have a cooling gradient that has the ability to cause different microstructural characteristics. These could be differences in grain size, lamellae size, and/or colony size (Filip, Kubiak and Sieniawski 2003). This is also seen in different heat treatments. A solutionizing and aging treatment in parts that have thicknesses greater than 3" may produce microstructures more similar to annealing than a solutionizing and aging treatment (Gilbert and Shannon 1991).

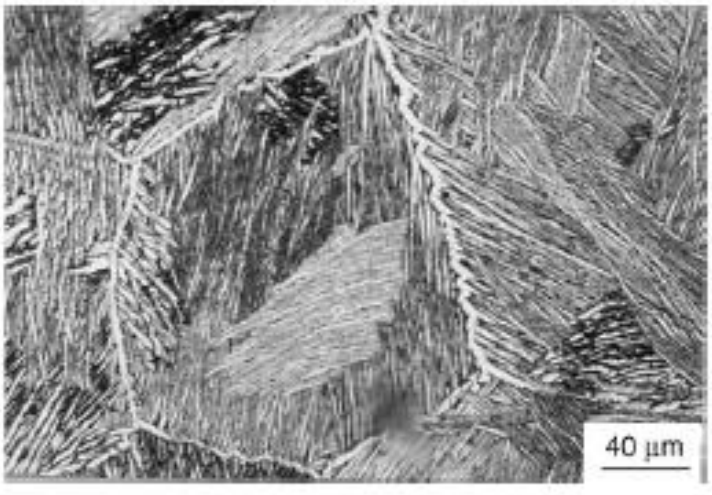

Figure 7. Ti-6Al-4V microstructure after cooling in air with a structure of α lamellae in a β matrix (Filip, Kubiak and Sieniawski 2003).

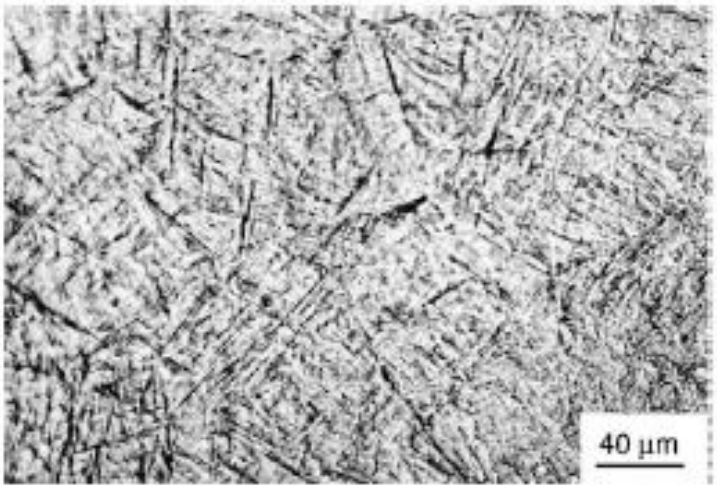

Figure 8. Ti-6Al-4V microstructure after quenching in water showing a martensitic structure (Filip, Kubiak and Sieniawski 2003).

Table 2. Table showing the effect of cooling rate on the composition of Ti-6Al-4V microstructures (Filip, Kubiak and Sieniawski 2003).

Cooling Rate (K s-1)	Composition Ti-6Al-4V
48	α'(α'')
40	α'(α'')
18	α'(α'')
9	α + α'(α'')
7	α + α'(α'')
3.5	α + α'(α'')trace + β
1.2	α + β
0.08	α + β
0.04	α + β
0.024	α + β
0.008	α + β
0.004	α + β

2.4.2 Fully Lamellar Microstructure

Some applications in industry require a fully lamellar microstructure. In order to create a fully lamellar microstructure there are a couple of processing methods that are used. The primary method, as outlined by the schematic in Figure 9, begins with homogenization by

first heating the workpiece above the β_T. The workpiece is then cooled at variable rates with the rate determined by the desired microstructural characteristics. An aging treatment below the β_T follows the homogenization treatment. During aging, temperature is more important than time. This is due to whether or not it is desirable for Ti_3Al particles in α to act as an age hardening mechanism. If Ti_3Al particles are present then an aging temperature is typically around 932 °F, which is approximately 122 °F below the Ti_3Al solvus temperature for Ti-6Al-4V. Alternatively, a stress relieving treatment may be desirable. If a stress relieving treatment is used the approximate aging temperature of 1112 °F is used (Lütjering 1998).

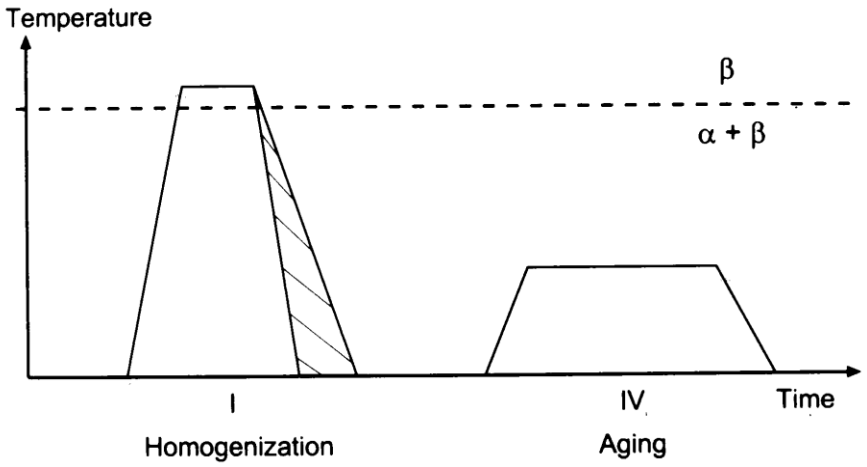

Figure 9. Processing parameters to achieve a fully lamellar microstructure (Lütjering 1998).

For a fully lamellar structure, Step I from the diagram in Figure 9, is the primary step that determines microstructural characteristics. In this step the temperature and cooling rate are both important to the process. This treatment typically produces large β grains which is important since the lamellar structure nucleates from the α phase at the grain boundaries. Therefore, the size of the grains and distribution of α at the grain boundaries can influence the final structure. Furthermore, the time and temperature influence the size of the α-lamellae, size of Widmanstätten colonies, and the grain boundary α layer.

The size of the Widmanstätten colonies is the primary factor that determines mechanical properties (Lütjering 1998). The colony size is responsible for the determination of the strength, elongation, and fracture properties of the material. Elongation may also be influenced by the size of the α layer at the grain boundary (Lütjering 1998).

In the aging step shown in Figure 9, the aging temperature is the chief characteristic of the treatment. The temperature of aging determines the presence and amount of Ti_3Al particles in the α phase as well as the amount of secondary α in β (Lütjering 1998). Both of these aspects influence the microstructural features of the material and play minor roles in the determination of mechanical properties. However, it is still the Widmanstätten colony size and α layer at the grain boundary that are the primary determining factors of the mechanical properties of the material (Lütjering 1998).

In a study conducted by Filip, Kubiak, and Sineawski (2003) the cooling rate also affects aspects of the lamellar structure. The thickness and length of the α phase in lamellar structures decreases with an increase in cooling rate. An increase of β stabilizing elements can also cause a decrease in the thickness and length of the α-phase. Furthermore, as the cooling rate increases the lamellar structure takes on a martensitic form, having to do with the mechanisms of the phase transformation (Filip, Kubiak and Sieniawski 2003). The range of cooling rates, and their effects on the phase composition, is seen in Table 2. Increased cooling rates from the β phase region yield a martensitic microstructure with a´(a´´). On the other hand, a decreased cooling rate yields a lamellar structure of stable α and β phases (Filip, Kubiak and Sieniawski 2003). The effect that the cooling rate ultimately has can be seen in Figure 10. An increased cooling rate is associated with an increase in strength (Filip, Kubiak and Sieniawski 2003).

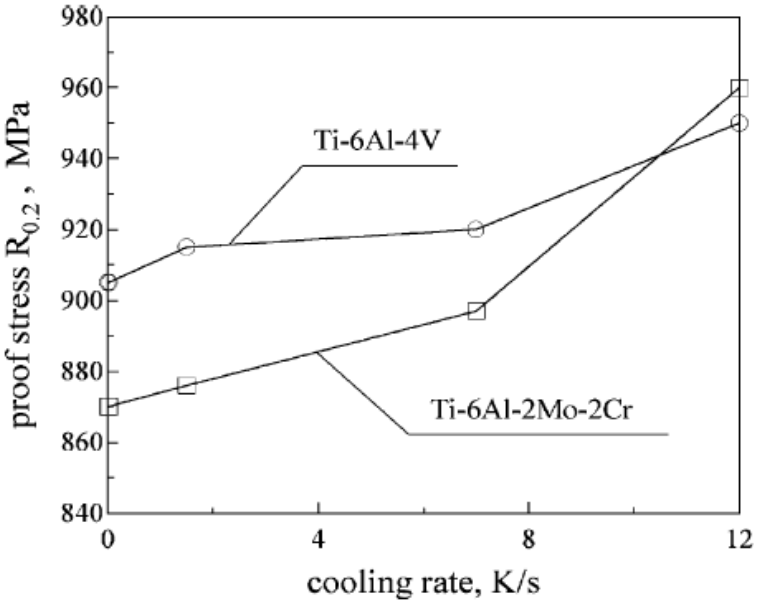

Figure 10. The effect of cooling rate on the mechanical properties of two α-β Ti alloys (Filip, Kubiak and Sieniawski 2003).

2.4.3 Widmanstätten Colonies

2.4.3.1 Formation of Widmanstätten Colonies

Formation of Widmanstätten colonies takes place upon cooling below the β_T. Upon cooling below the β_T, nucleation of the α phase within the β grains occurs. The nucleation of the α phase takes place in the form of plates with the longest dimension of these phases parallel to the $\{110\}_\beta$ plane. With continuous cooling, the α plates coarsen and grow constituting the Widmanstätten α phase. These α plates are characterized by an uneven distribution of the stabilizing elements Al and V present in the alloy (Gil, et al. 2001). Moving out from the center of the plate the α stabilizing element Al decreases and the amount of V, the β stabilizing element, increases. This uneven distribution along the radius of the α plates is maintained along the length of the α plate. The Widmanstätten colonies appear to grow from a grain boundary α layer into the β grain with sharp and even surface reliefs (Gil, et al. 2001).

Cooling rate has an effect on the Widmanstätten plate size. With a constant starting temperature a decrease in cooling rate is associated with an increase in plate size. Furthermore, the α plates form at slower cooling rates, and are shown to be thicker and become thinner as the cooling rate increases (Gil, et al. 2001). The reason for this is an increase in time which allows increased diffusivity and thus a more even growth of the α phase. Slower cooling rates are also characterized by intermittent colonies of α phase in the center of the grains which are different from the Widmanstätten α phase obtained, and which nucleate from the grain boundaries (Gil, et al. 2001).

The β grain size also affects the characteristics of the Widmanstätten colonies. Larger β grains are associated with a decrease in α plate width of the Widmanstätten colonies. These smaller plates are due to a decreased β → α transformation temperature which results from larger β grains (Gil, et al. 2001).

Orientation of the α colonies with respect to the direction of loading also influences the microstructure. Mirinov et. al. found that if the sample is compressed in the plane normal to the α lamellae, the lamellae become deformed. If the direction of loading is not perpendicular to the colonies then the α lamellae become aligned perpendicularly to the compressive loading axis. This alignment of α laths became uniform and results in a more homogenous microstructure (Mironov, et al. 2009). It should be noted, that this is observed for deformation occurring at high temperatures. Since deformation of the workpiece takes place at high temperatures in compression this may influence the microstructure of the part in the present study.

The morphology of the α and β laths is also influenced by the amount of strain applied. An increased strain results in thinner laths (Mironov, et al. 2009). However, these measurements may not be accurate if the sectioning is not conducted perpendicular to the laths.

The amount of strain again plays a role with a decreased strain related to larger variation in the orientation of α colonies, while a larger strain causes the α colonies to rotate and become more uniform throughout the sample. This in turn creates more accurate measurements (Mironov, et al. 2009). Thickness of the β laths appears unaffected by the strain, which is unexpected since the β-phase generally is thought to be more ductile than the α phase (Mironov, et al. 2009).

2.4.3.2 Grain Growth

When the temperature increases there is an increase in energy and as expected an increase in grain size over time. This is due to an increase in grain growth kinetics caused by the increase in temperature. At first, grain size increases rapidly, this occurs within the first 15-20 minutes of the heat treatment. After the increase in grain size for these first 15-20 minutes the rate of grain growth decreases (Gil, et al. 2001). The decrease in rate of grain growth is due to the grains expanding and creating a decrease in the ratio of grain boundary area to overall volume. Interfacial energy per unit volume decreases with this decreased ratio of grain boundary area to volume and in turn decreases the driving force for grain growth (Gil, et al. 2001). Finally, the grains reach a certain size where there is an insufficient driving force to continue growth at that specific temperature. This phenomena is explained in Figure 11 where the asymptotic relationship between time and grain growth is observed. Once a certain time is reached, in this case about 2000 s, grain growth ceases as the driving force is no longer present to continue grain growth. As is expected, the higher the temperature the more grain growth is allowed (Gil, et al. 2001).

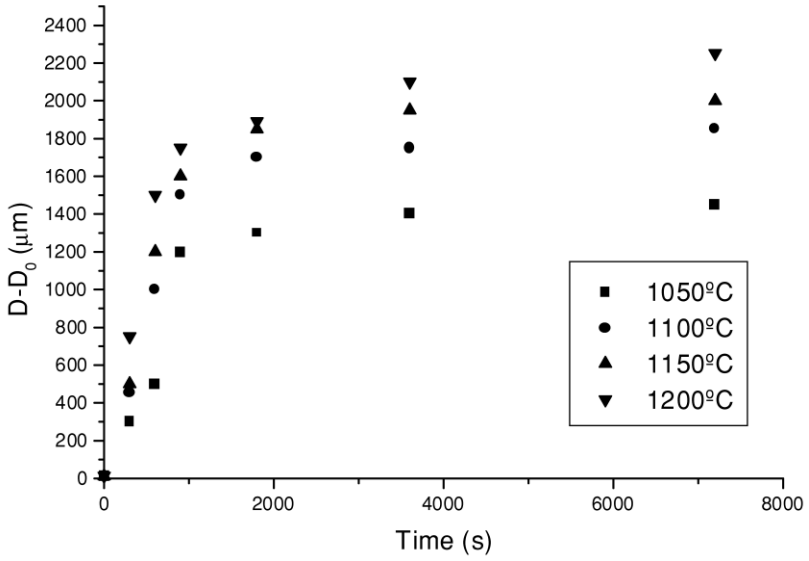

Figure 11. Depiction of the relationship between grain growth and time of different heat treatment. Notice the shape of the line and asymptote that forms (Gil, et al. 2001).

2.5 Mechanical Property Development

2.5.1 Influence of Fully Lamellar Microstructure

While all constituents of the microstructure are influential, only those of chief importance and that significantly alter the mechanical properties are discussed. This being said, the size of the Widmanstätten colonies is that of chief importance in fully lamellar structures for determining mechanical properties (Lütjering 1998). The colony size is a direct result of the cooling rate after the β heat treatment and is limited by the grain size. The grain size effectively acts as the determining factor of the effective slip length. The effect of slip length on the mechanical properties is shown in Figure 12. As is seen in Figure 12 the α colony size is inversely proportional to the yield strength, ductility, resistance to micro-crack propagation, and the HCF strength which refers to the resistance to crack nucleation. On the other hand, the alpha colony size is proportional to the formation and

propagation of macro-cracks. However, aspects of the crack such as its size and geometric features are also important (Lütjering 1998).

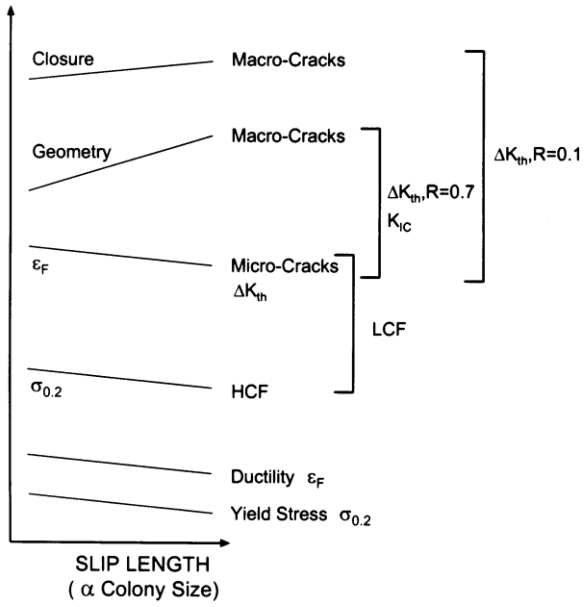

Figure 12. The effect of slip length, α colony size, on mechanical properties of Ti-6Al-4V shown schematically (Lütjering 1998).

2.5.2 Influence of Widmanstätten Colonies on Mechanical Properties

The effect that Widmanstätten colonies have on the mechanical properties of the workpiece are extensive. Work done by Lee et. al. shows that there is a relationship between colony size and spacing between lamellae to mechanical properties. This work shows that an increase in colony size and spacing between lamellae is associated with a decrease in yield strength, UTS, and elongation. The colony size has the most effect on strength while the spacing of the α-lamellae is the primary influence on elongation (Lee, et al. 2003).

As the effective grain size increases so does the slip length occurring during plastic deformation which creates preferential deformation at effective grain boundaries or grain boundary α layers. When the fractographs are observed it is noticed that they are

primarily characterized by ductile failure that consists of a dimpled surface (Lee, et al. 2003). This is due to the large number of voids that initiate at colony boundaries, grain boundary α layers, and α-β interfaces that propagate to form the dimpled fracture surface. It is also seen that the size of the dimples in the Widmanstätten structures are similar in size to the spacing of the α-lamellae (Lee, et al. 2003).

The final microstructure achieved from processing of the workpiece ultimately dictates the mechanical properties of the final part. However, it is the processing history of the part that dictates the final microstructure. Different applied stress in conjunction with the workpiece temperature during the deformation process has the ability to alter the mechanical properties. When deformation processes are complete a heat treatment is typically applied to achieve the desired microstructural characteristics.

This heat treatment, for large parts, typically takes the form of annealing and in this case a duplex anneal was used as compared to a recrystallization, beta, or mill anneal. These heat treatments produce different microstructures that may include: lamellar, martensitic, duplex, or equiaxed microstructures. However, given that a duplex anneal was used with a slow cooling rate the resulting microstructure would be a lamellar structure characterized by Widmanstätten colonies (Gilbert and Shannon 1991). It is the size and distribution of the Widmanstätten colonies along with other microstructural aspects like grain size and volume fraction of the phases that will ultimately affect the mechanical properties of the material (Mironov, et al. 2009).

2.6 Relevance to Study

General forging practices were utilized in the production of the part involved in this study. Certain aspects of the production process can influence the final microstructure of the part which in turn can alter the mechanical properties. Things such as strain rate as it applies to flow-softening, temperature of heat treatment, time held at temperature, and the cooling rate all have the ability to affect microstructure. This in turn affects the achieved mechanical

properties of the part. Different microstructures as well as characteristics of those microstructures have the ability to influence the mechanical properties of the final part. The most notable microstructural characteristics are grain size and Widmanstätten colony size which are directly influenced by processing and heat treatment.

3 METHODS

Tensile testing was the first step in the process in examining the possible anisotropic behavior and/or property variability throughout the part. While it was known that microstructure influences mechanical properties, it would have been irrelevant to conduct metallography without first knowing whether or not any anisotropic behavior existed. Once tensile testing was completed, the results of yield strength, ultimate tensile strength (UTS), and elongation were analyzed to see if any regions exhibited statistical differences. When regions were found to be statistically different, then metallography would be conducted on representative samples. These samples were then quantitatively analyzed in order to provide correlation to mechanical properties. Also, in order to qualitatively analyze any differences in UTS, fractography was also conducted using scanning electron microscopy.

3.1 Tensile Testing

3.1.1.1 Sample Selection

In order to determine any anisotropy in the part as well as variability between different regions, three regions were used from the part that did not originally meet specifications and one region was obtained from another part that did meet specifications. Figure 13 shows the locations of the regions of the part from which tensile and metallographic samples were taken. Test samples taken from regions 1A and 1B were samples that determined whether or not the part met specifications. Region 1A is from the same part as regions 2 and 3. However, region 1B is taken from another part that did meet specifications. The additional regions 2 and 3 were sampled to confirm whether or not properties were uniform throughout the part. Regions 2 and 3 were selected based on available material as well as to determine that the microstructure was consistent throughout the part. These locations had different geometries and sizes than region 1 which was the region that is tested for specification. Thus, be examining other regions variability of the microstructure was

able to be seen. The additional regions 2 and 3 were sampled from the same part as region 1A. Additional regions were not tested for specifications but were tested here to determine whether other regions of the part exhibited similar properties to region 1A.

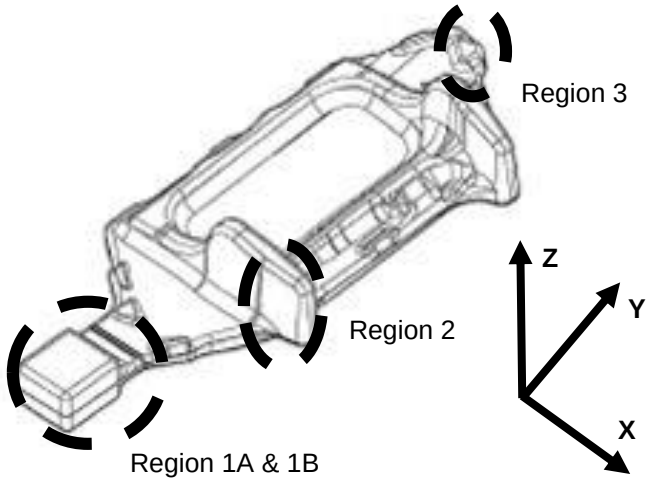

Figure 13. Location of regions from which samples were taken for tensile testing and metallographic analysis.

The assignment of tensile testing sample positions was based on the part specifications. However, some samples namely in regions 2 and 3 were chosen based on geometric constraints. It was important to get samples in each region that were all from the same orientation relative to the original axes. This allowed for better statistical analysis since a full design of experiment was not permitted. Locations from where the samples were taken can be seen in Figure 14 through Figure 17. Sample lengths were 2.5" and thus selection of sample locations was driven also by the amount of material from which samples could be taken.

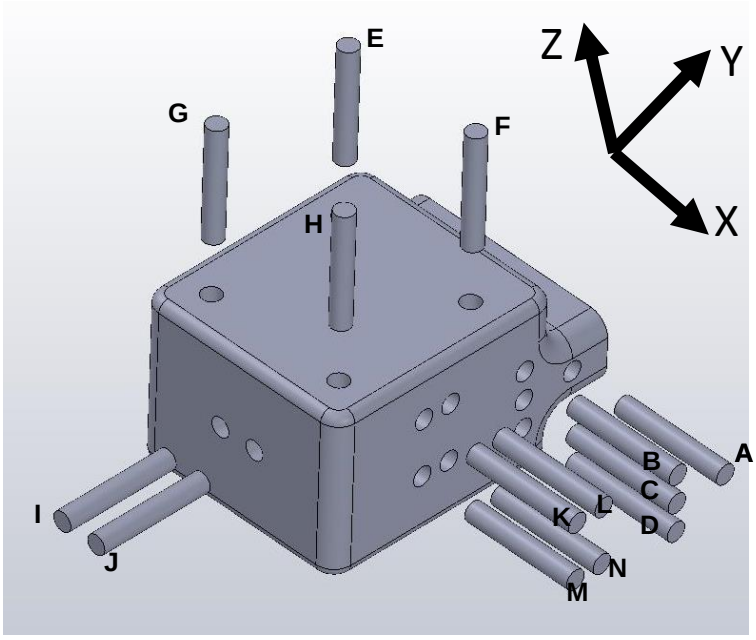

Figure 14. Location of tensile samples for region 1A.

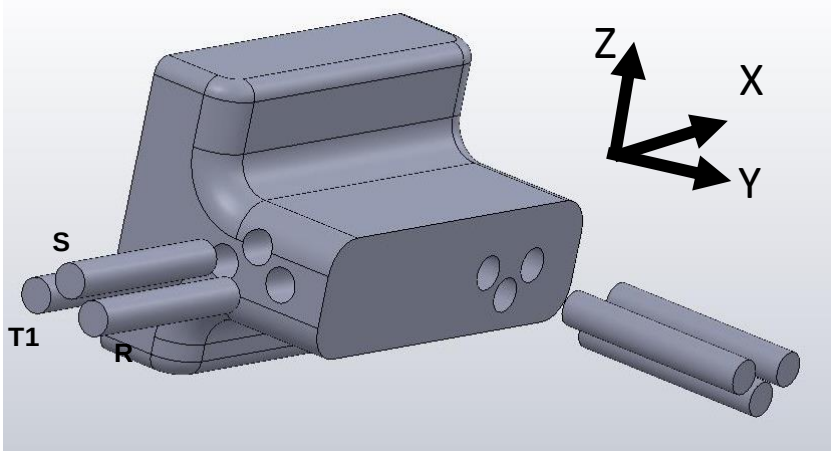

Figure 15. Location of tensile samples for region 1B.

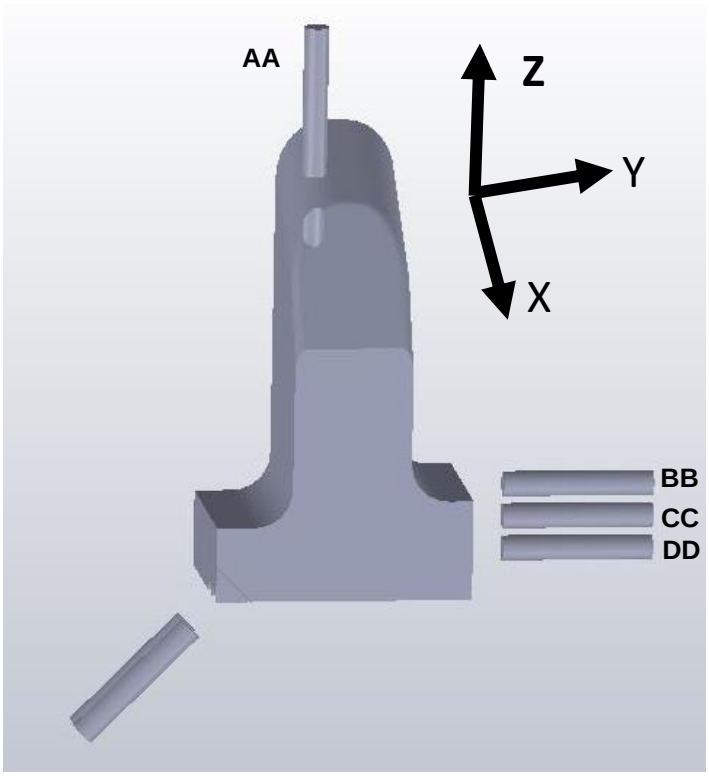

Figure 16. Locations of tensile samples in region 2.

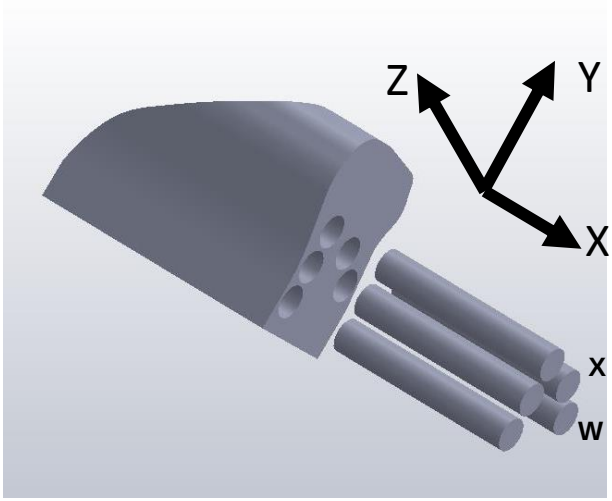

Figure 17. Locations of sample cuts in region 3.

The specifications for the part involved in this study were based primarily on tensile properties. Results obtained from tensile testing were then used to determine the next course of action. Values for yield strength, ultimate tensile strength (UTS), and elongation were those of primary concern.

3.1.1.2 Tensile Testing

Samples were machined to the specifications outlined in the ASTM E8M standard, which is the standard for tensile testing of metallic samples (ASTM International n.d.b.). Size of the machined samples were in accordance with the standard outlined in ASTM E8M for small-size specimens. In order to have as many samples as possible considering the constraint of the amount of usable material, smaller were used. These samples were threaded on either end and had a gauge length of 1.25 ± 0.005 in with a diameter of 0.25 ± 0.005 in and a length of the reduced section equal to 1.4 in. The radius of the fillet was 0.188 inches in accordance with the standard and yielded a total sample length of 2.5 in.

With the machined samples obtained, the standard operating procedure for using the Instron 5584 tensile tester with 150 kN load cell and Bluehill software was observed. The testing fixture consisted of wedge grips which held a secondary fixture containing a flat side that would be loaded in the wedge grips and a female threaded side opposite the flat side. Sizing of the threads was in accordance with the tensile test samples. This setup of wedge grips to threaded holder was used on both the crosshead and base of the Instron. In order to load the samples, the bottom side was first secured in the grips and the sample threaded into the secondary fixture. After the bottom was secured, the top was loaded into the secondary fixture and the crosshead lowered so that the secondary fixture could be loaded into the wedge grips. In order to not place too much load on the sample the bottom and top wedge grips were tightened equally and in alternating increments while monitoring the

applied load. If the applied load became too high the crosshead was slightly lowered in order to reduce any unwanted loading prior to testing.

Once samples were loaded the Bluehill software was started and sample dimensions were entered and the extensometer placed on the sample. The rate of crosshead motion was set to 0.0125 in/min until a strain of 1.25% when it was increased to 0.05 in/min for the rest of the testing cycle. After the test was completed the sample was taken out of the fixture and the top portion segregated from the bottom portion for later fractographic analysis. Results were then saved and the test repeated for subsequent samples until all tests had been completed.

3.2 Metallography

3.2.1 Sample Preparation and Acquisition

3.2.1.1 Sectioning

Metallographic sample bars were taken directly adjacent to tensile test bars. These samples were roughly ½” wide and 3” in length with a thickness of about ¼”. The bars were then taken and a rough cut made about halfway down the bar using a Leco MSX-250A wet abrasive chop saw. One half of the bars was then sectioned using an Allied Tech Cut 4 precision saw with a diamond abrasive wafering blade. Two cuts were made at ¼” intervals to yield a length equivalent to the thickness. Further cuts were made to each of the smaller bars halfway along the width of the bar. The progression of cuts as they relate to the original sample bar can be seen in Figure 18.

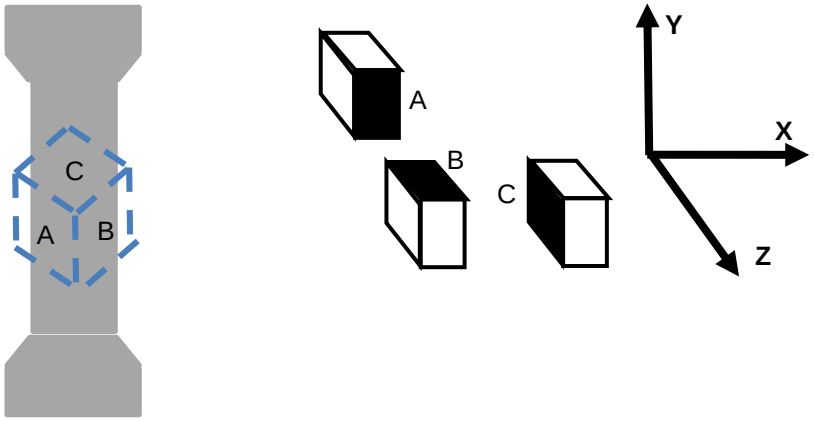

Figure 18. Diagram of the progression of cuts made for micrograph samples and orientation relative to circular rod tensile sample.

As mentioned previously, metallographic samples were taken from areas directly adjacent to the tensile test specimen. The orientation of the metallographic samples were cut so that each side: A, B, or C was the same when related back to the original axes. As far as the relationship of the different metallographic samples, the A sample was related back to the X-Y plane in regards to the original axes. The B sample was related back to the X-Z plane in the original part and sample C was related back to the Y-Z plane from the original part's axes. The orientation of the samples relative to the tensile sample are also shown in Figure 18.

3.2.1.2 Mounting and Polishing

With the sample cuts achieved and the surfaces marked, the samples were placed face down in a Leco PR-32 mounting press. Enough bakelite powder was then added to give a final sample height of roughly ½". The ram was then raised and the heating process started. Samples were heated for 13 minutes and then a cool down cycle was initiated. Once this was complete samples were removed from the mounting press and the corners ground at a 45° angle on a lubricated belt grinder.

With the samples mounted and the edges ground, samples were then ground using silica abrasive grinding paper. Grits used for grinding were 240, 360, 480, 600, and 800 in that order. Each sample was rotated 90° after the previous grit with enough passes to successfully remove scratches produced by the previous grit.

In order to polish the samples, 8” wheels were used. The first wheel contained an Allied Tech nylon woven pad with a 9 µm diamond slurry in glycol suspension. An ethylene glycol, ethanol, and water mixture was used as necessary to lubricate the polishing pads. When polishing on the 9 µm pad was achieved, as verified by light microscopy, samples were polished using a 1 µm grit diamond slurry in glycol suspension on an Allied Tech Microcloth. Again, the efficacy of the polish was verified by light microscopy. Once samples had been polished using the 1 µm suspension a final polish was conducted. This polish was conducted using a 0.05 µm alumina/silica abrasive in glycol suspension on an Allied Tech Red Final C polishing cloth.

3.2.1.3 Image Acquisition and Box Micrograph Construction

Image acquisition was achieved using ImageQ software in conjunction with an optical microscope and polarized filter. In total there were two magnifications used to acquire images 50x and 100x. The 50x images were those used to construct the box micrographs and the 100x images used for quantifying microstructure. Prior to a set of images being acquired the auto exposure and contrast tool was used. This was done for each metallographic sample prior to image acquisition.

In order to create one side of the box micrograph a series of 50x images were captured and stitched together. Images were acquired starting in the upper left corner of the sample and taken first left to right with overlapping features from image to image. Once a full row had been acquired the position was moved down, making sure to include overlap in order for the software to be able to stitch together the

images. From here images were acquired within the row in the opposite direction of those from the previous row. Once all images were acquired a micron bar was superimposed on the first image of the series. Since images were acquired in the TIFF format they were converted to JPG format to allow compatibility with the panorama creator software.

The panorama creator software used to stitch the images together was i2k Quickage by Dual Align. This process was done in multiple steps in order to create the most accurate final image. Three rows were selected and stitched together. After the process had completed the first two rows of the previous image were deselected and the next two rows selected and the images stitched together with this taking place until there were no more rows to stitch together. Once this process of stitching together three rows at a time was complete, the created images of three rows were all selected and stitched together to make the final image consisting of one side of one of the box micrographs. From here this entire process was repeated until all final images were obtained.

It was found that once all of the images were stitched together there was not enough contrast to accurately determine the grain boundaries. In order to remedy this, copies of the images were made and the gamma value of the image was reduced in order to highlight microstructural features such as grain boundaries and Widmanstätten colonies. For each image the gamma was reduced to between 0.15 and 0.20 in order to obtain the most contrast. However, once the gamma was reduced some images were too dark. Thus the brightness for those images was increased by 30% to 50% depending on the specific images needs.

3.2.2 Quantitative Metallography

3.2.2.1 Grain Size

Grain size was determined by manual counts based on the standard ASTM E112-12 (ASTM International n.d.a.). This specific standard outlined multiple ways to determine grain size, yet only one method was used. For this study, the Abrams three-circle procedure was used. The method involves overlaying three concentric circles over the image. Typically, the total line distance should be 500mm. However, it was found that this would create too large of circles and thus an alternative line distance was used still allowing the same outcome.

For the Abrams approach to be accurate it was recommended that there should be between 40 to 100 intersections per set of concentric circles. In this case, a diameter of 750 microns for the first circle was used with each concentric circle having an increased diameter of 750 microns for a diameter of the final third circle of 2250 microns. Five sets of concentric circles were then overlaid on the image using ImageJ software with the downloaded concentric circles plugin. Care was taken to ensure that none of the sets of circles overlapped.

Once all images had the sets of circles overlaid, intersections of the circles and grain boundaries were tallied manually. These counts were then put into Microsoft Excel for the corresponding image and circle. Then the following formula was used to calculate the average number of intercepts per length:

$$\bar{N}_L = \frac{N_i}{L/M} \qquad (1)$$

Where, N_i is the number of intercepts, L is the total test line length, and M is the magnification used. In this case the total line length was equivalent to 14137 microns.

When this was completed the inverse of the previous calculation was taken to calculate the average grain size in units of microns/grain.

3.2.2.2 Grain Shape

The grain shape was measured by determining the aspect ratio of the grains. For this test the aspect ratio in the “a” and “b” directions was taken with the “a” direction corresponding to the x-axis of the image and the “b” direction the y-axis of the image. In total ten grains were sampled per image with the “a” and “b” coordinates measured using ImageJ software. These measurements were then put into Excel and the aspect ratio calculated by dividing the “a” measurement by the “b” measurement. This would mean that a value of 1 would give equiaxed grains. These measurements were also organized and analyzed as they corresponded to the axes of the original image.

3.2.2.3 Phase Volume Fraction

In order to determine the volume fraction of α and β, the images of the sample at 100x were opened individually with ImageJ. For each image the sharpen process in ImageJ was used to enhance the contrast between α and β. Once this was done the image was converted to binary using ImageJ. Threshold was then set so that the darker regions were highlighted. Highlighted regions were then measured using the command Analyze > Analyze Particles and the % area recorded in Excel. This process was then duplicated for each of the 100x images, across all of the samples.

3.2.2.4 Widmanstätten Colonies

In order to calculate the size of the Widmanstätten colonies the same standard was used as that for grain size (ASTM International n.d.a.). However, instead of using the Abrams concentric circles method, an alternative method was used. For this method the Heyn Lineal Intercept procedure was utilized. This procedure involves overlaying

an x-shaped image over the original image. In this case two lines, each 2500 microns in length, were overlaid over different areas of one of the 50x images post gamma reduction. In order to create the cross hair shaped lines, the “Specify Line” plugin was used which can be found on the NIH’s website. Using the “Specify Line” plugin the endpoints of a line can be entered into a dialog box and the resulting line displayed. This line was then overlaid on the image. All told, a total of four cross hairs were overlaid over the image. Once the cross hairs were overlaid, intercepts of the Widmanstätten colonies were tallied manually and recorded in Excel.

3.3 Statistical Analysis

The method utilized for statistical analysis was the analysis of variance (ANOVA). This method compares the residual values of the data versus the mean of the residuals to see if any of the variables exhibit statistical differences. A p-value less than the significance level indicates that at least one of the variables exhibits a statistical difference. In this case the significance level used was 10%. The larger significance level was used so as to more easily identify differences in either the tensile properties or microstructural properties. As suchm, the Type I error was sacrificed; however, this was allowable since it was more important to identify differences in measurements.

When conducting ANOVA several assumptions must be met. These assumptions are: normality, constant variance, and independence. Whether or not assumptions are met can be determined from plots of the deleted residuals. Normality is satisfied if the normal probability plot of the residuals adheres to the diagonal line. The assumption of constant variance is met if the versus fits plot of the residuals maintains even spacing of all residuals. Independence is confirmed based on the versus fits plot, if there is a random scattering of points above and below zero then the assumption is met. Examples of the plots that meet the assumptions can be found in Figure 19.

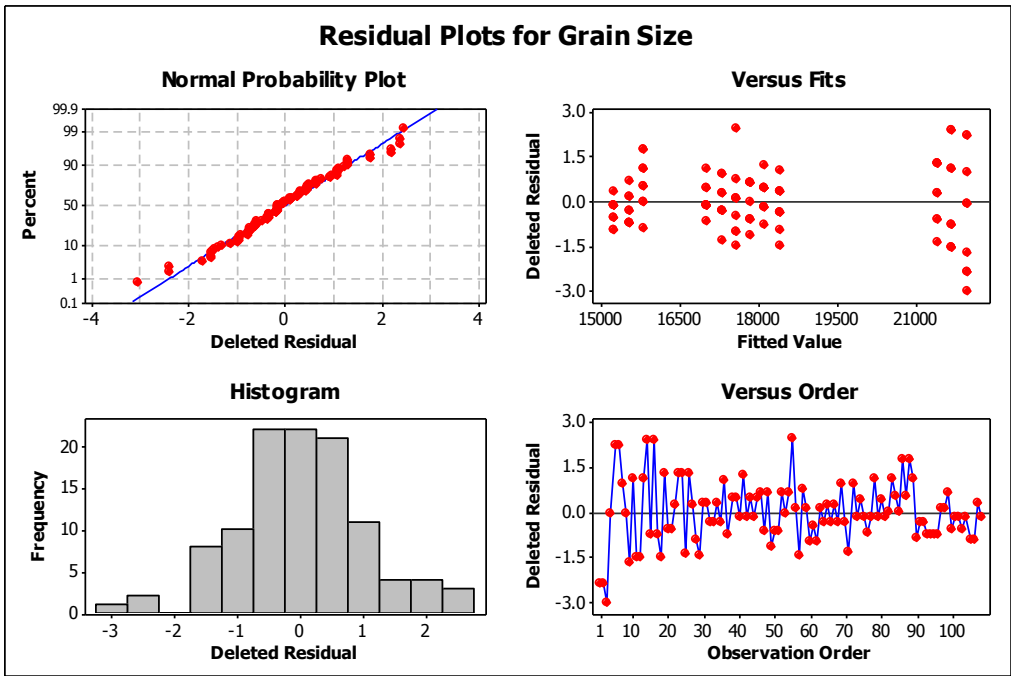

Figure 19. Example of graphs of the residuals that meet the assumptions for ANOVA.

Once all assumptions are met then a Tukey's Pairwise comparison was conducted. This test looks at all variables and compares the residuals to determine which variables are statistically different from one another. The Tukey's Pairwise comparison was conducted with a 90% confidence level in accordance with the significance level. Once comparisons were conducted Ven diagrams were constructed to visually represent differences between variables if differences existed.

3.4 Fractography

Tensile test samples from the corresponding metallographic images as well as the other two orientations in region 1A would not fit in the SEM vacuum chamber. In order to get the samples to fit in the vacuum chamber the threaded portion of the tensile sample was cut off preserving the fracture surfaces. Once samples were cut to size they had to be cleaned of the cutting fluid before being used in the scanning electron microscope (SEM). In order to clean the samples a Chicago Electric ultrasonic cleaner was used. The first cleaning

treatment used acetone for two consecutive three minute cycles. This treatment was done for all samples. After the acetone cleaning cycle samples were immersed in the ultrasonic cleaner bath, this time with deionized water, and cycled through for two more consecutive three minute cycles. Again, this was completed for all samples.

Obtaining images for fractography was accomplished using a Philips Quanta 200 ESEM. First, pertinent information about the SEM operating conditions was recorded to maintain a record of the performance of the SEM. From here, the standard operating procedure was followed. The filament voltage was set to 20 kV and the spot size to 4.0. In order to determine locations for high magnification images, an overall picture was captured for each sample. Following the capturing of the entire surface, selected areas were then magnified to 150x or 300x depending on the size of the feature being examined. The positions of magnified images were chosen according to features that were present at those locations that represented the overall sample.

4 RESULTS AND DISCUSSION

4.1 Tensile Testing

After tensile testing data was conducted stress-strain curves were created for regions 1A, 1B, 2, and 3 and are seen in Figure 20 through Figure 23 respectively. The stress-strain diagram for region 1A showed that most of the samples exhibited similar yield strengths but had a variety of UTS values. The elastic region is also not completely linear for almost all samples except for sample B potentially due to slippage of the grips during testing. Region 1B showed even more variation in UTS between samples, especially due to the limited number of samples. The same is true of region 3 UTS values. However, region 2 exhibits little variation in yield strength and UTS values.

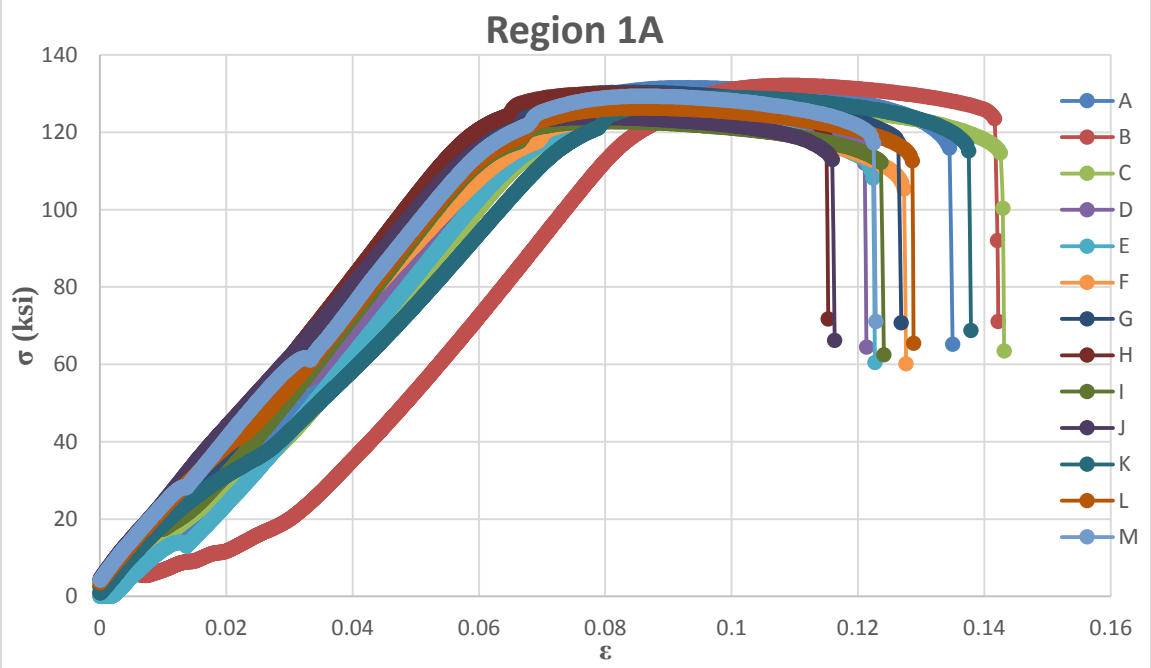

Figure 20. Stress-strain curves for the tensile testing results for region 1A.

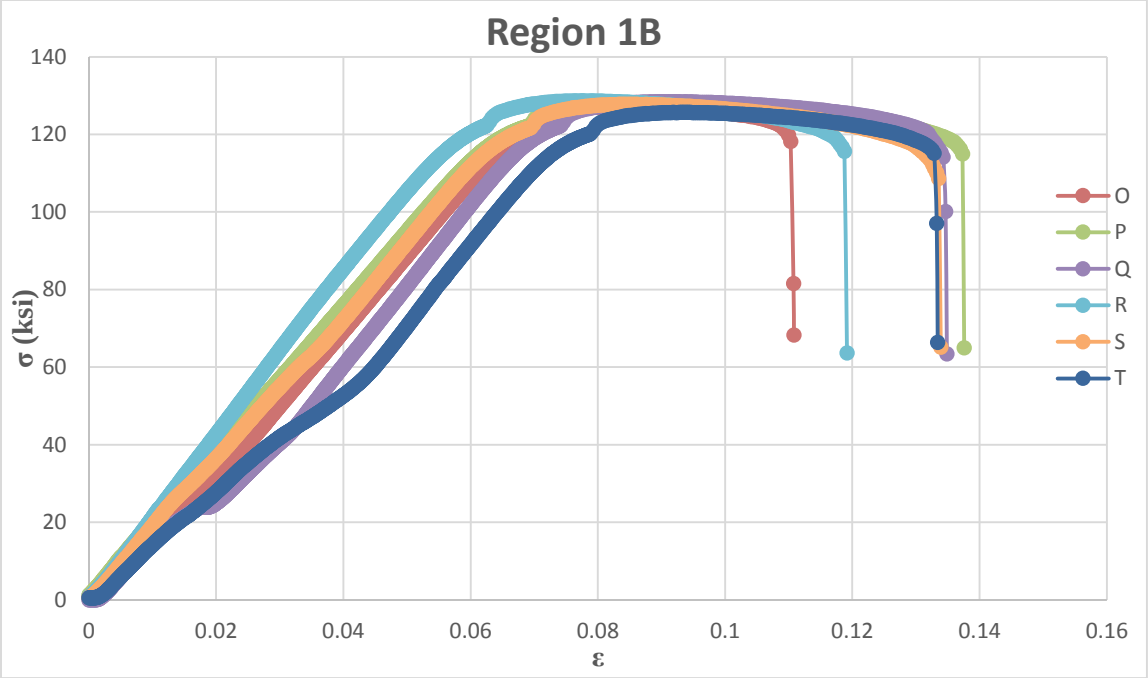

Figure 21. Stress-strain curves for the tensile testing results for region 1B.

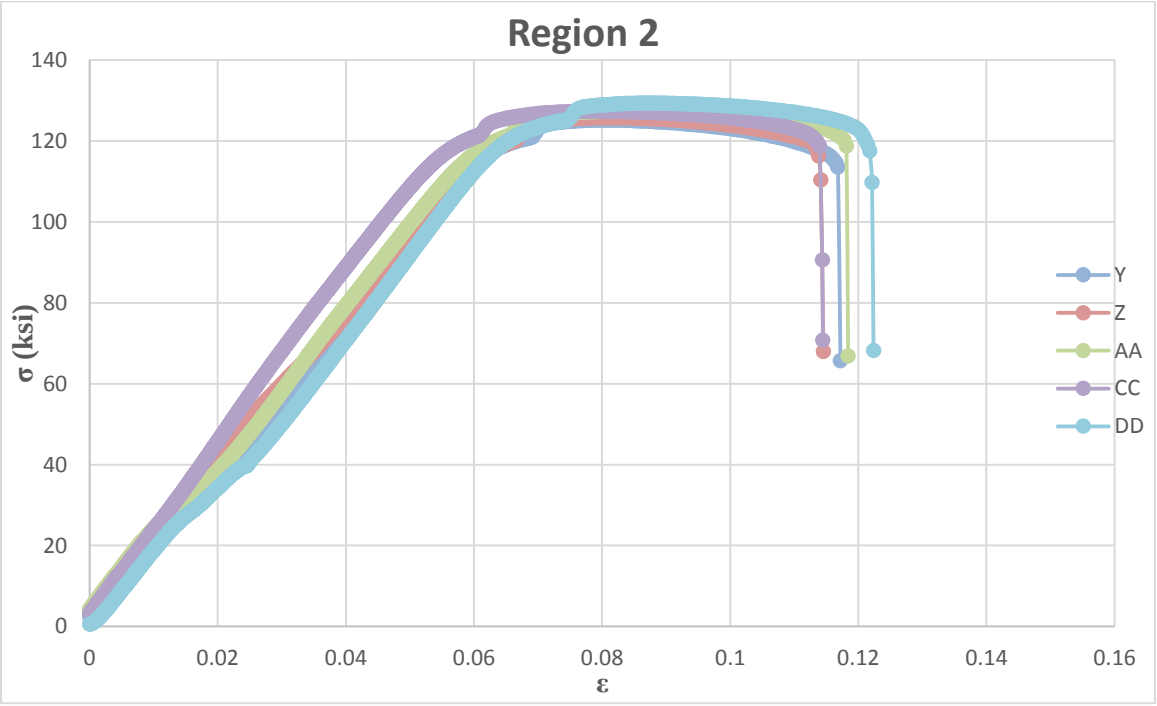

Figure 22. Stress-strain curves for the tensile testing results for region 2.

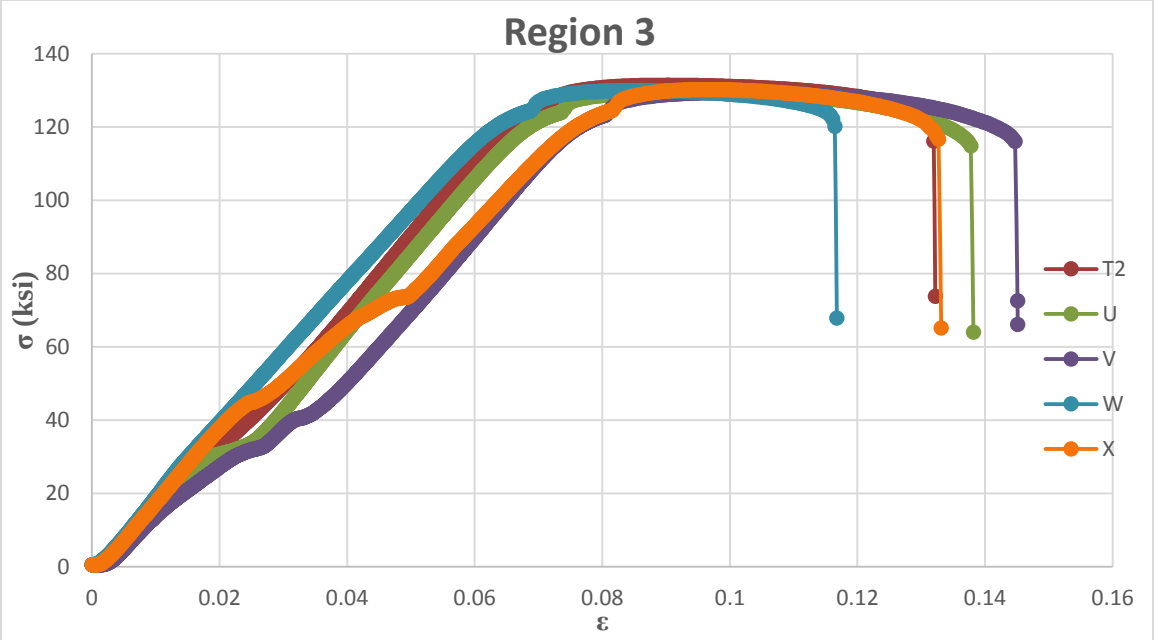

Figure 23. Stress-strain curves for the tensile testing results for region 3.

4.1.1 Yield Strength

The yield strength of regions 1A and 1B are properties that are outlined in the part specification. As such, analysis of whether or not they were similar was required as well as the determination of any anisotropic behavior that existed in the part from which region 1A was taken. A summary of the results for the yield strength based on region can be found in Table 3. From these results it was seen that there was less variability in region 1B, which was taken from the part that met specification, relative to that of region 1A. This variability was undesirable and was one of the reasons for the part not meeting specifications. A boxplot of the data was included to show a visual representation of the data.

Table 3. Results of yield strength data obtained from tensile testing separated by region.

Region	Mean Yield Strength (ksi)	Standard Deviation (ksi)	Number of Samples
1A	116.05	2.78	13
1B	117.31	1.05	6
2	117.48	2.26	4
3	120.06	0.941	5

The values obtained for yield strength were less than those found by Lütjering (1998) for Ti-6Al-4V which had a yield strength of roughly 135 ksi. One possible reason for this is that the values obtained by Lütjering were for samples with a much smaller grain size. This smaller grain size would have impeded the movement of dislocations more and ultimately resulted in higher yield strength values in Lütjering's study than those obtained here. Another reason for the different values obtained by Lütjering as compared to this study is that the microstructure obtained by Lütjering was a duplex structure as compared to a Widmanstätten colony structure.

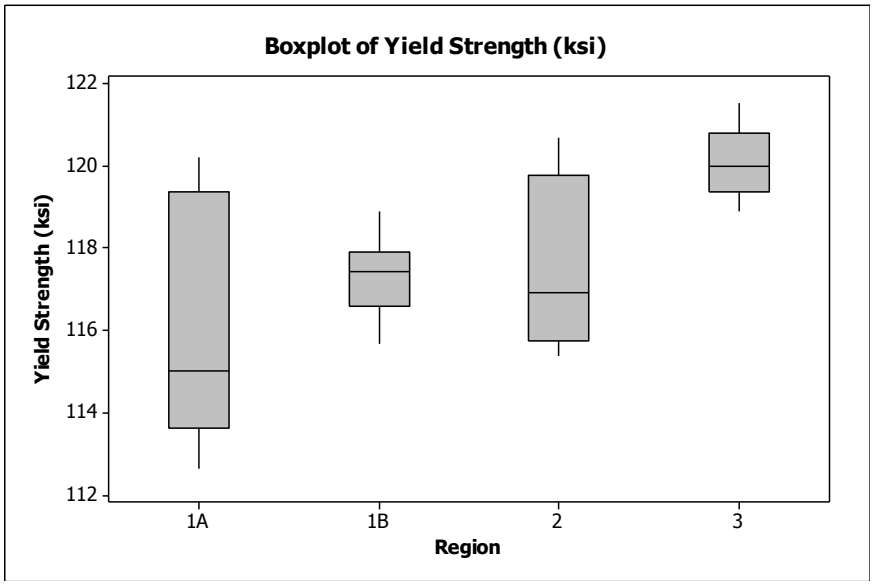

Figure 24. Boxplot of yield strength data obtained from tensile testing separated by region.

It was also noticed that region 2 had a relatively high variation of yield strength values while region 3 had the least amount of variability. Some of the variability may have been explained by the sampling locations, since samples in region 3 were all taken closely together. Regions 1A and 2 were larger regions with the samples spread throughout the regions which may have created more variability than the samples taken adjacent to one another in region 3. Also, with the larger dimensioned regions an uneven cooling rate may have existed. This uneven cooling rate would have affected the microstructure and also the mechanical properties. In order to draw conclusions from the ANOVA test the assumptions were tested by looking at the necessary plots of the residuals. After analyzing the residuals it was found that all of the assumptions were met.

An ANOVA test was used to determine if any statistical differences existed between regions or sample orientation. It was found with a 10% significance level that at least one region was different from the others ($p = 0.076$) but failed to find a difference between sample orientation ($p = 0.927$). The Minitab output may be found in Appendix A as well as the plots of the residuals. As seen from the summary of data in Table 3, region 1A has the lowest yield strength; however, since the standard deviation was so large it was statistically similar to regions 1B and 2. As was seen in the Ven diagram for the yield strength data (Figure 25), regions 1A, 1B, and 2 all were statistically similar. In addition, regions 1B, 2, and 3 were also statistically similar. This meant that region 1A and region 3 were regions with statistically dissimilar yield strengths in accordance with a Tukey's Pairwise Comparison test with a 90% confidence interval.

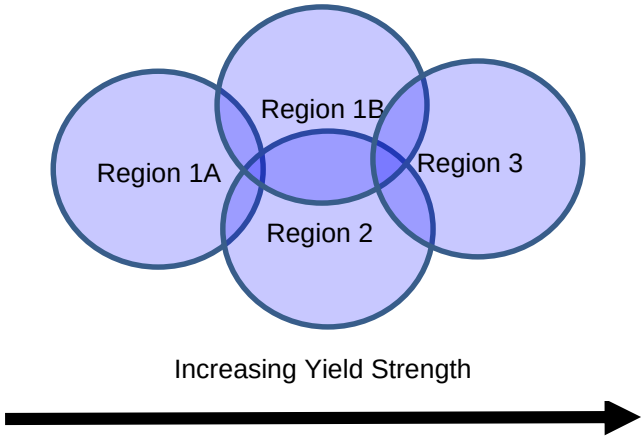

Figure 25. Ven diagram of Tukey's pairwise comparison results for yield strength data.

4.1.2 Ultimate Tensile Strength

A summary of the tensile testing data for the UTS can be found in Table 4. As observed from the data, region 3 had visually higher UTS values with a much lower standard deviation. The reason for this may be that samples were all taken with close proximity to one another within region 3 which in turn yielded more precise data. Region 1A on the other hand had a much larger standard deviation, possibly due to a relative increase in distance between samples and inclusion of multiple orientations. When looking at the boxplot of the data in Figure 26 it was seen that the values for region 3 were larger than that of region 1B, region 2, and potentially region 1A. However, due to the large standard deviation exhibited by the data for region 1A, it was harder to draw specific differences between region 1A and region 3. The actual determination of a difference, if any existed, was determined by statistical analysis using ANOVA.

Table 4. Results of UTS data obtained from tensile testing separated by region.

Region	Mean UTS (ksi)	Standard Deviation (ksi)	Number of Samples
1A	127.50	3.36	13
1B	127.57	1.08	6
2	126.42	1.13	4
3	130.13	0.79	5

When these values were compared again to those found by Lütjering (1998) they were also lower. Values for UTS found by Lütjering were of roughly 143 ksi. Again the grain size would have played a key role in accounting for the lower UTS in the study conducted by Lütjering as compared to this study.

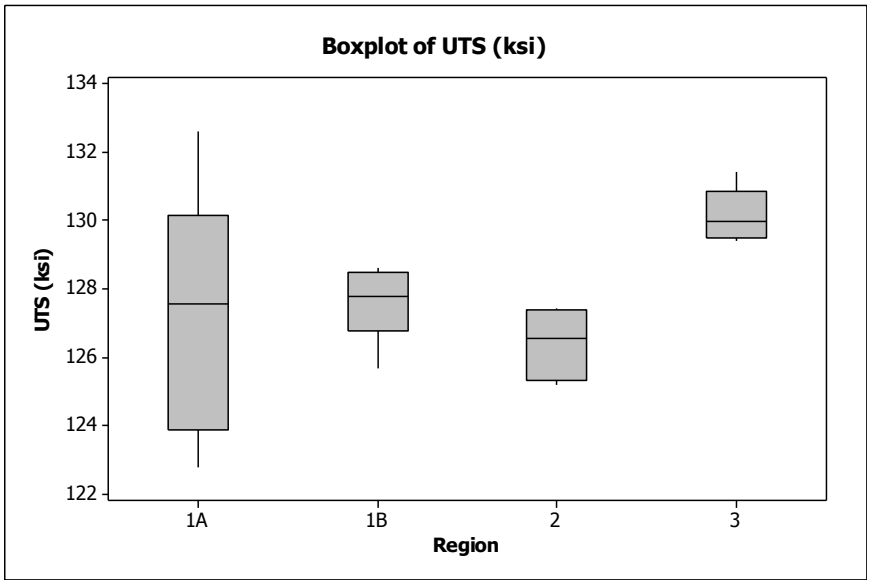

Figure 26. Boxplot of UTS results for tensile testing separated by region.

Upon conducting statistical analysis using ANOVA with a significance level of 10%, statistical differences were found between regions ($p = 0.047$) but not between orientations ($p = 0.140$) of the samples. A 10% significance level was used rather than that of 5% so that any differences that may have existed were found and it was acceptable to sacrifice Type I error. However, for the results to be valid the ANOVA assumptions of: normality, constant variance, and independence must have been met. Assumptions for ANOVA were tested and all of the ANOVA assumptions were met.

Therefore, the conclusion that statistically significant differences existed between regions was valid. In order to determine which regions were statistically different from others a Tukey's Pairwise Comparison was conducted.

The Minitab output, found in Appendix B, includes the results from the Tukey's pairwise comparison test, ANOVA, and plots of the residuals. From the Tukey's test, conducted with a 90% confidence level, it was found that regions 2, 1A, and 1B were all statistically similar. In addition, regions 1B and 3 were statistically similar. These results were displayed in the Ven diagram found in Figure 27. In the Ven diagram, the regions that are statistically similar overlap. This meant that region 3 was statistically different from regions 1A and 2, which had statistically lower UTS values. It should be remembered that region 1A and region 1B came from different parts and region 1B exhibited properties that passed specification. Region 1A and region 1B came from different regions of which region 1B was previously found to have met specifications. After the Tukey's pairwise comparison it was found that the mean values of the UTS data were statistically similar for regions 1A and 1B. However, it was previously found that the part from which region 1A was taken did not meet specification and required additional heat treatments. This was not reflected in these results, most likely due to the large variation of data within region 1A and region 1B as compared to other regions.

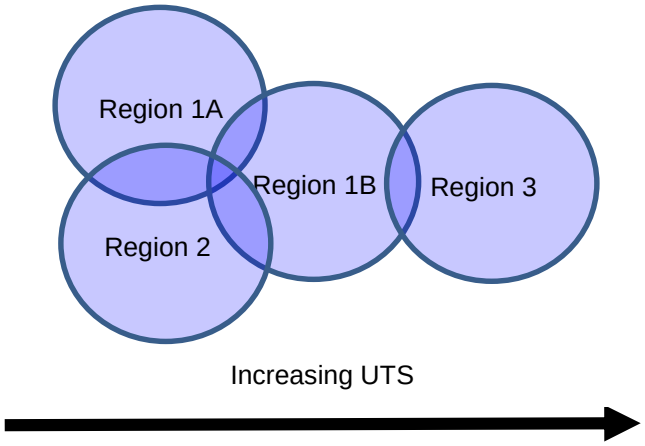

Figure 27. Ven diagram for the Tukey's pairwise comparison results of UTS data.

4.1.3 Elongation

It can be seen in the stress-strain curves that region 1b and region 2 have a smaller elongation than that of region 1A and region 3 (Table 5). This was somewhat corroborated by the statistical analysis conducted on the elongation based on region and taking into account the effects of orientation using ANOVA. With an α significance level of 10%, it was seen that the region variable had a statistically significant effect on the elongation ($p = 0.059$); however, the test failed to find a statistically significant difference based on sample orientation ($p = 0.164$). Furthermore, a Tukey's Pairwise Comparison was conducted with a 90% simultaneous confidence interval. From the Tukey's comparison it was found that regions 1A, 1B, and 3 were all statistically similar to one another. In addition, regions 1B, 1A, and 2 were all statistically similar as well. This meant that regions 2 and 3 were statistically different as these were the regions where the groupings did not overlap. Table 5 shows the mean and standard deviations of the elongation data based on the region of the part. In Figure 28 the data can be seen in graphical form divided by region. As can be seen from the graph, region 2 exhibits smaller values and a smaller range than that of the other regions. This shows that

regions 2 and 3 had statistically different elongation. The Minitab output of the results can be found in Appendix C.

Table 5. Results table for the elongation values obtained from tensile testing separated by region.

Region	Mean Elongation (%)	Standard Deviation (%)	Number of Samples
1A	12.86	1.056	13
1B	12.93	1.063	6
2	11.60	0.462	4
3	13.28	0.912	5

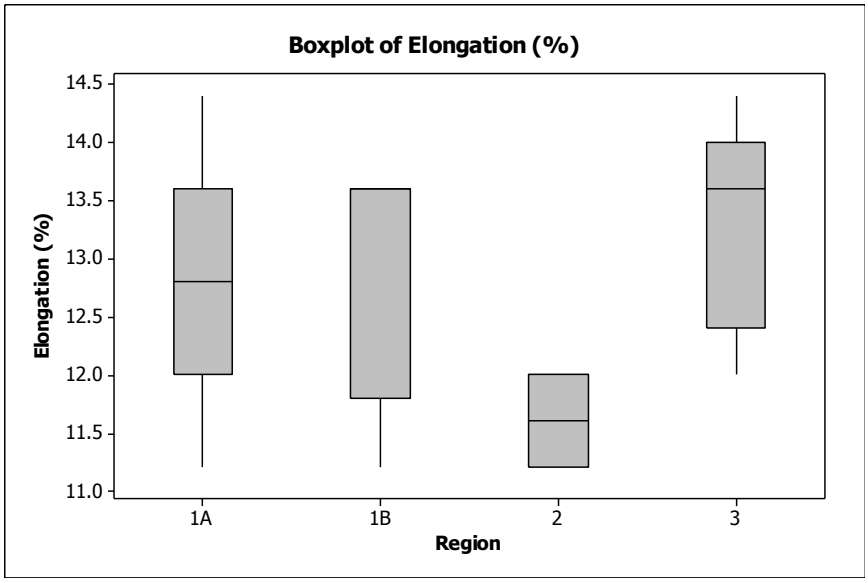

Figure 28. Boxplot of the elongation data from tensile testing divided into regions.

From the deleted residuals plots seen in Figure 29 it was found that the data was not entirely normal and has the potential to not meet the assumption of constant variance. Both normality and constant variance are assumptions that must be met in order to accurately interpret the results. The versus fits plot of the deleted residuals showed that there may have been some uneven scattering of points along the y-axis, yet due to the lack of data on the lower end of the x-axis this was not fully determinable. Also, the normal probability plot of the residuals showed that since the data did not adhere to the

normal line, the data was not normal. With sufficient data points, typically 30 or more, the normality assumption may be overlooked based on the Central Limit Theorem. Since there are just 30 data points the Central Limit Theorem could have been applied. Although, the lack of normality coupled with the fact that the data may not have exhibited constant variance shows that it may have been unreliable for determination of statistical differences in elongation of the samples.

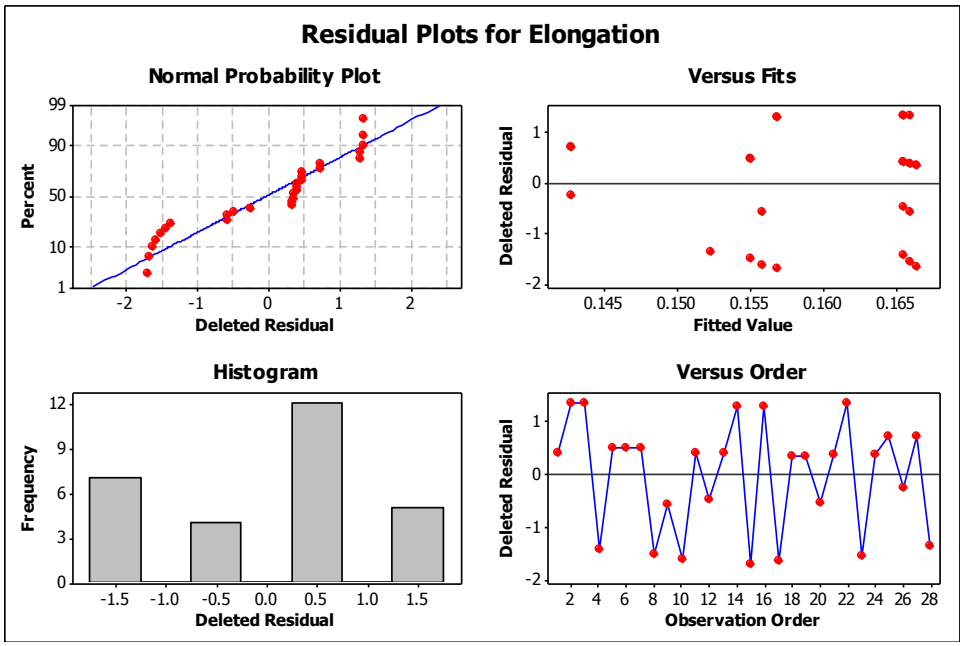

Figure 29. Plots of the deleted residuals for elongation data obtained from tensile testing.

Not all of the assumptions for ANOVA were met for the elongation data for a couple of reasons. One possible reason that the data did not meet the requirements was complications during data collection. When the samples were put in the secondary fixture and the wedge grips of the primary fixture were tightened the fixtures were not tightened enough. If the fixtures were not fully tightened, there is the potential that the secondary fixture may have slipped within the wedge grips possibly corrupting data. Since the secondary fixture would have slipped in line with the sample the software would have read this as the sample elongating when it really was not. This can be somewhat corroborated by the stress-strain curves across nearly all samples. In the stress-strain

curves the elastic portion of the curve is not as straight as it should be for all of the curves. This non-linear behavior could be explained by the slipping of the secondary fixture in the wedge grips. Since this happened for almost all of the data it was not possible to discard the data. Also, some of the slippage that occurred was corrected in the stress-strain curves and raw data, yet could not be fully corrected without jeopardizing the other measurements.

4.2 Metallography

The four aspects of the microstructure that were evaluated were: grain size, grain shape, volume fraction of β-phase, and size of Widmanstätten colonies. These tests were carried out on samples from the x-orientation relative to the original sample axes and conducted based on micrographs for one sample in each region. Tests on the box micrographs yielded data for each plane in each region.

The three images from each metallography sample were organized into a box micrograph (Figure 30). Sampling of the images allowed the orientation of the image to be statistically analyzed. Upon conducting ANOVA for all of the different measurements with a 10% significance level, the test failed to find was a statistical difference based on orientation for all measurements. This finding somewhat correlated to the tensile testing data in which the orientation of the test sample also did not exhibit statistical differences. However, this comparison is weaker as the tensile samples were taken from different areas of the associated region whereas the metallography samples were taken adjacent to just one tensile sample.

Box micrographs (Figure 30) all appeared fairly similar upon visual inspection. However, when each image was examined separately and quantitative metallography was conducted there were statistical differences in microstructural characteristics. These differences existed between regions from which the samples were taken. The exact differences varied based on the microstructural characteristic that was analyzed.

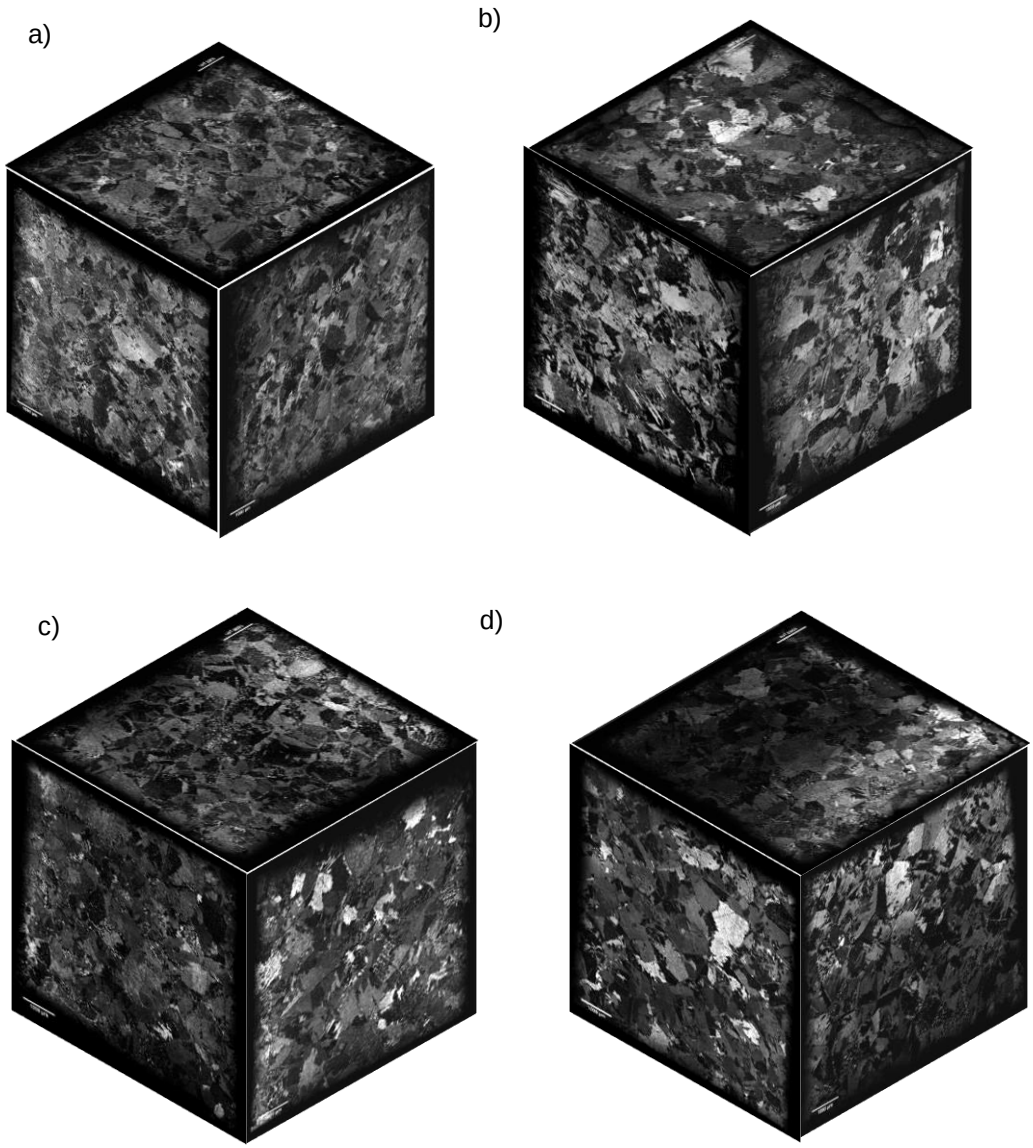

Figure 30. Box micrographs resulting from metallography for: a) region 1A, b) region 1B, c) region 2, and d) region 3.

4.2.1 Widmanstätten Colony Size

Size of the Widmanstätten colonies can influence the yield strength of the material being tested (Lütjering 1998). Therefore, statistical analysis was done to determine the differences between samples. A summary of the data can be found in Table 6. The summary of data shows that again regions 2 and 3 exhibit the lowest variability as well as a smaller colony size. This can be further seen in the boxplot of the data found in Figure 31. In the boxplot a visual difference could be found between regions. This was confirmed with ANOVA and a Tukey's Pairwise Comparison.

Table 6. Summary of the size of Widmanstätten colony size.

Region	Mean Colony Size (microns/colony)	Standard Deviation (microns/colony)	Number of Samples
1A	173.40	9.56	12
1B	171.20	18.90	12
2	127.81	4.63	12
3	122.60	7.12	12

In a study conducted by Ding, Guo, and Wilson (2002) the colony size was much smaller than that presented herein only abou 75 microns in diameter. However, the grain size of those samples was also smaller. This would make sense since the Widmanstätten colonies nucleate from the grain boundaries. Therefore, it would be expected that a sample with a smaller grain size would exhibit smaller sized colonies.

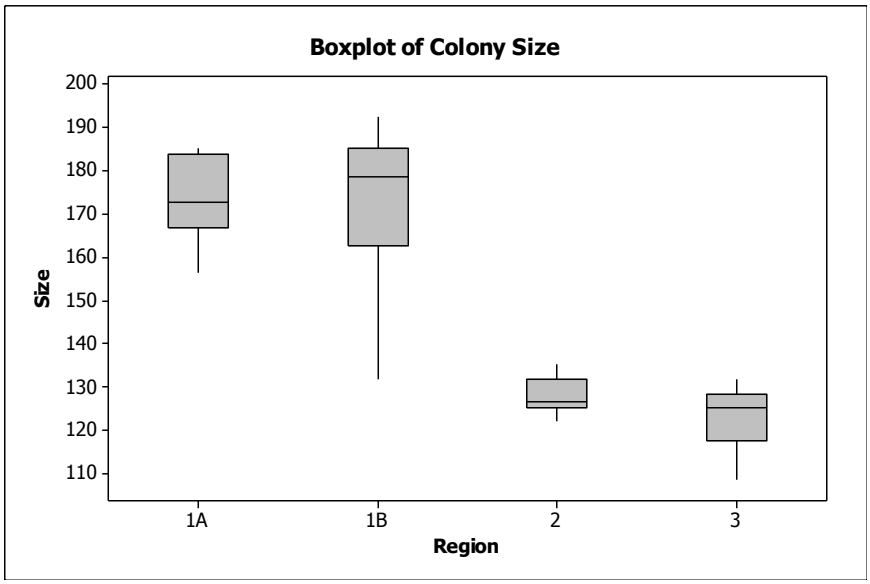

Figure 31. Boxplot of data for the size of Widmanstätten colonies.

Like the other statistical analysis completed, the assumptions of the ANOVA were first checked. These assumptions were checked based on plots of the deleted residuals found in Appendix D. After analyzing the residuals it was found that all of the assumptions were met. Next, ANOVA and a Tukey's Pairwise Comparison were conducted to find if any differences existed in the measurements pertaining to the size of the Widmanstätten colonies. With a 10% significance level, it was found that after adjusting for the effects of the orientation that there was at least one region that exhibited a mean difference in the size of the Widmanstätten colonies than the other regions ($p < 0.001$). Also, the ANOVA failed to find a statistical difference in colony size based on the orientation of the image ($p = 0.150$). The full data output from Minitab can be found in Appendix D. With the ANOVA successfully completed the exact differences were compared using Tukey's comparisons. A visual representation of the differences in colony size is seen in Figure 32. Region 1A exhibits visually larger Widmanstätten colonies than region 3.

a) 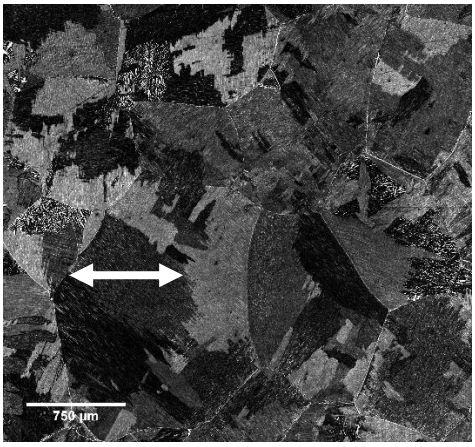

b) 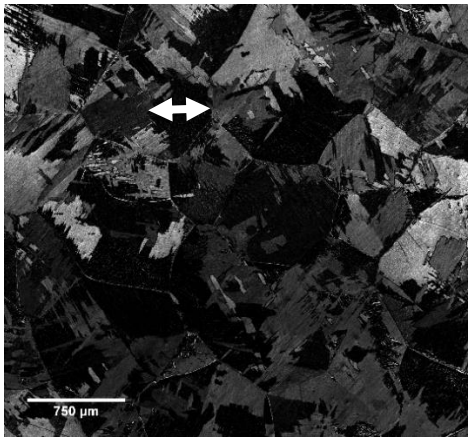

Figure 32. Examples of the differences in colony size with white lines showing the colony width a) sample from region 1A and b) sample from region 3.

A Tukey's Pairwise Comparison was used to tell which regions were statistically different from one another. To visually represent the differences that existed a Ven diagram was created (Figure 33). This diagram showed that regions 1A and 1B were statistically similar to one another but different from regions 2 and 3.

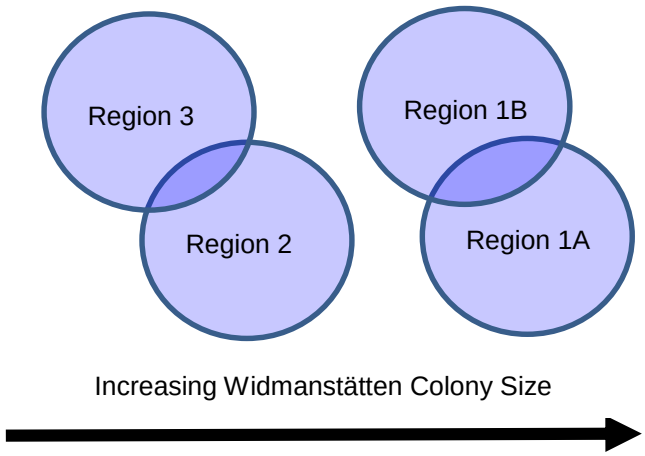

Figure 33. Ven diagram showing the differences in Widmanstätten colony size.

4.2.2 Grain Size

Since grain size was found through research to influence the mechanical properties of the material, quantitative analysis of grain size was performed. A table of the results can be found in Table 7. Furthermore, a boxplot of the data may be found in Figure 34 which shows the smaller grain size of region 2 as compared to the other regions.

Table 7. Results of grain size data from quantitative metallography.

Region	Mean Grain Size (microns/grain)	Standard Deviation (microns/grain)	Number of Samples
1A	21700	2762	27
1B	18128	1221	27
2	15541	1522	27
3	17309	1449	27

Ding, Guo, and Wilson (2002) conducted a study on the effect of strain rate on grain size. In their study the rough grain diameter was only a few hundred microns. This in turn resulted in their values of yield strength and UTS being lower than those found in the samples used for this study.

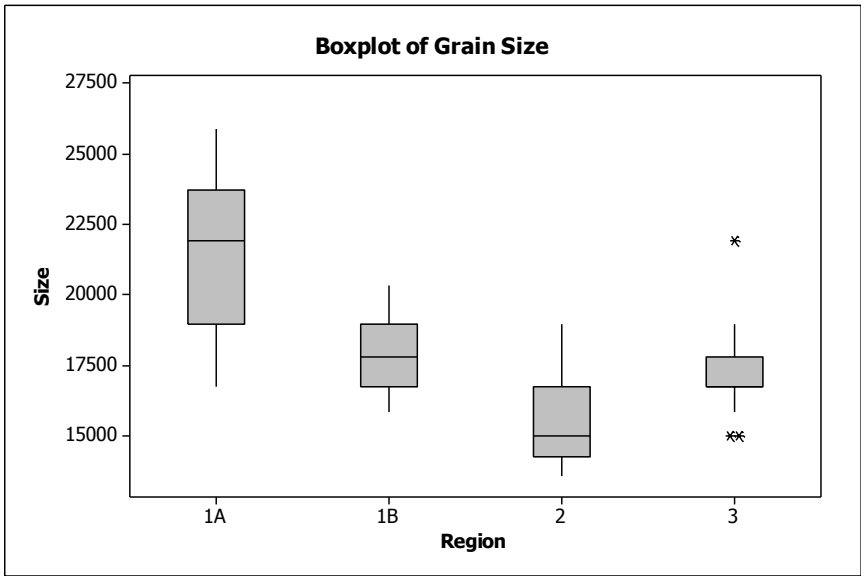

Figure 34. Boxplot of the data for Grain Size showing significantly larger grain size in region 1A.

The assumptions for ANOVA were checked and found to be met allowing conclusions to be drawn. It was found that with a significance level of 10%, the region from which the sample was taken ($p < 0.001$) had a statistically significant effect on the grain size while after taking into account the orientation of the micrograph. While the orientation of the image failed to exhibit a statistical difference in grain size ($p = 0.416$). In order to see if the differences in grain size correlated to the mechanical properties a Tukey's comparison was conducted. A visual comparison of region 1A, which had the largest grain size and region 3, the smallest can be seen in Figure 35.

a)

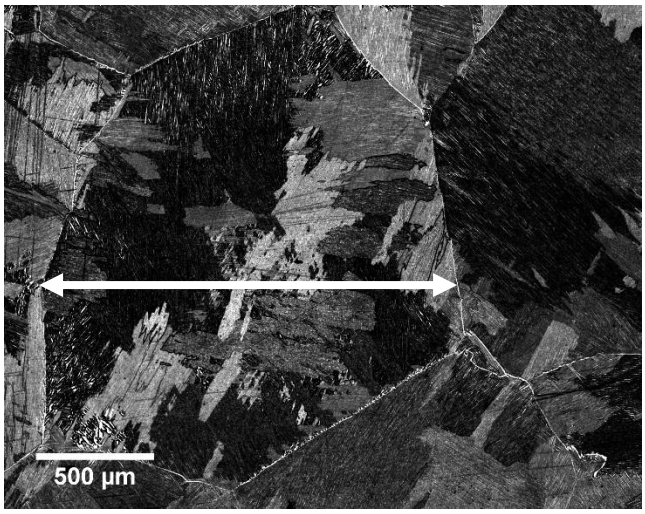

b)

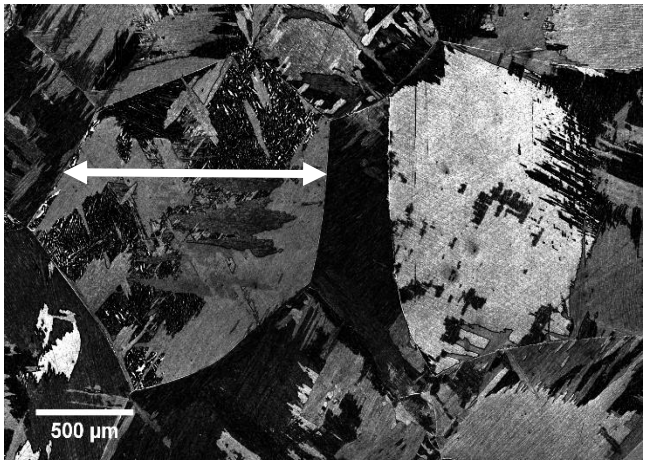

Figure 35. An example of the differences in grain size a) example from region 1A and b) example from region 3.

The Tukey's Pairwise Comparison was used with a confidence level of 90%. Results from the comparison were put in a Ven diagram (Figure 36). This Ven diagram shows that the only two regions that were statistically similar were regions 3 and 1B. It should also be noted that region 2 exhibited the smallest grain size while region 1A exhibited the largest grain size.

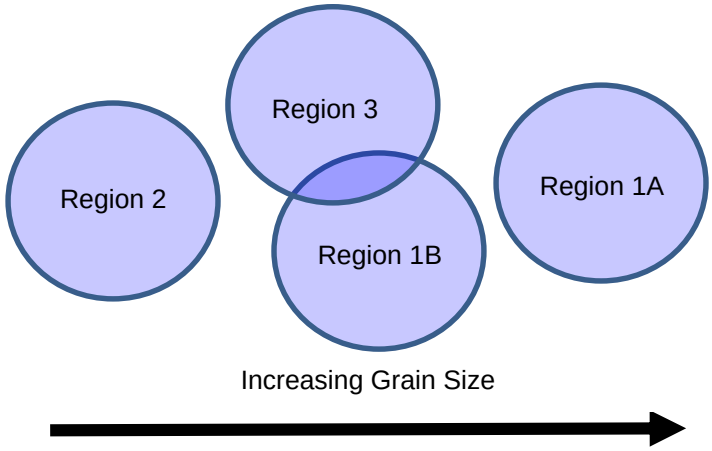

Figure 36. Ven diagram of the Tukey's comparison result for grain size measurements.

4.2.3 Grain Shape

The aspect ratio of the grains or grain shape was used to determine whether or not there were any elongated grains. Ideally, all of the grains would have an aspect ratio of 1:1 which would mean statistically similar x-axis and y-axis components. If this was the case then the heat treatment was successful in recrystallizing and growing grains. However, if the aspect ratio of the x-axis and y-axis components of the grains was not 1:1 then there was potentially some residual influence of the deformation process. A table summarizing the values obtained from the measurements can be found below in Table 8. Additionally, a boxplot summary based on region of the aspect ratio can be found in Figure 37. The data summary and boxplot showed that there was no statistical difference between regions as far as the aspect ratio of the grains was concerned. Furthermore, the ANOVA test also failed to find a difference based on orientation of the image.

Table 8. Summary of the results of grain shape.

Region	Grain Shape – Aspect Ratio	Standard Deviation	Number of Samples
1A	1.06	0.17	27
1B	1.00	0.20	27
2	1.01	0.18	27
3	1.08	0.20	27

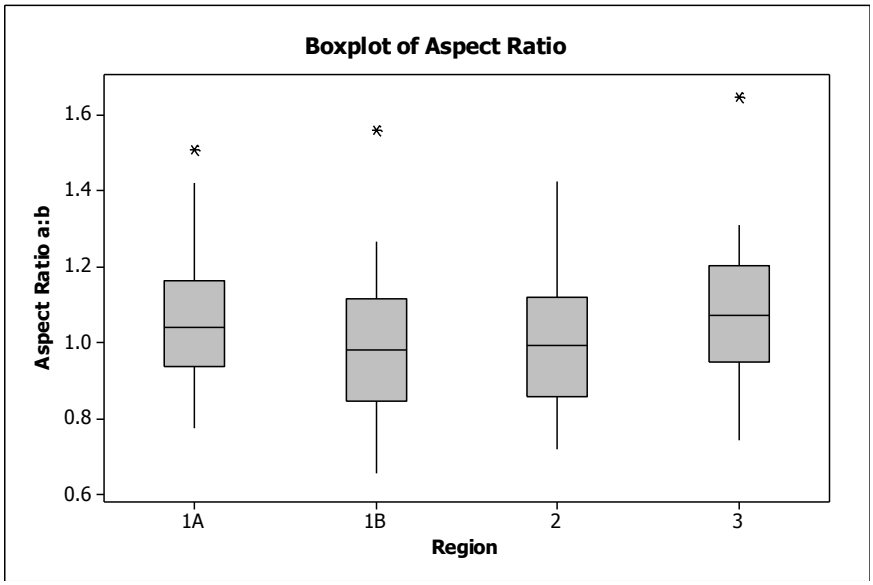

Figure 37. Boxplot summary of aspect ratio of grains.

An ANOVA and Tukey's pairwise comparison were conducted for the aspect ratio of the grains. The Minitab output of the results for the two tests can be found in Appendix F. However, the ANOVA assumptions were first checked using the plots of deleted residuals found in Appendix F. From the plots it was seen that all assumptions were met.

The ANOVA test was conducted with a 10% significance level. After conducting the ANOVA there failed to be a statistical difference between regions ($p = 0.328$) or between image orientation ($p = 0.3122$). Also, since all of the ranges of data for each region and orientation had an aspect ratio value that spanned 1 it was determined that the grains were equiaxed. This meant that there was no elongation of the grains that may have

resulted from the deformation process. An image representative of the average grain shape (Figure 38) shows that the grains were indeed equiaxed.

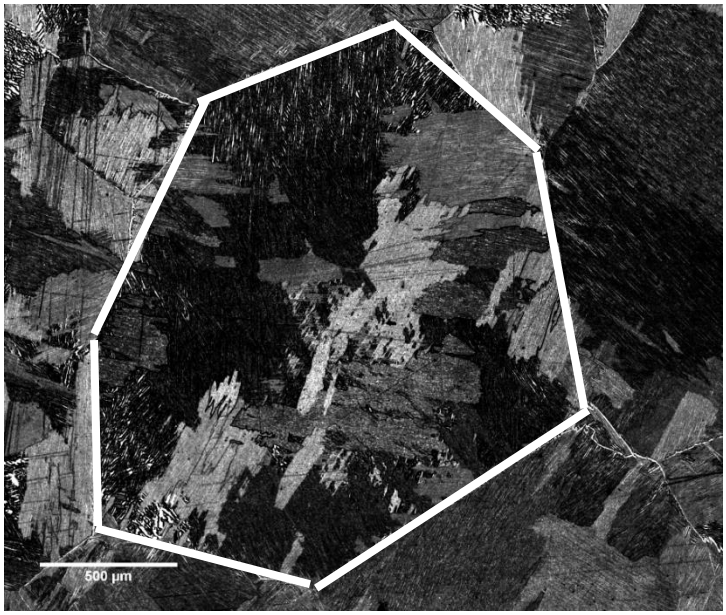

Figure 38. An example of the equiaxed grain shape from region 1A roughly outline in white.

4.2.4 β-phase

The β-phase was thought to be more ductile and softer than the α-phase. As such, analysis of the volume fraction of β-phase as well as the distribution was conducted. First, general statistics of the mean and standard deviation of volume fraction and particle count were conducted. Resulting statistics can be found in Table 9 and Table 10. It was found from the tables that both regions 2 and 3 exhibited the lowest variance for both volume fraction and particle count. However, in this case sampling had no effect as all measurements were taken from three orientations of one sample. Boxplots of the data can be found in Figure 39 and Figure 40. The distribution and variance was seen in the boxplots and showed what was found in the summary statistics. The reason for analyzing both the percent area and the particle count was that each could tell different things

about the phases. A measure of the percent area would give the total amount of β phase while the particle count could account for the spacing and density of the β phase.

Table 9. Summary of the results for the volume fraction of β-phase based on region.

Region	% Area β-phase	Standard Deviation (% area)	Number of Samples
1A	67.439	6.354	60
1B	69.04	8.69	60
2	63.792	3.373	60
3	63.601	4.070	60

Table 10. Summary of the results for the number of β particles present based on region.

Region	Particle Count of β-phase	Standard Deviation	Number of Samples
1A	16311	10198	60
1B	24455	12297	60
2	19625	4987	60
3	21976	7085	60

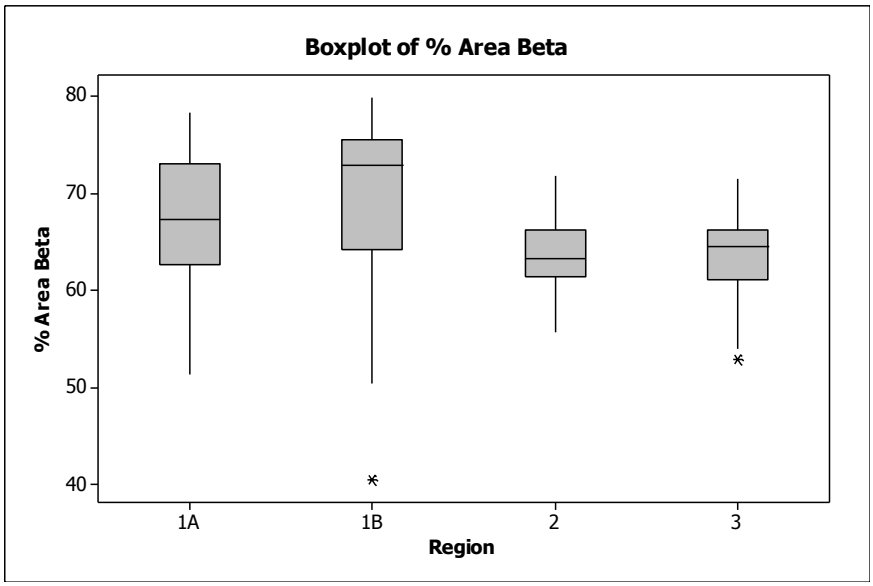

Figure 39. Boxplot of the measurements of the volume fraction of β-phase.

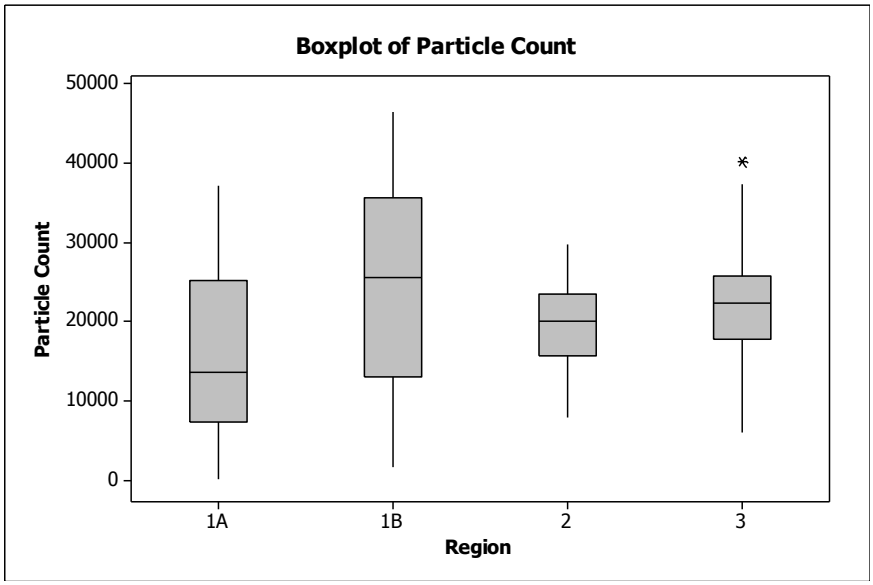

Figure 40. Boxplot of particle counts of β-phase from quantitative metallography.

Residuals were analyzed based on the plots found in Appendix G and Appendix H and all assumptions were met. An ANOVA and Tukey's Pairwise Comparison were then conducted on the volume fraction and particle count measurements. The Minitab output of the results can be found in Appendix G and Appendix H. From the output it was determined with a 10% significance level and after adjusting for the effects of orientation

that there was a statistically significant difference between at least one of the regions for the volume fraction of β-phase ($p < 0.001$). Furthermore, when testing the β-phase particle counts it was found with a 10% significance and after adjusting for orientation that at least one region was different from the others ($p < 0.001$). In order to determine the exact differences, a Tukey's Pairwise Comparison was used. A visual representation of the differences in volume fraction of β can be found in Figure 41. This shows that the sample from region 1A had a smaller volume fraction of β than that of region 3.

a)

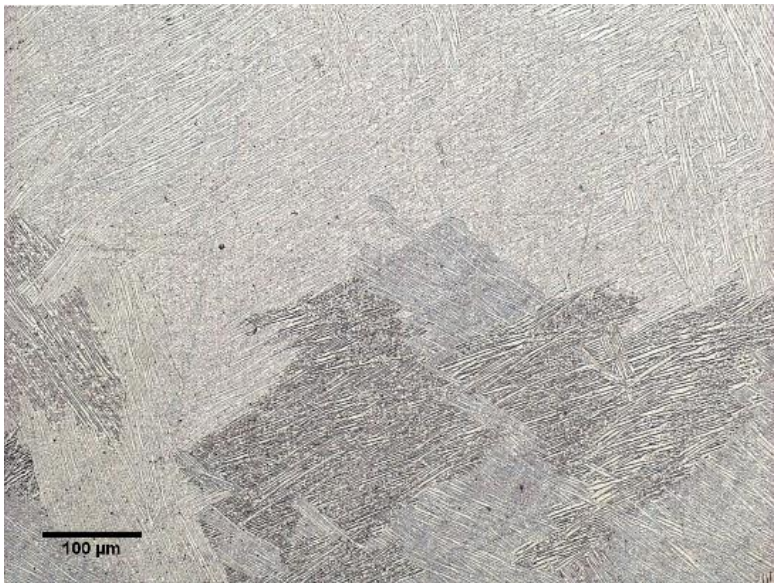

b)

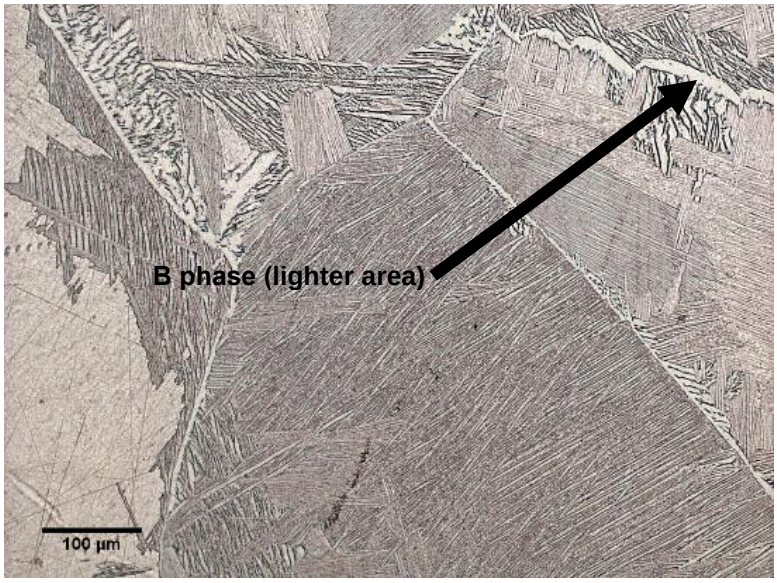

Figure 41. Example of the differences in volume fraction of β a) region 1A with lower volume fraction and b) region 3 with higher volume fraction of β.

The particle count is useful in determining spatial density of the β phase. Those regions with a higher particle count are correlated with a denser concentration of β phase. Ultimately the measurements of volume fraction were ultimately insignificant. This is due to how the lamellar structure being measured lined up with the sectioning of the sample. Since multiple measurements were taken across one sample and there were multiple

lamellar colonies with different orientations this meant that the measurements were irrelevant. The only way that appropriate measurements could have been taken, was if all the lamellar colonies were oriented in the same direction. However, the sectioning of the samples would have also had to be the in the same orientation across all samples. In this case this would be impossible since part of the strengthening mechanism that is needed is based on the lamellar colonies being oriented differently between colonies. Therefore, the creation of Ven diagrams would not be relevant since the measurements were too variable.

4.3 Fractography

Fractography helped to act as a possible correlation factor for UTS differences that existed. Images of the fracture surface can provide a qualitative look at what may have caused any differences in the UTS. Locations of the magnified images relative to the entire fracture surface can be found in overlaid on the image of the entire fracture surface located in the appendix for the corresponding sample. The fractographs for the images can be found in the appendix corresponding to the sample as outlined in Table 11.

Table 11. List of appendix corresponding to fractography samples based on region and orientation.

Sample	Region	Orientation Relative to Original Axes	Appendix Location
C	1A	x-direction	Appendix I
R	1B	x-direction	Appendix J
Y	2	x-direction	Appendix K
X	3	x-direction	Appendix L
I	1A	y-direction	Appendix M
F	1A	z-direction	Appendix N

Fractographs indicated that the samples primarily failed in a ductile failure mode. This ductility could be seen by a dimpled fracture surface (Figure 42) as well in the elongation data. For the data in this study the elongation of roughly 12% was slightly higher than that found in samples tested by Filip, Kubiak, and Sieniawski (2003). However, there were also regions of interlamellar decohesion and trans-lamellar failure. These last two failure modes are brittle failure modes. The reason that it was suspected that these brittle regions were interlamellar decohesion and trans-lamellar failure has to do with the size of the features. Characteristic features of these regions corresponded to widths similar to that of the lamellae found in the metallographic specimens. Thus it was thought that the reason for failure had to do with the alternating alpha and beta phases and differences in their structures. This was corroborated by Lee et. al. (2003) where it was found that shear bands in their torsional fracture surface lined up with lamellae size. Lee et. al. theorize this was due to one phase failing preferentially compared to the other. This then created fracture areas that then propagated in a ductile manner throughout the rest of the surface. An example of interlamellar decohesion is seen in Figure 43. Another example, this of trans-lamellar failure, is seen in Figure 44.

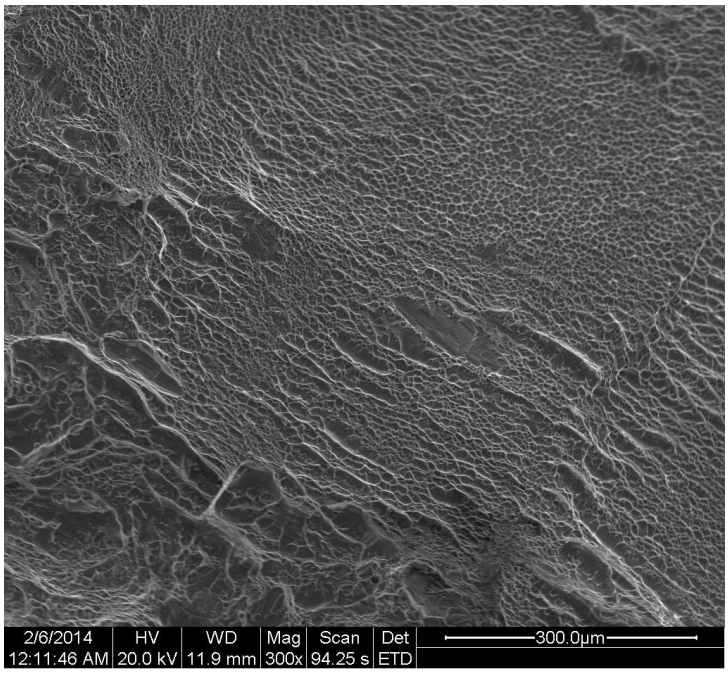

Figure 42. Example of ductile failure mode with dimpled surface taken from location 3 from the sample from region 1B.

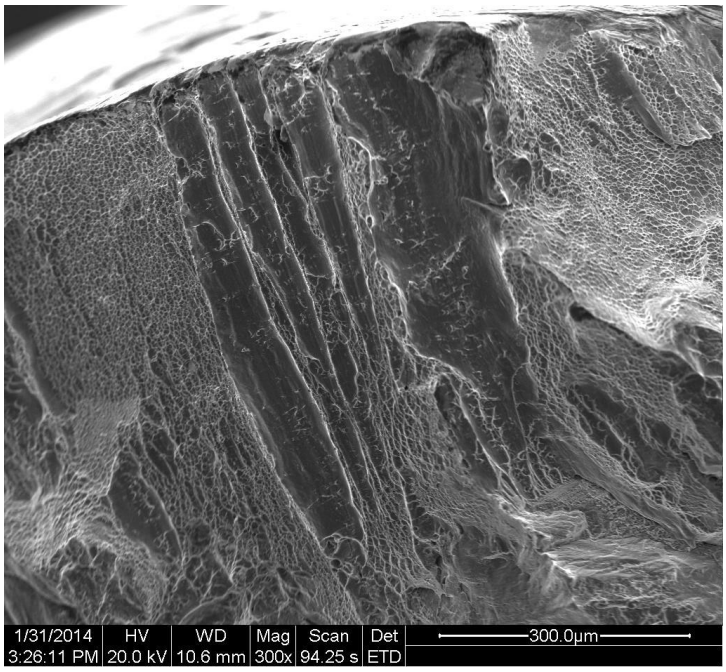

Figure 43. Example of interlamellar decohesion taken from location 1 from region 1A.

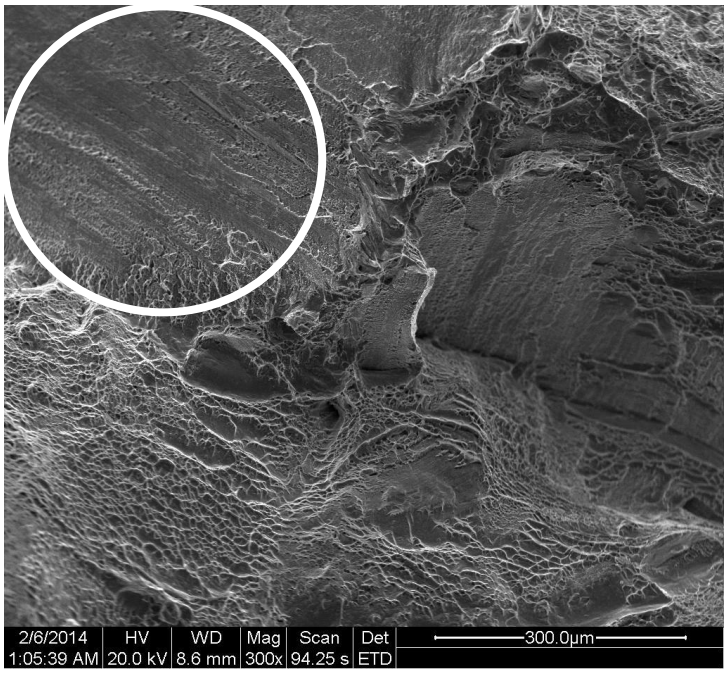

Figure 44. Example of trans-lamellar failure taken from location 2 of region 3 outlined by the white circle.

In the areas of interlamellar decohesion, it was seen that adjacent lamellae failed in different ways. Some lamellae failed in a more ductile manner while those adjacent to them failed in a brittle manner. Lamellae that failed in a more ductile manner were most likely the β lamellae as the beta phase is thought to be more ductile than the alpha phase (Kuhlman 2005). The reason for the β lamellae failing in a ductile manner as compared to the α lamellae has to do with the crystal structure of the two phases. With a BCC structure, the β lamellae would have been more ductile and had a lower UTS than the HCP α lamellae. Thus the β lamellae would fail first being pulled in tension and failing in a ductile manner until the α lamellae, the stronger phase, failed in a more brittle manner.

The areas of the fracture surface that were deemed trans-lamellar failure were done so for multiple reasons. Firstly, the areas of this failure type were too small to be trans-granular failure. However, they were approximately the same size as the Widmanstätten colonies found for that sample. Also, there was some surface relief in the form of ridges. The spacing

of these ridges corresponded to the width of lamellae found in the metallographic samples which was on the order of 10 – 20 microns. Therefore, these brittle regions were found to have failed through trans-lamellar failure of the Widmanstätten colony. Similar failures were also seen by Lee et. al. (2003) with the only difference being that samples failed in torsion. However, the fracture surfaces still resulted in similar features.

Fractographs were analyzed to determine if any differences existed between images that might correspond to the differences in UTS based on region. A summary of relevant differences can be found in Table 12. Results from the table indicated that there were different failure modes across the regions in the x- direction. Also, within region 1A there were different failure modes depending on the orientation of the tensile test sample.

Table 12. Summary of features found in fractographs.

Sample	Region	Orientation Relative to Original Axes	Characteristics
C	1A	x-direction	Areas of ductile failure and interlamellar decohesion
R	1B	x-direction	Areas of ductile failure and interlamellar decohesion
Y	2	x-direction	Areas of ductile failure, interlamellar decohesion, and trans-lamellar failure
X	3	x-direction	Areas of ductile failure and trans-lamellar failure
I	1A	y-direction	Areas ductile failure, interlamellar decohesion, and trans-lamellar failure
F	1A	z-direction	Areas of ductile failure, interlamellar decohesion, and trans-lamellar failure

4.4 Correlations Between Mechanical Properties and Microstructure

The yield strength was one of the determining factors of whether or not the part met specifications. As was seen, there were differences between regions with regards to the yield strength. Region 3 had a statistically higher yield strength than region 1A. Thus, an explanation was required. The three aspects of the microstructure typically found to influence the yield strength are: grain size, volume fraction of β, and the size of the Widmanstätten colonies.

There was a relationship between all three of the microstructural characteristics and yield strength. It was found that yield strength increased in the order: region 1A, region 1B, region 2, and region 3. Grain size increased in the order: region 2, region 3, region 1B, and region 1A while the size of the Widmanstätten colonies increased in the order: region 3, region 2, region 1B, and region 1A. This showed that regions with a smaller grain and colony size had an increased yield strength. A visual representation of this can be found in Figure 45 and Figure 46. Due to the microstructural features this was expected as the smaller grain size and colonies created more obstacles to impede the movement of dislocations. These results were similar to those found by (Lütjering 1998). Where it was discovered that a decreased colony size resulted in an increase in yield strength. Again, the mechanism for this was the creation of more obstacles to block the movement of dislocations resulting in higher yield strengths (Lütjering 1998).

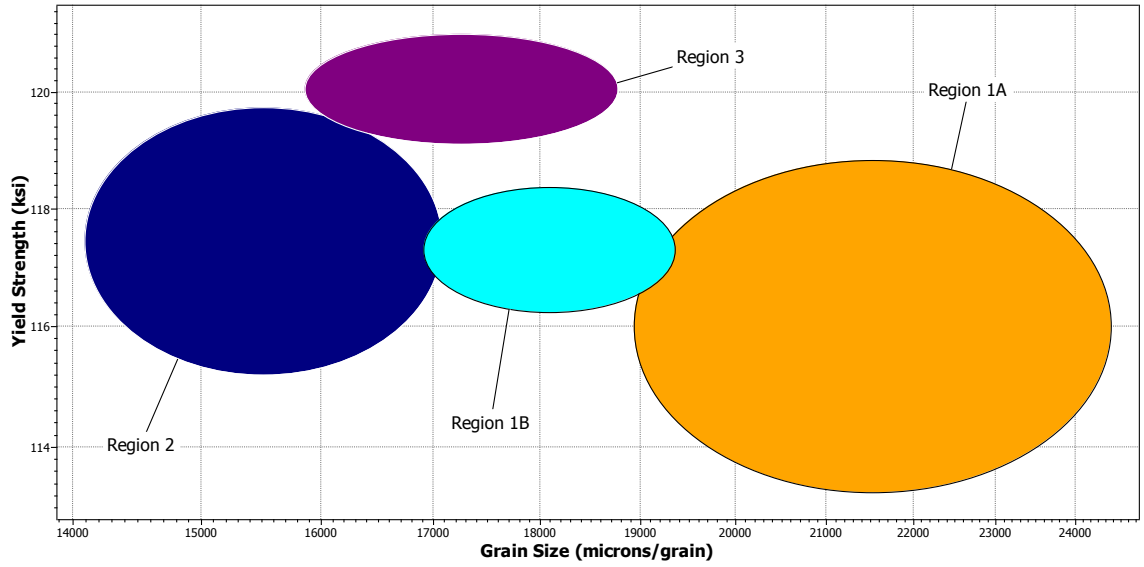

Figure 45. Shows the comparison between grain size and yield strength.

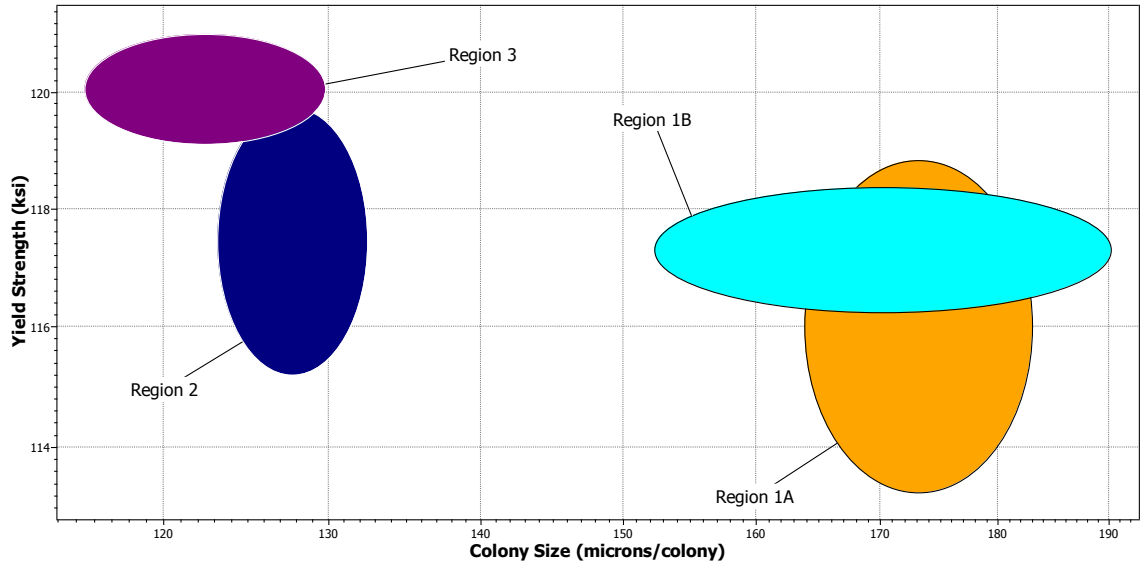

Figure 46. Shows the comparison between Widmanstätten colony size and yield strength.

Microstructural characteristics were statistically different based on the region of the part from which samples were taken. One potential cause for this could have been during the heat treatment. The sample was air cooled and thus a temperature gradient may have formed due to different sizes and thicknesses of different regions of the part. This would mean that

smaller regions like that of region 3 would have cooled quicker than larger regions which would have had an effect on microstructural characteristics. This increased cooling rate in the smaller regions would have explained the smaller grain size and in turn the smaller Widmanstätten colony size (Gil, et al. 2001). In order to quantify whether or not a temperature gradient may have had an influence a double y-axis plot was used for two different plots. The first plot was of yield strength and colony size versus the thickness (Figure 47) of the region of the part from which the sample was taken. While, the second plot shows yield strength and grain size versus the thickness (Figure 48) of the region. From these plots it is clearly seen that there is a relationship between yield strength and thickness of the part. As the thickness of the part increases the yield strength decreases. This corresponds to an opposite effect with the grain size and colony size. When the thickness is increases the colony size and grain size increases. The most likely explanation is that there is a temperature gradient created so that thicker regions cool slower and create a larger grain size and larger colony size resulting in lower yield strengths.

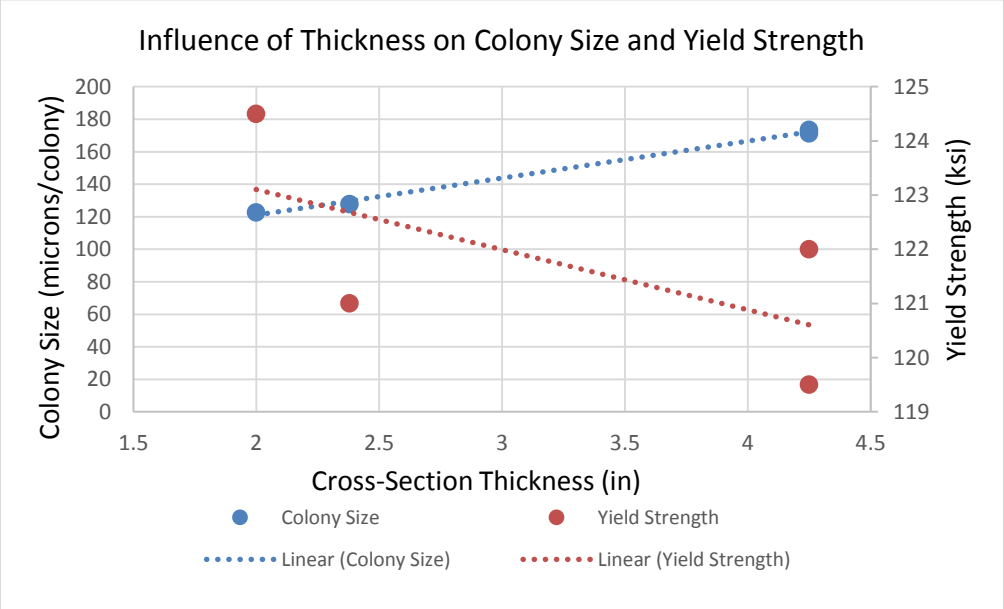

Figure 47. Plot showing the effect of thickness on the relationship between colony size and yield strength.

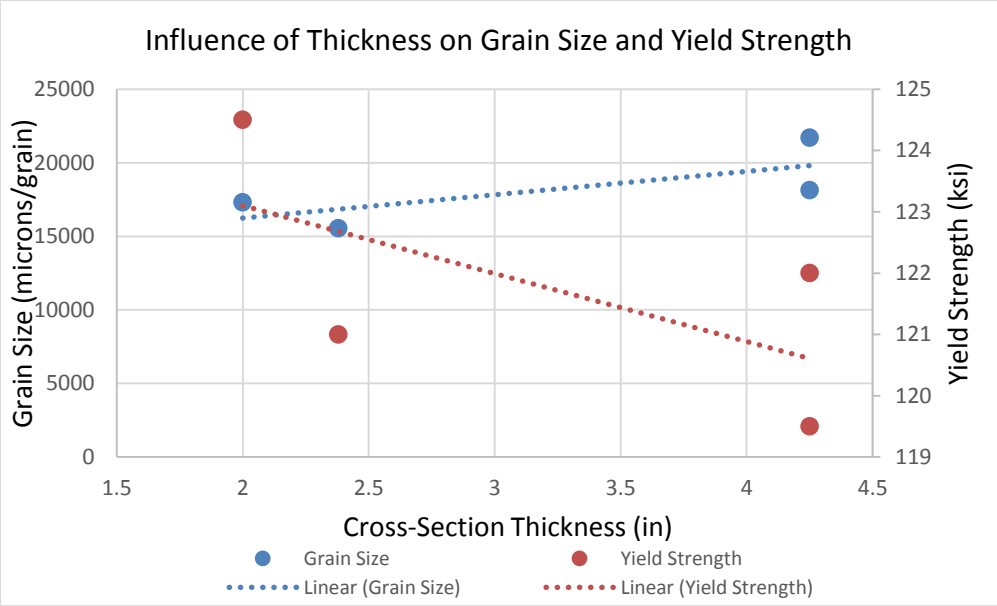

Figure 48. Plot showing the effect of thickness on the relationship between grain size and yield strength.

To correct this uneven cooling rate an alternative cooling method would be recommended. It would be beneficial to use a method that would achieve a slightly faster and more even cooling rate. However, quenching should not be used as this method produces a faster cooling rate and different microstructure than desired (Gilbert and Shannon 1991).

Another aspect of the processing history that affects the mechanical properties is the applied strain rate. Different strain rates can be associated with flow-softening. A near constant flow stress is beneficial in achieving more uniform microstructural characteristics. As such the strain rate may need to be altered to achieve more uniform flow stress to help with more uniform grain size. Achieving this would be difficult as it would mean potentially retooling or altering the shape and design of the preform. By creating a more uniform grain size it will also help create more uniform Widmanstätten colonies during the heat treatment (Ding, Guo and Wilson 2002). The reason for a potentially different strain in different regions of the part has to do with the contours of the part. Smaller cross sections have to be deformed more and could be creating a smaller and more unequal grain size throughout the part prior to heat

treatment. This would then result in the unequal grain size post heat treatment. In order to determine if this situation exists it is recommended to take samples from different regions of the part and examine the microstructure as it relates from the middle to the edge of the part in increments. By doing this it would be seen if the grain size varies between regions as well as if it varies within the regions.

Ultimate tensile strength was another mechanical property that was found to exhibit differences. It was noted earlier that regions 2 and 1A, while statistically similar to one another, were statistically lower than region 3. In order to gain an understanding of these differences fractography was conducted. From fractography it was found that the samples from regions 1A and 1B exhibited interlamellar decohesion which was not present in the sample from region 3. One reason this might have influenced the UTS was that it would have created areas for crack propagation. Similar fracture surfaces were found by Lee et. al. (2003) that showed that fracture surfaces were primarily ductile with areas of failure at the lamellar interfaces. The reason this created lower ultimate tensile strength is that the regions of brittle failure created fracture areas that then propagated in a ductile manner. With a larger number of the interlamellar decohesion and trans-lamellar failure, a lower ultimate tensile strength would be achieved.

The volume fraction of β was also looked at with regards to its effect on elongation. A higher content of β phase was found by Kim to increase the ductility of samples (Kim 2001). However, in the present study, conclusions as to differences in elongation could not be interpreted due to the conditions for the ANOVA test not being met. On the other hand, the volume fraction of β was able to be analyzed and it was found that region 1A and region 1B were statistically similar to one another, yet different from that of the grouping of similar elongation for regions 2 and 3. As such, it could be deduced that had there been data that could have been interpreted, there might have been an increase in ductility in regions 2 and 3 as compared to regions 1A and 1B. However, this was speculation and would require follow up.

5 CONCLUSIONS

After conducting tensile testing, quantitative metallography, and fractography of heat treated forged Ti-6Al-4V several conclusions were able to be drawn. The first was that there was a statistically significant difference in mean UTS and mean yield strength that was dependent on the region of the part from which samples were selected. However, there was no evidence to suspect that the orientation of the sample relative to the die parting line and axis of loading had an effect on mechanical properties. Furthermore, the data for elongation did not meet the ANOVA assumptions and thus no conclusions were able to be drawn from the data.

As far as quantitative metallography was concerned, there were also statistically significant differences based on region. Again, there was no statistically significant effect of orientation on the metallography data. Measurements of Widmanstätten colony size, grain size, and volume fraction of β all showed a statistically significant regional dependence. The Widmanstätten colony size ranged from about 120-175 microns/colony with the grain diameter ranging from 1500-2200 microns/grain. The volume fraction was ultimately deemed irrelevant due to inaccuracy of measurements caused by an effect of lamellar orientation when sectioning samples. Furthermore, the grain shape showed equiaxed grains across all regions.

Fractography was also conducted and showed a qualitative representation of the fracture surfaces. Magnified images were taken of regions showing characteristics of the overall fracture surface. These images showed qualitative differences based on region. The most notable difference was that regions 1A and 1B exhibited areas of interlamellar decohesion which was not present in region 3. Also, all samples had areas with dimpled surfaces indicating that there was significant ductile failure. These observations along with data from quantitative metallography were then correlated to the differences in mechanical properties. A decrease in grain size and Widmanstätten colony size was associated with a higher yield strength. This was concurrent with research and was expected as these smaller grain and colony sizes would have more easily impeded the movement of dislocations. The UTS was also found to be associated with

differences in the fractographs. Those areas that exhibited a lower UTS were characterized by interlamellar decohesion. This was again concurrent with research that found that this failure mode created an increase in voids and more preferential crack propagation.

It is recommended that several changes be made to the process. The first recommendation is to use an alternative cooling method by circulating the air more evenly around the part. This would hopefully achieve a quicker cooling rate to create more refined grains and smaller colonies so as to strengthen the part and reduce the variability of microstructural features due to the temperature gradient. This would help to maintain uniform grain size and Widmanstätten colony size throughout the part. Also, an investigation into the flow stress during deformation is recommended to confirm that the workpiece is behaving as modeled during deformation. This would involve taking microstructural samples before the heat treatment from different regions of the part through the thickness to determine if differences exist within regions and/or between regions prior to heat treatment. If these differences occurred it could mean the part is not being held at temperature as long as needed for the appropriate microstructure to occur.

REFERENCES

ASTM International. n.d.a. "Standard Test Methods for Determining Average Grain Size." *ASTM* E112 (12): 1-37.

ASTM International. n.d.b. "Standard Test Methods for Tension Testing of Metallic Materials." *ASTM International* E8M: 1-27.

Ding, R., Z.X. Guo, and A. Wilson. 2002. "Microstructural evolution of a Ti-6Al-4V alloy during thermomechanical processing." *Materials Science and Engineering* 327 (A): 233-245.

Filip, R., K. Kubiak, and J. Sieniawski. 2003. "The effect of microstructure on the mechanical properties of two-phase titanium alloys." *Journal of Materials Processing and Technology* 133: 84-89.

Gil, F.J., M.P. Ginebra, J.M. Manero, and J.A. Planell. 2001. "Formation of α-Widmanstätten structure: effects of grain size and cooling rate on the Widmanstätten morphologies and on mechanical properties in Ti6Al4V alloy." *Journal of Alloys and Compounds* (329): 142-152.

Gilbert, R, and C.R. Shannon. 1991. "Heat Treating of Titanium and Titanium Alloys." *ASM Handbook* (ASM International) 4 (Heat Treating): 913-923.

Kim, T. 2001. "Volume fraction aspects of the heterogeneous microstructures in superplastic Ti-6Al-4V." *Journal of Materials Science Letters* 20: 1443-1445.

Kuhlman, G W. 2005. "Forging of Titanium Alloys." *ASM Handbook* 14 (A): 331-353.

Lee, Dong-Geun, Sunghak Lee, Chong Soo Lee, and Sunmoo Hur. 2003. "Effects of Microstructural Factors on Quasi-Static and Dynamic Deformation Behaviors of Ti-6Al-4V Alloys with Widmanstätten Structures." *Metallurgical and Materials Transactions* 34A: 2541-2548.

Lütjering, G. 1998. "Influence of processing on microstructure and mechanical properties of (α+β) titanium alloys." *Materials Science & Engineering* (A243): 32-45.

Mironov, S, M Murzinova, S Zherebtsov, G.A. Salischev, and S.L. Semiatin. 2009. "Microstructure evolution during warm working of Ti–6Al–4V with a colony-α microstructure." *Acta Materiala* (47): 2470-2481.

Poondla, N., T.S. Srivatsan, A. Patnaik, and M. Petraroli. 2009. "A study o fthe microstructure and hardness of two titanium alloys: Commercially pure and Ti-6Al-4V." *Journal of Alloys and Compounds* 486: 162-167.

Sieniawski, J., W. Ziaja, K. Kubiak, and M. Motyka. 2013. "Microstructure and Mechanical Properties of High Strength Two-Phase Titanium Alloys." In *Titanium Alloys - Advances in Properties Control*. InTech. doi:10.5772/56197.

Stefanescu, D.M., and R. Ruxanda. 2004. "Solidification Structures of Titanium Alloys." *ASM Handbook* 9 (Metallography and Microstructures): 116-126.

APPENDICES

Appendix A. Minitab output of the ANOVA and Tukey's results for Yield Strength.

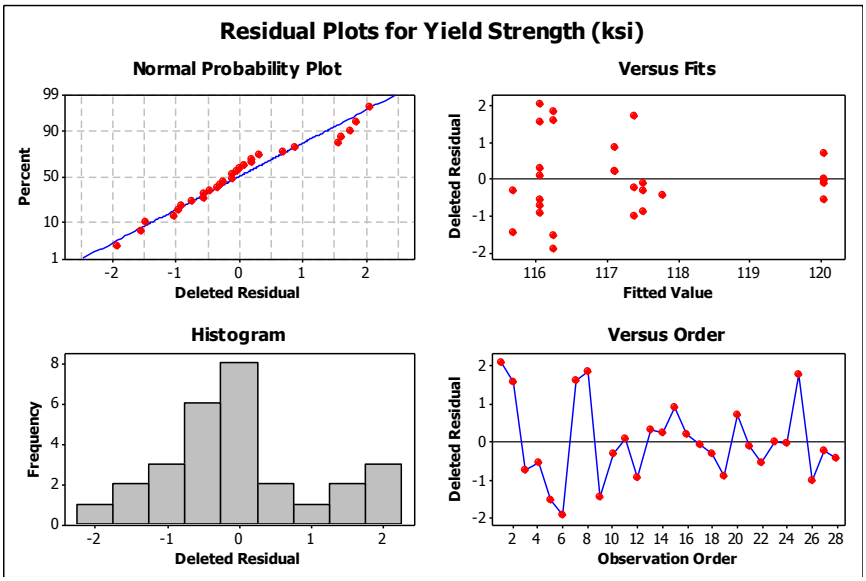

Analysis of Variance for Yield Strength (ksi), using Adjusted SS for Tests

Source	DF	Seq SS	Adj SS	Adj MS	F	P
Region	3	58.451	41.600	13.867	2.62	0.076
Orientation	2	0.805	0.805	0.402	0.08	0.927
Error	22	116.221	116.221	5.283		
Total	27	175.477				

S = 2.29843 R-Sq = 33.77% R-Sq(adj) = 18.72%

Expected Mean Squares, using Adjusted SS

	Source	Expected Mean Square for Each Term
1	Region	(3) + Q[1]
2	Orientation	(3) + Q[2]
3	Error	(3)

Error Terms for Tests, using Adjusted SS

	Source	Error DF	Error MS	Synthesis of Error MS
1	Region	22.00	5.283	(3)
2	Orientation	22.00	5.283	(3)

Variance Components, using Adjusted SS

Source	Estimated Value
Error	5.28

Grouping Information Using Tukey Method and 90.0% Confidence for Yield Strength (ksi)

Region	N	Mean	Grouping
3	5	120.4	A
2	4	117.7	A B
1B	6	117.4	A B
1A	13	116.0	B

Means that do not share a letter are significantly different.

Tukey 90.0% Simultaneous Confidence Intervals
Response Variable Yield Strength (ksi)
All Pairwise Comparisons among Levels of Region
Region = 1A subtracted from:

Region	Lower	Center	Upper	+---------+---------+---------+------
1B	-1.602	1.450	4.502	(--------*--------)
2	-1.967	1.718	5.402	(----------*---------)
3	0.570	4.404	8.237	(----------*----------)
				+---------+---------+---------+------
				-3.5 0.0 3.5 7.0

Region = 1B subtracted from:

Region	Lower	Center	Upper	+---------+---------+---------+------
2	-3.412	0.2674	3.947	(----------*---------)
3	-0.723	2.9535	6.630	(---------*----------)
				+---------+---------+---------+------
				-3.5 0.0 3.5 7.0

Region = 2 subtracted from:

Region	Lower	Center	Upper	+---------+---------+---------+------
3	-1.132	2.686	6.504	(----------*----------)
				+---------+---------+---------+------
				-3.5 0.0 3.5 7.0

Grouping Information Using Tukey Method and 90.0% Confidence for Yield Strength (ksi)

Orientation	N	Mean	Grouping
Z	4	118.1	A
X	11	117.9	A
Y	13	117.6	A

Means that do not share a letter are significantly different.

Tukey 90.0% Simultaneous Confidence Intervals
Response Variable Yield Strength (ksi)
All Pairwise Comparisons among Levels of Orientation
Orientation = X subtracted from:

```
Orientation   Lower   Center  Upper  -----+---------+---------+---------+-
Y           -2.946  -0.3964  2.153  (------------*-----------)
Z           -2.856   0.1853  3.227   (--------------*--------------)
                          -----+---------+---------+---------+-
                            -2.0       0.0       2.0       4.0
```

Orientation = Y subtracted from:

```
Orientation   Lower  Center  Upper  -----+---------+---------+---------+-
Z           -3.005  0.5816  4.168  (-----------------*-----------------)
                          -----+---------+---------+---------+-
                            -2.0       0.0       2.0       4.0
```

Appendix B. Minitab output of the ANOVA and Tukey's results for UTS.

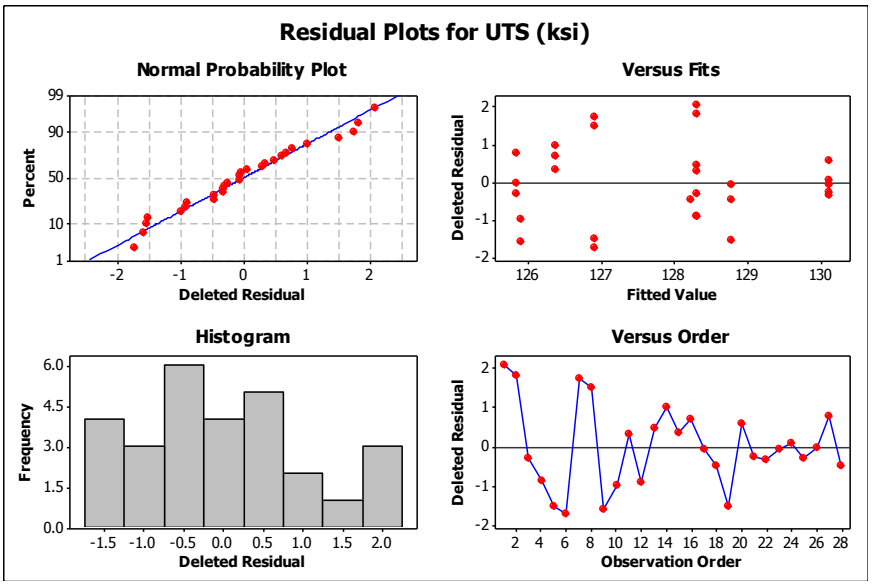

Analysis of Variance for UTS (ksi), using Adjusted SS for Tests

Source	DF	Seq SS	Adj SS	Adj MS	F	P
Region	3	36.101	52.306	17.435	3.11	0.047
Orientation	2	24.164	24.164	12.082	2.15	0.140
Error	22	123.495	123.495	5.613		
Total	27	183.760				

S = 2.36926 R-Sq = 32.80% R-Sq(adj) = 17.52%

Expected Mean Squares, using Adjusted SS

	Source	Expected Mean Square for Each Term
1	Region	(3) + Q[1]
2	Orientation	(3) + Q[2]
3	Error	(3)

Error Terms for Tests, using Adjusted SS

	Source	Error DF	Error MS	Synthesis of Error MS
1	Region	22.00	5.613	(3)
2	Orientation	22.00	5.613	(3)

Variance Components, using Adjusted SS

Source	Estimated Value
Error	5.613

Grouping Information Using Tukey Method and 90.0% Confidence for UTS (ksi)

Region N Mean Grouping
3 5 131.3 A
1B 6 127.5 A B
1A 13 127.0 B
2 4 127.0 B

Means that do not share a letter are significantly different.

Tukey 90.0% Simultaneous Confidence Intervals
Response Variable UTS (ksi)
All Pairwise Comparisons among Levels of Region
Region = 1A subtracted from:

```
Region   Lower    Center  Upper   --+---------+---------+---------+----
1B      -2.680   0.46678  3.613       (--------*--------)
2       -3.873  -0.07529  3.723    (----------*----------)
3        0.279   4.23031  8.182              (----------*----------)
                          --+---------+---------+---------+----
                         -3.5       0.0       3.5       7.0
```

Region = 1B subtracted from:

```
Region   Lower   Center  Upper   --+---------+---------+---------+----
2       -4.335  -0.5421  3.251   (---------*----------)
3       -0.026   3.7635  7.553             (----------*----------)
                         --+---------+---------+---------+----
                        -3.5       0.0       3.5       7.0
```

Region = 2 subtracted from:

```
Region   Lower  Center  Upper   --+---------+---------+---------+----
3       0.3697   4.306  8.242              (----------*-----------)
                        --+---------+---------+---------+----
                       -3.5       0.0       3.5       7.0
```

Grouping Information Using Tukey Method and 90.0% Confidence for UTS (ksi)

Orientation N Mean Grouping
X 11 129.5 A
Z 4 128.1 A
Y 13 127.1 A

Means that do not share a letter are significantly different.

Tukey 90.0% Simultaneous Confidence Intervals
Response Variable UTS (ksi)
All Pairwise Comparisons among Levels of Orientation
Orientation = X subtracted from:

```
Orientation   Lower  Center   Upper  -------+---------+---------+---------
Y           -5.036  -2.408  0.2195  (--------*--------)
Z           -4.540  -1.404  1.7314    (---------*----------)
                          -------+---------+---------+---------
                             -3.0       0.0       3.0
```

Orientation = Y subtracted from:

```
Orientation   Lower  Center  Upper  -------+---------+---------+---------
Z           -2.693   1.004  4.701          (-----------*------------)
                          -------+---------+---------+---------
                             -3.0       0.0       3.0
```

Appendix C. Minitab output of the ANOVA and Tukey's results for Elongation.

Analysis of Variance for Elongation (%), using Adjusted SS for Tests

Source	DF	Seq SS	Adj SS	Adj MS	F	P
Region	3	7.0450	7.6775	2.5592	2.88	0.059
Orientation	2	3.4918	3.4918	1.7459	1.97	0.164
Error	22	19.5203	19.5203	0.8873		
Total	27	30.0571				

S = 0.941959 R-Sq = 35.06% R-Sq(adj) = 20.30%

Expected Mean Squares, using Adjusted SS

	Source	Expected Mean Square for Each Term
1	Region	(3) + Q[1]
2	Orientation	(3) + Q[2]
3	Error	(3)

Error Terms for Tests, using Adjusted SS

	Source	Error DF	Error MS	Synthesis of Error MS
1	Region	22.00	0.8873	(3)
2	Orientation	22.00	0.8873	(3)

Variance Components, using Adjusted SS

Source	Estimated Value
Error	0.8873

Least Squares Means for Elongation (%)

Region	Mean	SE Mean
1A	12.70	0.2765
1B	12.78	0.4307
2	11.64	0.5337
3	13.51	0.5431
Orientation		
X	13.20	0.3598
Y	12.43	0.2727
Z	12.36	0.5899

Grouping Information Using Tukey Method and 90.0% Confidence

Region	N	Mean	Grouping
3	5	13.5	A
1B	6	12.8	A B
1A	13	12.7	A B
2	4	11.6	B

Means that do not share a letter are significantly different.

Tukey 90.0% Simultaneous Confidence Intervals
Response Variable Elongation (%)
All Pairwise Comparisons among Levels of Region
Region = 1A subtracted from:

```
Region   Lower  Center   Upper  ---+---------+---------+---------+---
1B      -1.170   0.081  1.3317        (-----*------)
2       -2.570  -1.060  0.4501  (-------*------)
3       -0.758   0.813  2.3838          (-------*-------)
                        ---+---------+---------+---------+---
                        -2.0       0.0       2.0       4.0
```

Region = 1B subtracted from:

```
Region   Lower  Center   Upper  ---+---------+---------+---------+---
2       -2.649  -1.141  0.3672  (------*-------)
3       -0.775   0.732  2.2387          (-------*------)
                        ---+---------+---------+---------+---
                        -2.0       0.0       2.0       4.0
```

Region = 2 subtracted from:

```
Region   Lower  Center  Upper  ---+---------+---------+---------+---
3       0.3079   1.873  3.438              (------*-------)
                        ---+---------+---------+---------+---
                        -2.0       0.0       2.0       4.0
```

Grouping Information Using Tukey Method and 90.0% Confidence

Orientation	N	Mean	Grouping
X	11	13.2	A
Y	13	12.4	A
Z	4	12.4	A

Means that do not share a letter are significantly different.

Tukey 90.0% Simultaneous Confidence Intervals
Response Variable Elongation (%)
All Pairwise Comparisons among Levels of Orientation
Orientation = X subtracted from:

```
Orientation   Lower   Center   Upper    -+---------+---------+---------+-----
Y           -1.816  -0.7708  0.2740       (---------*----------)
Z           -2.085  -0.8380  0.4086    (------------*-----------)
                              -+---------+---------+---------+-----
                            -2.0      -1.0       0.0       1.0
```

Orientation = Y subtracted from:

```
Orientation   Lower    Center  Upper    -+---------+---------+---------+-----
Z           -1.537  -0.06715  1.403         (-------------*--------------)
                              -+---------+---------+---------+-----
                            -2.0      -1.0       0.0       1.0
```

Appendix D. Minitab output of the ANOVA and Tukey's results for the size of the Widmanstätten colonies.

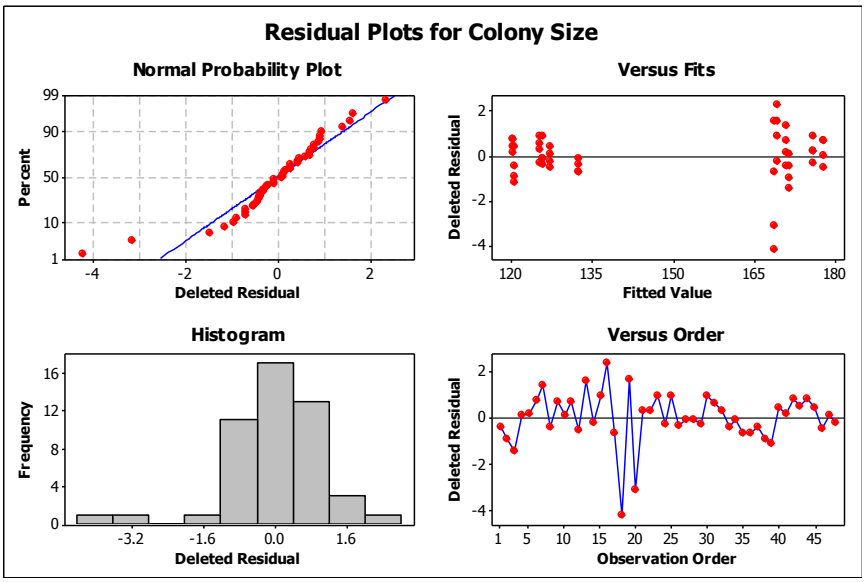

Analysis of Variance for Size, using Adjusted SS for Tests

Source	DF	Seq SS	Adj SS	Adj MS	F	P
Region	3	26808.6	26808.6	8936.2	71.72	0.000
Orientation	2	495.4	495.4	247.7	1.99	0.150
Error	42	5233.0	5233.0	124.6		
Total	47	32537.0				

S = 11.1622 R-Sq = 83.92% R-Sq(adj) = 82.00%

Unusual Observations for Size

Obs	Size	Fit	SE Fit	Residual	St Resid
16	192.308	169.168	3.946	23.139	2.22 R
18	131.579	168.699	3.946	-37.120	-3.56 R
20	138.889	168.699	3.946	-29.810	-2.86 R

R denotes an observation with a large standardized residual.

Expected Mean Squares, using Adjusted SS

	Source	Expected Mean Square for Each Term
1	Region	(3) + Q[1]
2	Orientation	(3) + Q[2]
3	Error	(3)

Error Terms for Tests, using Adjusted SS

	Source	Error DF	Error MS	Synthesis of Error MS
1	Region	42.00	124.6	(3)
2	Orientation	42.00	124.6	(3)

Variance Components, using Adjusted SS

Source	Estimated Value
Error	124.6

Least Squares Means for Size

Region	Mean	SE Mean
1A	173.4	3.222
1B	171.2	3.222
2	127.8	3.222
3	122.6	3.222
Orientation		
A	146.7	2.791
B	146.3	2.791
C	153.3	2.791

Grouping Information Using Tukey Method and 90.0% Confidence

Region	N	Mean	Grouping
1A	12	173.4	A
1B	12	171.2	A
2	12	127.8	B
3	12	122.6	B

Means that do not share a letter are significantly different.

Tukey 90.0% Simultaneous Confidence Intervals
Response Variable Size
All Pairwise Comparisons among Levels of Region
Region = 1A subtracted from:

Region	Lower	Center	Upper	-+---------+---------+---------+-----
1B	-12.96	-2.20	8.56	(----*----)
2	-56.35	-45.59	-34.83	(----*-----)
3	-61.56	-50.80	-40.04	(-----*----)
				-+---------+---------+---------+-----
				-60 -40 -20 0

Region = 1B subtracted from:

```
Region   Lower  Center   Upper  -+---------+---------+---------+-----
2       -54.15  -43.39  -32.63       (----*-----)
3       -59.37  -48.60  -37.84    (-----*----)
                        -+---------+---------+---------+-----
                       -60       -40       -20         0
```

Region = 2 subtracted from:

```
Region   Lower  Center  Upper  -+---------+---------+---------+-----
3       -15.98  -5.213  5.549                    (----*-----)
                        -+---------+---------+---------+-----
                       -60       -40       -20         0
```

Grouping Information Using Tukey Method and 90.0% Confidence

Orientation	N	Mean	Grouping
C	16	153.3	A
A	16	146.7	A
B	16	146.3	A

Means that do not share a letter are significantly different.

Tukey 90.0% Simultaneous Confidence Intervals
Response Variable Size
All Pairwise Comparisons among Levels of Orientation
Orientation = A subtracted from:

```
Orientation   Lower   Center   Upper  ---+---------+---------+---------+---
B           -8.785  -0.4695   7.846  (-----------*-----------)
C           -1.748   6.5683  14.884            (----------*-----------)
                          ---+---------+---------+---------+---
                           -7.0       0.0       7.0      14.0
```

Orientation = B subtracted from:

```
Orientation   Lower  Center  Upper  ---+---------+---------+---------+---
C           -1.278   7.038  15.35            (-----------*-----------)
                          ---+---------+---------+---------+---
                           -7.0       0.0       7.0      14.0
```

Appendix E. Minitab output of the ANOVA and Tukey's results for grain size.

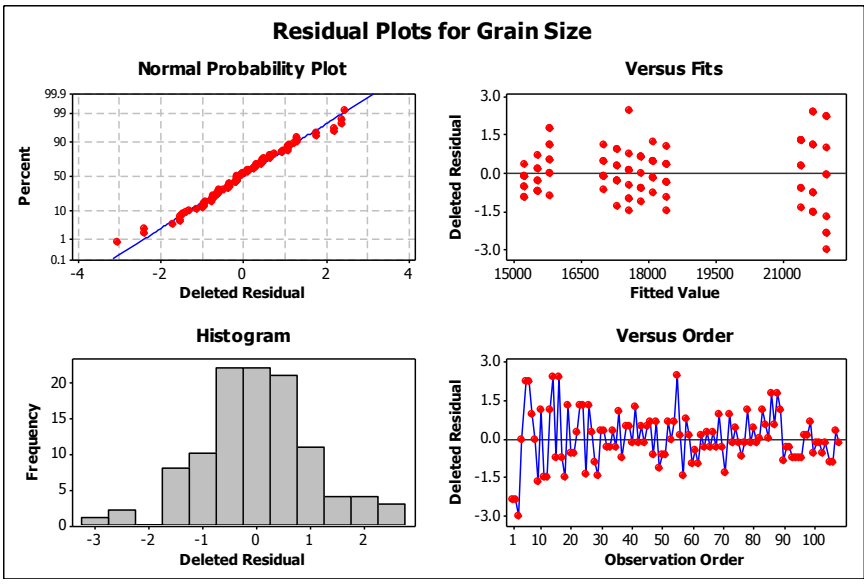

Analysis of Variance for Size, using Adjusted SS for Tests

Source	DF	Seq SS	Adj SS	Adj MS	F	P
Region	3	542988861	542988861	180996287	53.37	0.000
Orientation	2	5999315	5999315	2999657	0.88	0.416
Error	102	345925657	345925657	3391428		
Total	107	894913833				

S = 1841.58 R-Sq = 61.35% R-Sq(adj) = 59.45%

Unusual Observations for Size

Obs	Size	Fit	SE Fit	Residual	St Resid
1	17797.1	21987.9	434.1	-4190.7	-2.34 R
2	17797.1	21987.9	434.1	-4190.7	-2.34 R
3	16750.2	21987.9	434.1	-5237.6	-2.93 R
5	25886.7	21987.9	434.1	3898.9	2.18 R
6	25886.7	21987.9	434.1	3898.9	2.18 R
14	25886.7	21700.5	434.1	4186.2	2.34 R
16	25886.7	21700.5	434.1	4186.2	2.34 R
55	21904.1	17597.6	434.1	4306.5	2.41 R

R denotes an observation with a large standardized residual.

Expected Mean Squares, using Adjusted SS

	Source	Expected Mean Square for Each Term
1	Region	(3) + Q[1]
2	Orientation	(3) + Q[2]
3	Error	(3)

Error Terms for Tests, using Adjusted SS

	Source	Error DF	Error MS	Synthesis of Error MS
1	Region	102.00	3391428	(3)
2	Orientation	102.00	3391428	(3)

Variance Components, using Adjusted SS

Source	Estimated Value
Error	3391428

Least Squares Means for Size

Region	Mean	SE Mean
1A	21700	354.4
1B	18128	354.4
2	15541	354.4
3	17309	354.4
Orientation		
A	18458	306.9
B	18171	306.9
C	17881	306.9

Grouping Information Using Tukey Method and 90.0% Confidence

Region	N	Mean	Grouping
1A	27	21699.7	A
1B	27	18128.5	B
3	27	17309.4	B
2	27	15541.3	C

Means that do not share a letter are significantly different.

Tukey 90.0% Simultaneous Confidence Intervals
Response Variable Size
All Pairwise Comparisons among Levels of Region
Region = 1A subtracted from:

Region	Lower	Center	Upper	----+---------+---------+---------+--
1B	-4734	-3571	-2409	(---*---)
2	-7321	-6158	-4996	(--*---)
3	-5553	-4390	-3228	(---*---)
				----+---------+---------+---------+--
				-6000 -3000 0 3000

Region = 1B subtracted from:

Region	Lower	Center	Upper	----+---------+---------+---------+--
2	-3750	-2587	-1425	(--*---)
3	-1982	-819	343	(---*---)
				----+---------+---------+---------+--
				-6000 -3000 0 3000

Region = 2 subtracted from:

```
Region  Lower  Center  Upper  ----+---------+---------+---------+--
3       605.6   1768   2931                      (---*---)
                      ----+---------+---------+---------+--
                      -6000     -3000         0      3000
```

Grouping Information Using Tukey Method and 90.0% Confidence

Orientation	N	Mean	Grouping
A	36	18457.9	A
B	36	18170.6	A
C	36	17880.6	A

Means that do not share a letter are significantly different.

Tukey 90.0% Simultaneous Confidence Intervals
Response Variable Size
All Pairwise Comparisons among Levels of Orientation
Orientation = A subtracted from:

```
Orientation  Lower  Center  Upper  -----+---------+---------+---------+-
B           -1190  -287.3  615.0       (--------------*--------------)
C           -1480  -577.3  325.1  (--------------*--------------)
                        -----+---------+---------+---------+-
                        -1200      -600         0       600
```

Orientation = B subtracted from:

```
Orientation  Lower  Center  Upper  -----+---------+---------+---------+-
C           -1192  -290.0  612.4       (--------------*--------------)
                        -----+---------+---------+---------+-
                        -1200      -600         0       600
```

Appendix F. Minitab output of the ANOVA and Tukey's results for grain aspect ratio.

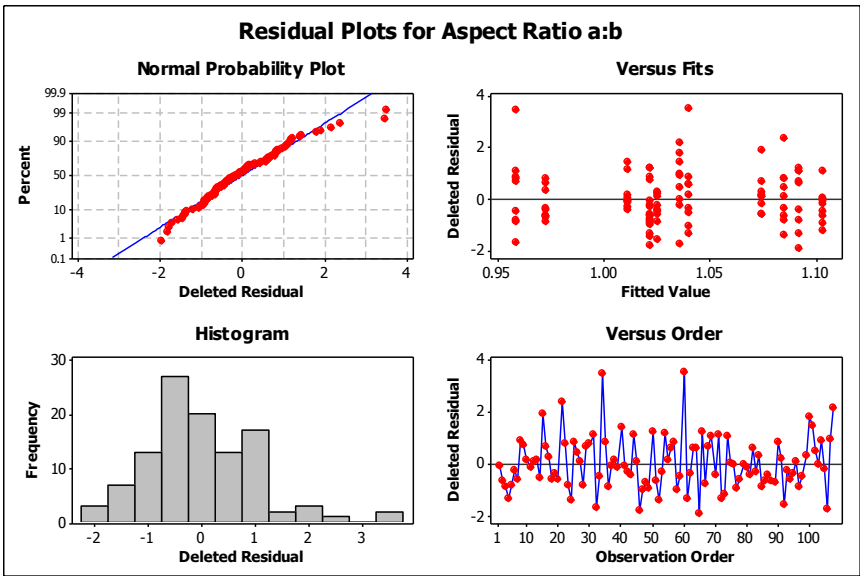

Analysis of Variance for Aspect Ratio a:b, using Adjusted SS for Tests

Source	DF	Seq SS	Adj SS	Adj MS	F	P
Region	3	0.12159	0.12159	0.04053	1.16	0.328
Orientation	2	0.08225	0.08225	0.04112	1.18	0.312
Error	102	3.55658	3.55658	0.03487		
Total	107	3.76041				

S = 0.186731 R-Sq = 5.42% R-Sq(adj) = 0.78%

Unusual Observations for Aspect Ratio a:b

Obs	Aspect Ratio a:b	Fit	SE Fit	Residual	St Resid
21	1.50888	1.08482	0.04401	0.42405	2.34 R
34	1.56057	0.95866	0.04401	0.60191	3.32 R
60	1.64623	1.03979	0.04401	0.60643	3.34 R
108	1.42242	1.03569	0.04401	0.38673	2.13 R

R denotes an observation with a large standardized residual.

Expected Mean Squares, using Adjusted SS

	Source	Expected Mean Square for Each Term
1	Region	(3) + Q[1]
2	Orientation	(3) + Q[2]
3	Error	(3)

Error Terms for Tests, using Adjusted SS

	Source	Error DF	Synthesis Error MS	of Error MS
1	Region	102.00	0.03487	(3)
2	Orientation	102.00	0.03487	(3)

Variance Components, using Adjusted SS

Source	Estimated Value
Error	0.03487

Least Squares Means for Aspect Ratio a:b

Region	Mean	SE Mean
1A	1.0602	0.03594
1B	0.9972	0.03594
2	1.0110	0.03594
3	1.0783	0.03594
Orientation		
A	0.9981	0.03112
B	1.0505	0.03112
C	1.0613	0.03112

Grouping Information Using Tukey Method and 90.0% Confidence

Region	N	Mean	Grouping
3	27	1.1	A
1A	27	1.1	A
2	27	1.0	A
1B	27	1.0	A

Means that do not share a letter are significantly different.

Tukey 90.0% Simultaneous Confidence Intervals
Response Variable Aspect Ratio a:b
All Pairwise Comparisons among Levels of Region
Region = 1A subtracted from:

Region	Lower	Center	Upper	------+---------+---------+---------+-
1B	-0.1809	-0.06298	0.05489	(---------*---------)
2	-0.1670	-0.04914	0.06874	(---------*---------)
3	-0.0997	0.01815	0.13602	(---------*--------)
				-----+---------+---------+---------+-
				-0.12 0.00 0.12 0.24

Region = 1B subtracted from:

Region	Lower	Center	Upper	------+---------+---------+---------+-
2	-0.1040	0.01385	0.1317	(---------*---------)
3	-0.0367	0.08114	0.1990	(---------*---------)
				-----+---------+---------+---------+-
				-0.12 0.00 0.12 0.24

Region = 2 subtracted from:

```
Region    Lower   Center   Upper  -----+---------+---------+---------+-
3      -0.05058  0.06729  0.1852            (---------*--------)
                          -----+---------+---------+---------+-
                           -0.12      0.00      0.12      0.24
```

Grouping Information Using Tukey Method and 90.0% Confidence

Orientation	N	Mean	Grouping
C	36	1.1	A
B	36	1.1	A
A	36	1.0	A

Means that do not share a letter are significantly different.

Tukey 90.0% Simultaneous Confidence Intervals
Response Variable Aspect Ratio a:b
All Pairwise Comparisons among Levels of Orientation
Orientation = A subtracted from:

```
Orientation    Lower   Center   Upper   --+---------+---------+---------+----
B           -0.03910  0.05239  0.1439         (------------*-------------)
C           -0.02831  0.06318  0.1547           (------------*------------)
                              --+---------+---------+---------+----
                             -0.070     0.000     0.070     0.140
```

Orientation = B subtracted from:

```
Orientation    Lower   Center   Upper   --+---------+---------+---------+----
C           -0.08071  0.01079  0.1023   (-------------*------------)
                              --+---------+---------+---------+----
                             -0.070     0.000     0.070     0.140
```

Appendix G. Minitab output of the ANOVA and Tukey's results for volume fraction of β.

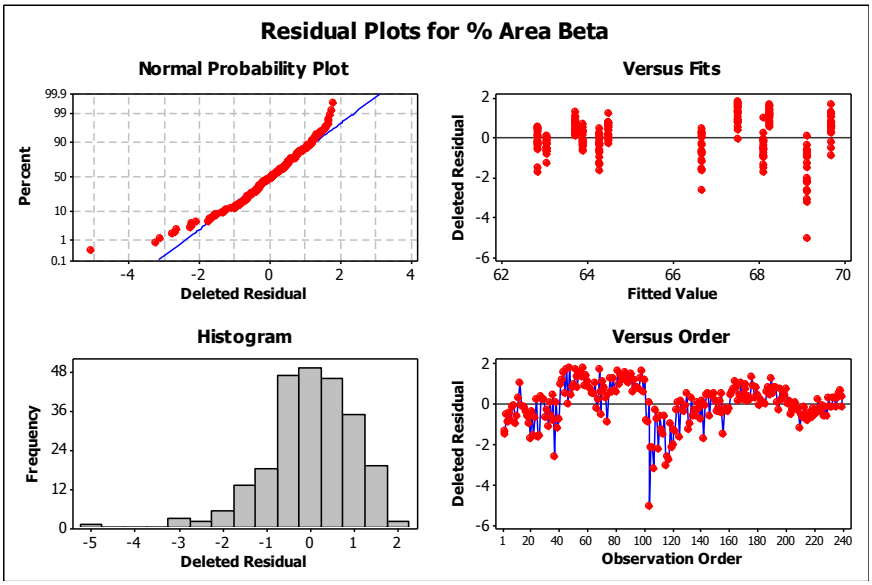

Analysis of Variance for % Area Beta, using Adjusted SS for Tests

Source	DF	Seq SS	Adj SS	Adj MS	F	P
Region	3	1317.13	1317.13	439.04	12.23	0.000
Orientation	2	85.93	85.93	42.97	1.20	0.304
Error	234	8401.50	8401.50	35.90		
Total	239	9804.56				

S = 5.99198 R-Sq = 14.31% R-Sq(adj) = 12.48%

Unusual Observations for % Area Beta

Obs	% Area Beta	Fit	SE Fit	Residual	St Resid
37	51.2820	66.6632	0.9474	-15.3812	-2.60 R
104	40.5010	69.1386	0.9474	-28.6376	-4.84 R
105	56.2150	69.1386	0.9474	-12.9236	-2.18 R
106	56.1580	69.1386	0.9474	-12.9806	-2.19 R
107	50.4450	69.1386	0.9474	-18.6936	-3.16 R
110	55.9800	69.1386	0.9474	-13.1586	-2.22 R
115	51.0940	69.1386	0.9474	-18.0446	-3.05 R
116	53.6000	69.1386	0.9474	-15.5386	-2.63 R
117	53.0910	69.1386	0.9474	-16.0476	-2.71 R
119	56.2020	69.1386	0.9474	-12.9366	-2.19 R
120	57.0220	69.1386	0.9474	-12.1166	-2.05 R

R denotes an observation with a large standardized residual.

Expected Mean Squares, using Adjusted SS

	Source	Expected Mean Square for Each Term
1	Region	(3) + Q[1]
2	Orientation	(3) + Q[2]
3	Error	(3)

Error Terms for Tests, using Adjusted SS

	Source	Error DF	Error MS	Synthesis of Error MS
1	Region	234.00	35.90	(3)
2	Orientation	234.00	35.90	(3)

Variance Components, using Adjusted SS

Source	Estimated Value
Error	35.90

Least Squares Means for % Area Beta

Region	Mean	SE Mean
1A	67.44	0.7736
1B	69.04	0.7736
2	63.79	0.7736
3	63.60	0.7736
Orientation		
A	66.65	0.6699
B	65.19	0.6699
C	66.06	0.6699

Grouping Information Using Tukey Method and 90.0% Confidence

Region	N	Mean	Grouping
1B	60	69.0	A
1A	60	67.4	A
2	60	63.8	B
3	60	63.6	B

Means that do not share a letter are significantly different.

Tukey 90.0% Simultaneous Confidence Intervals
Response Variable % Area Beta
All Pairwise Comparisons among Levels of Region
Region = 1A subtracted from:

Region	Lower	Center	Upper	---+---------+---------+---------+---
1B	-0.918	1.603	4.125	(-------*------)
2	-6.169	-3.647	-1.125	(-------*------)
3	-6.360	-3.838	-1.316	(------*------)
				---+---------+---------+---------+---
				-7.0 -3.5 0.0 3.5

Region = 1B subtracted from:

```
Region   Lower  Center   Upper  ---+---------+---------+---------+---
2       -7.772  -5.250  -2.728   (------*------)
3       -7.963  -5.441  -2.919  (------*-------)
                        ---+---------+---------+---------+---
                        -7.0      -3.5       0.0       3.5
```

Region = 2 subtracted from:

```
Region   Lower   Center  Upper  ---+---------+---------+---------+---
3       -2.713  -0.1910  2.331              (------*-------)
                        ---+---------+---------+---------+---
                        -7.0      -3.5       0.0       3.5
```

Grouping Information Using Tukey Method and 90.0% Confidence

```
Orientation   N  Mean  Grouping
A            80  66.6  A
C            80  66.1  A
B            80  65.2  A
```

Means that do not share a letter are significantly different.

Tukey 90.0% Simultaneous Confidence Intervals
Response Variable % Area Beta
All Pairwise Comparisons among Levels of Orientation
Orientation = A subtracted from:

```
Orientation   Lower  Center   Upper  -------+---------+---------+---------
B            -3.412  -1.456  0.4999  (---------*--------)
C            -2.540  -0.584  1.3720      (---------*---------)
                          -------+---------+---------+---------
                            -2.0       0.0       2.0
```

Orientation = B subtracted from:

```
Orientation   Lower  Center  Upper  -------+---------+---------+---------
C            -1.084  0.8721  2.828            (--------*---------)
                          -------+---------+---------+---------
                            -2.0       0.0       2.0
```

Appendix H. Minitab output of the ANOVA and Tukey's results for the particle count of β.

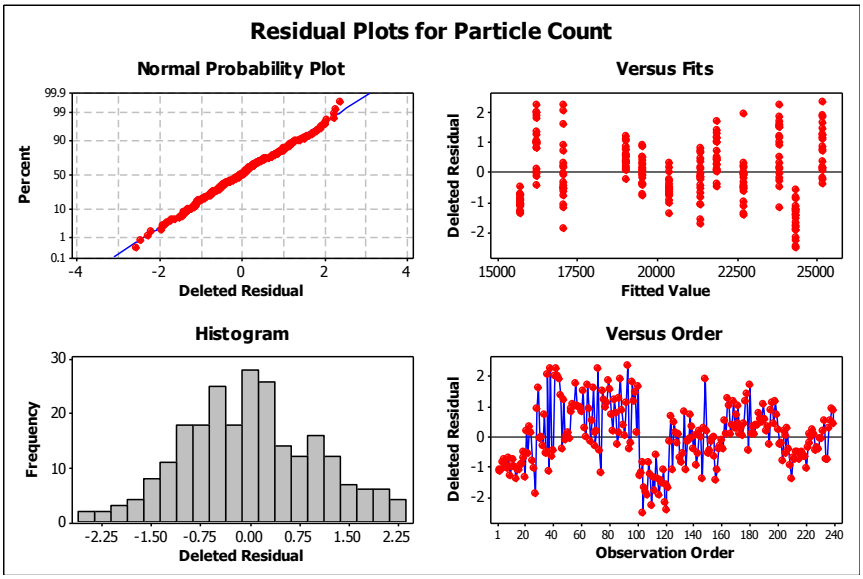

Analysis of Variance for Particle Count, using Adjusted SS for Tests

Source	DF	Seq SS	Adj SS	Adj MS	F	P
Region	3	2165667388	2165667388	721889129	8.70	0.000
Orientation	2	75355659	75355659	37677829	0.45	0.636
Error	234	19412795360	19412795360	82960664		
Total	239	21653818406				

S = 9108.27 R-Sq = 10.35% R-Sq(adj) = 8.43%

Unusual Observations for Particle Count

Obs	Particle Count	Fit	SE Fit	Residual	St Resid
36	35375.0	17045.3	1440.1	18329.7	2.04 R
38	37103.0	17045.3	1440.1	20057.7	2.23 R
41	34281.0	16202.8	1440.1	18078.2	2.01 R
42	36525.0	16202.8	1440.1	20322.2	2.26 R
43	34236.0	16202.8	1440.1	18033.2	2.01 R
72	43928.0	23829.0	1440.1	20099.0	2.23 R
93	46297.0	25188.6	1440.1	21108.4	2.35 R
104	1672.0	24346.1	1440.1	-22674.1	-2.52 R
110	4061.0	24346.1	1440.1	-20285.1	-2.26 R
119	4618.0	24346.1	1440.1	-19728.1	-2.19 R
120	2355.0	24346.1	1440.1	-21991.1	-2.45 R

R denotes an observation with a large standardized residual.

Expected Mean Squares, using Adjusted SS

	Source	Expected Mean Square for Each Term
1	Region	(3) + Q[1]
2	Orientation	(3) + Q[2]
3	Error	(3)

Error Terms for Tests, using Adjusted SS

	Source	Error DF	Synthesis Error MS	of Error MS
1	Region	234.00	82960664	(3)
2	Orientation	234.00	82960664	(3)

Variance Components, using Adjusted SS

Source	Estimated Value
Error	82960664

Grouping Information Using Tukey Method and 90.0% Confidence for Particle Count

Region	N	Mean	Grouping
1B	60	24454.6	A
3	60	21976.2	A B
2	60	19625.4	B C
1A	60	16311.3	C

Means that do not share a letter are significantly different.

Tukey 90.0% Simultaneous Confidence Intervals
Response Variable Particle Count
All Pairwise Comparisons among Levels of Region
Region = 1A subtracted from:

Region	Lower	Center	Upper	----+---------+---------+---------+--
1B	4310.0	8143	11977	(------*-----)
2	-519.2	3314	7147	(------*-----)
3	1831.6	5665	9498	(-----*------)
				----+---------+---------+---------+--
				-6000 0 6000 12000

Region = 1B subtracted from:

Region	Lower	Center	Upper	----+---------+---------+---------+--
2	-8663	-4829	-995.8	(-----*-----)
3	-6312	-2478	1355.0	(------*-----)
				----+---------+---------+---------+--
				-6000 0 6000 12000

Region = 2 subtracted from:

```
Region  Lower  Center  Upper  ----+---------+---------+---------+--
3      -1483    2351   6184            (-----*-----)
                       ----+---------+---------+---------+--
                       -6000        0      6000     12000
```

Grouping Information Using Tukey Method and 90.0% Confidence for Particle Count

Orientation	N	Mean	Grouping
B	80	21325.9	A
C	80	20483.4	A
A	80	19966.3	A

Means that do not share a letter are significantly different.

Tukey 90.0% Simultaneous Confidence Intervals
Response Variable Particle Count
All Pairwise Comparisons among Levels of Orientation
Orientation = A subtracted from:

```
Orientation  Lower  Center  Upper  -----+---------+---------+---------+-
B           -1614  1359.6   4333          (----------*----------)
C           -2456   517.1   3491       (----------*----------)
                       -----+---------+---------+---------+-
                        -2500        0      2500      5000
```

Orientation = B subtracted from:

```
Orientation  Lower  Center  Upper  -----+---------+---------+---------+-
C           -3816  -842.6   2131  (----------*----------)
                       -----+---------+---------+---------+-
                        -2500        0      2500      5000
```

Appendix I. SEM images of the fracture surface for region 1A in the x-direction corresponding to tensile Sample C.

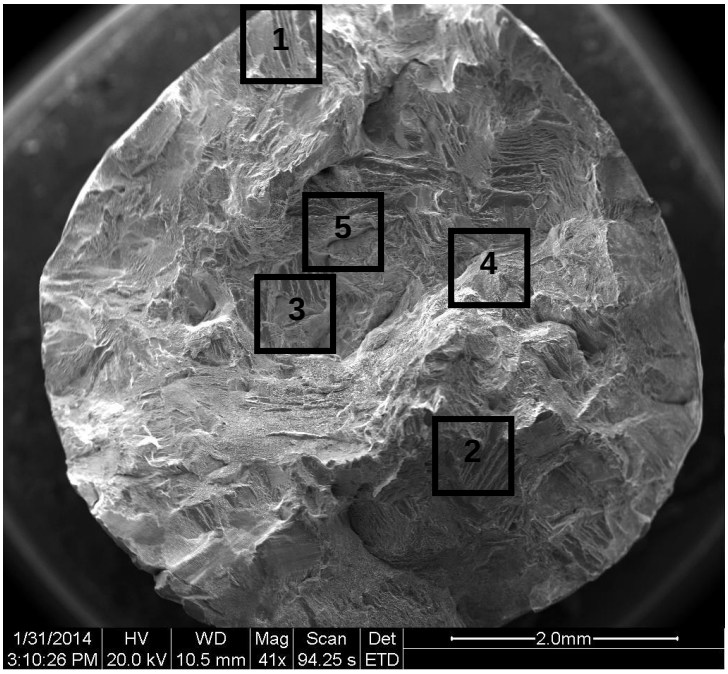

SEM image of the entire fracture surface with locations of magnified images labeled

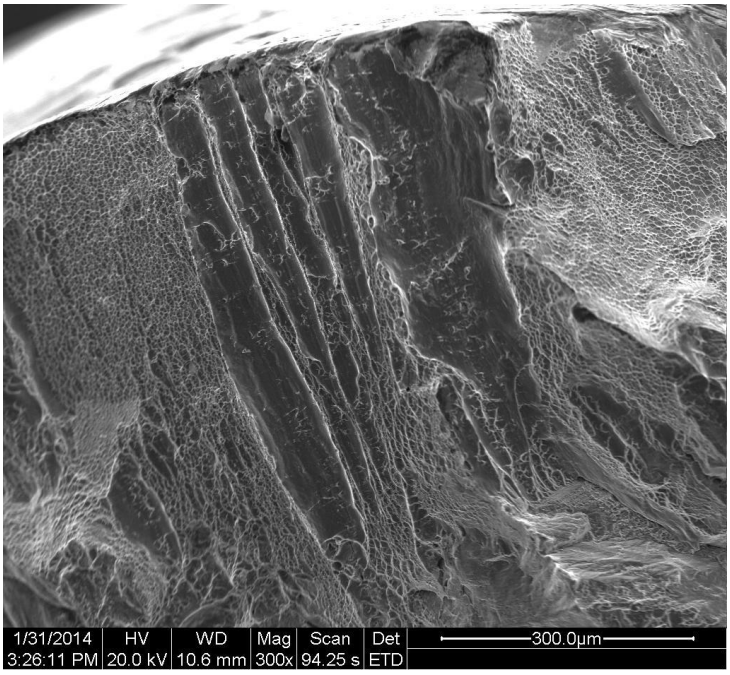

Location 1 image showing interlamellar decohesion.

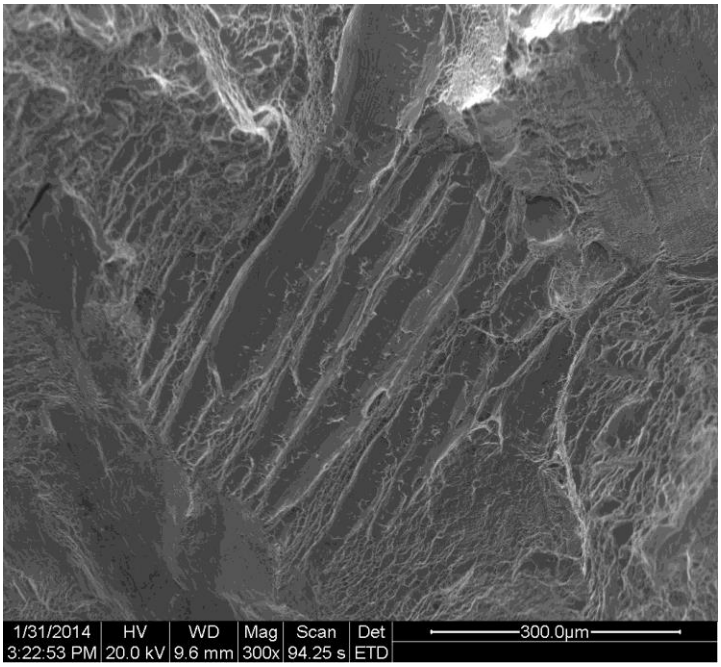

Location 2 showing more interlamellar decohesion

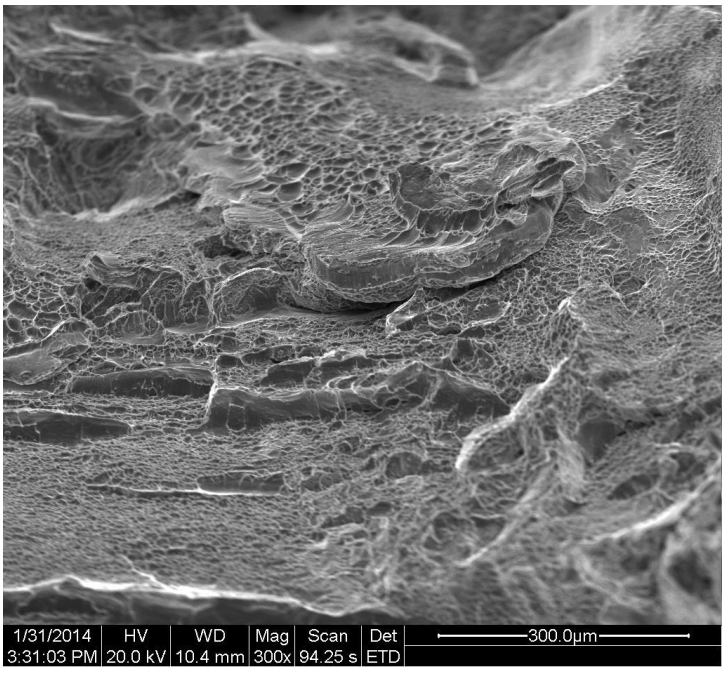

Location 3 showing a dimpled surface corresponding to a ductile failure region.

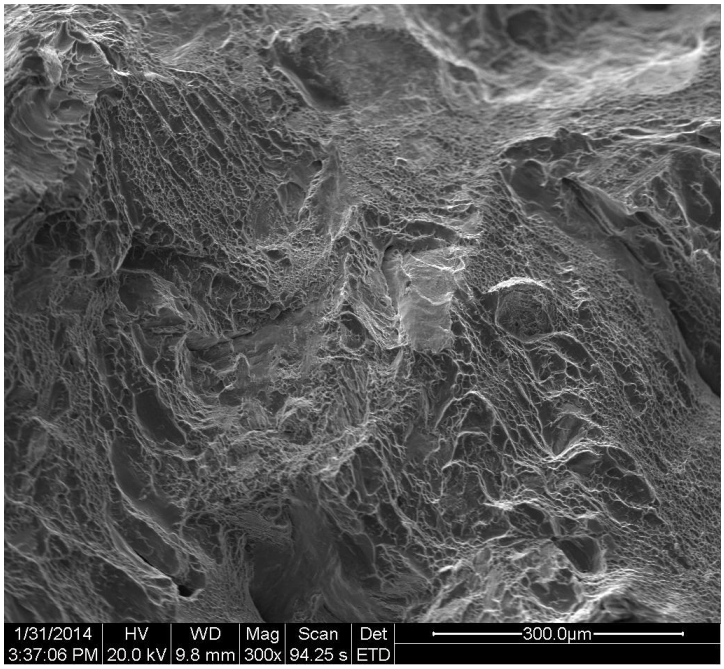

Location 4 showing dimpled surface corresponding to ductile failure.

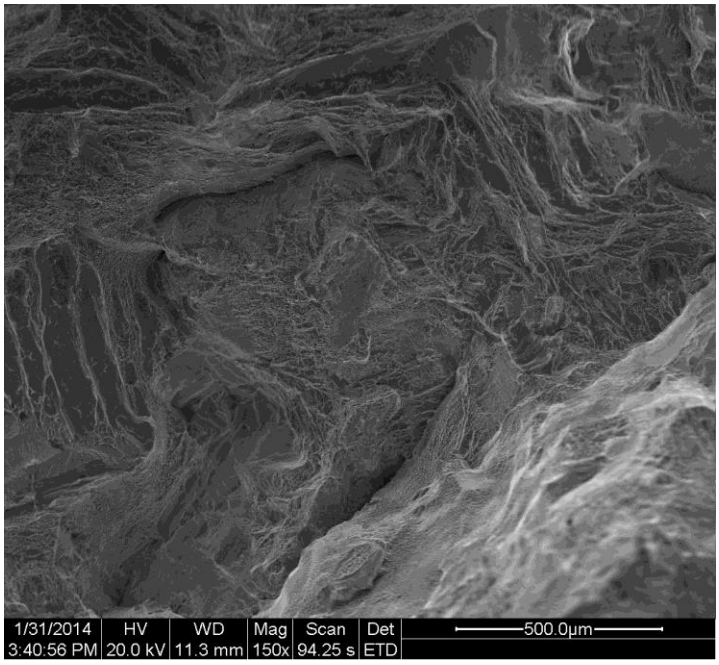

Location 5 showing mixed mode with interlamellar decohesion to the left and more ductile failure in the surrounding area.

Appendix J. SEM images of the fracture surfaces for region 1B in the x-direction corresponding to tensile Sample R.

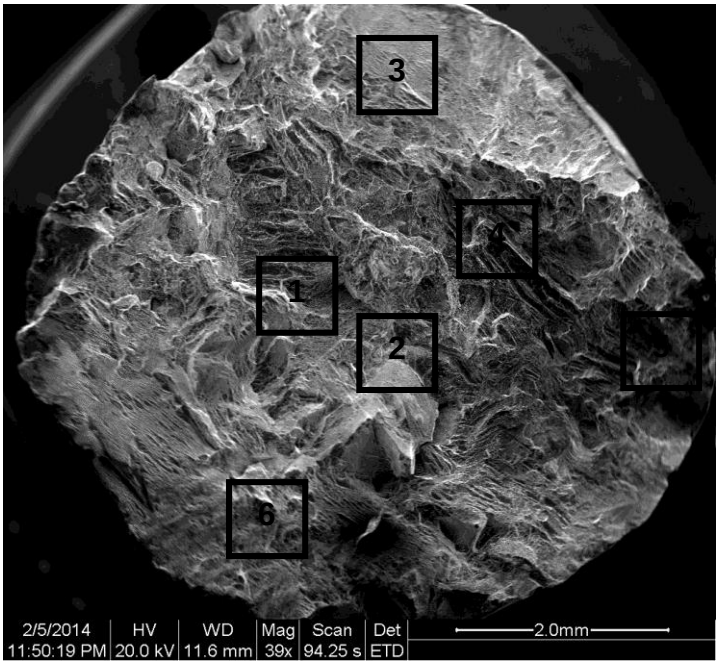

Image of the entire fracture surface with locations of magnified images identified.

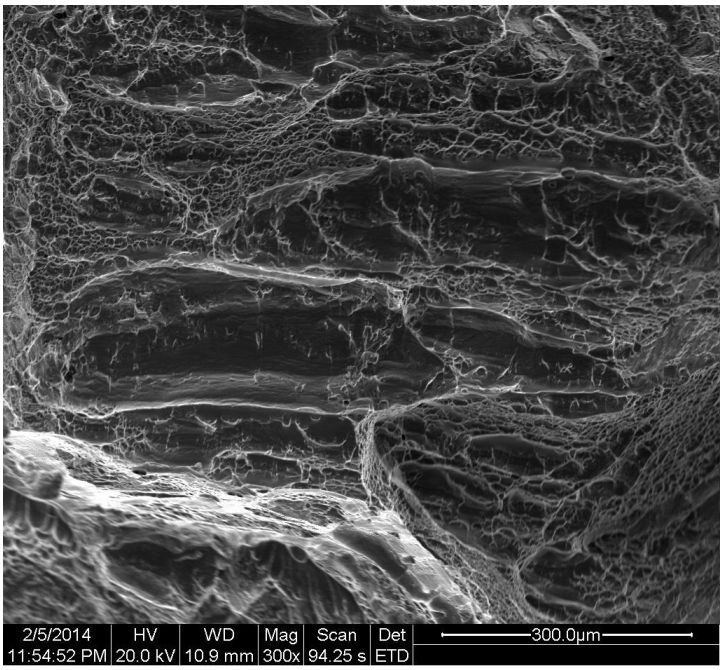

Location 1 showing interlamellar decohesion.

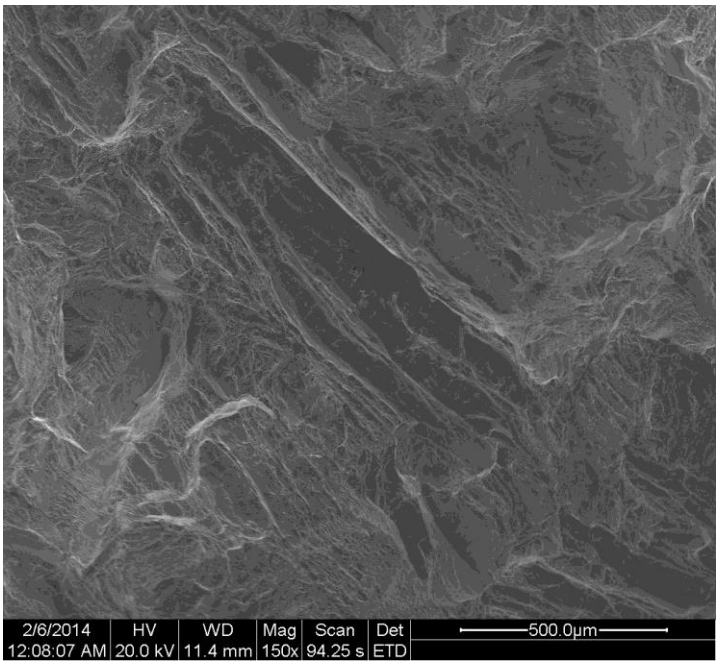

Location 2 showing trans-lamellar brittle failure

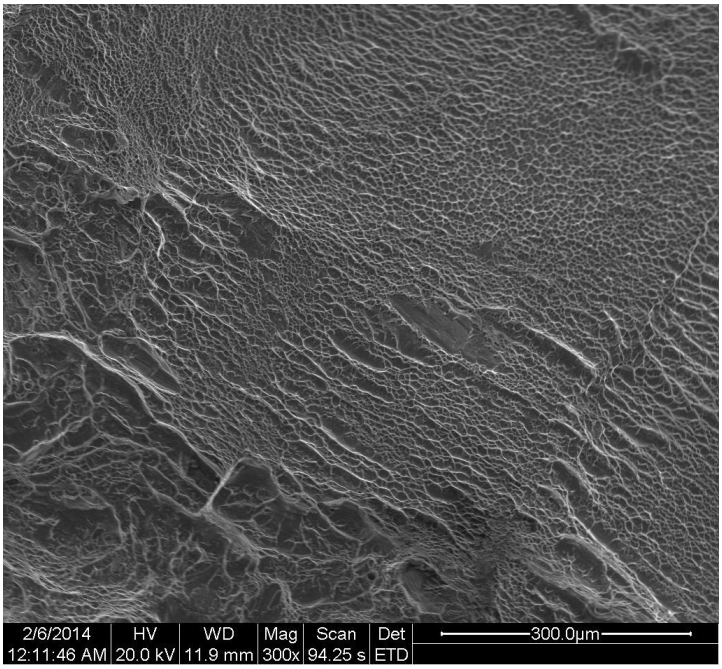

Location 3 showing dimpled ductile failure region.

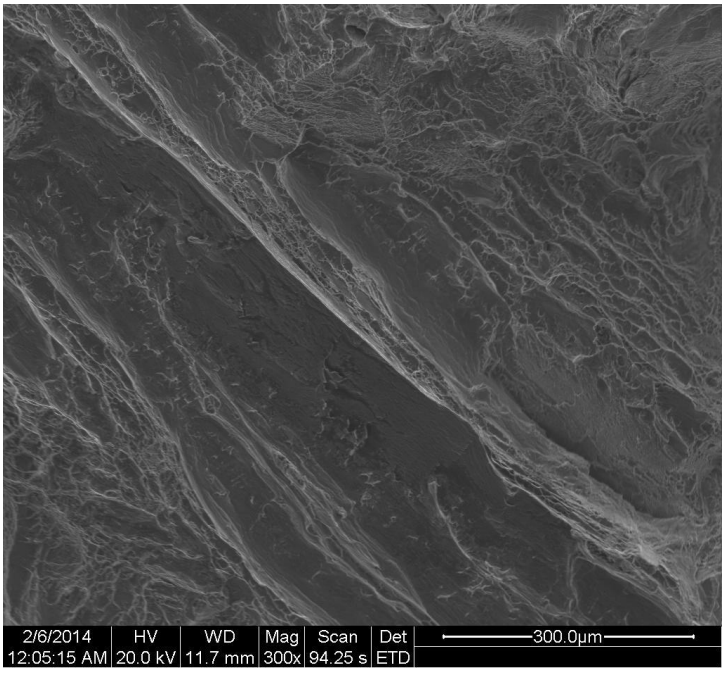

Location 4 showing interlamellar decohesion.

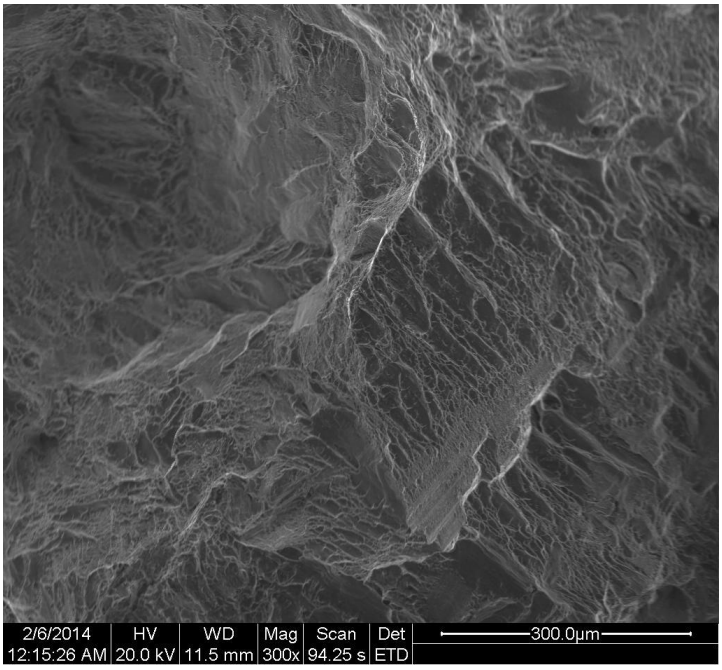

Location 5 showing interlamellar decohesion.

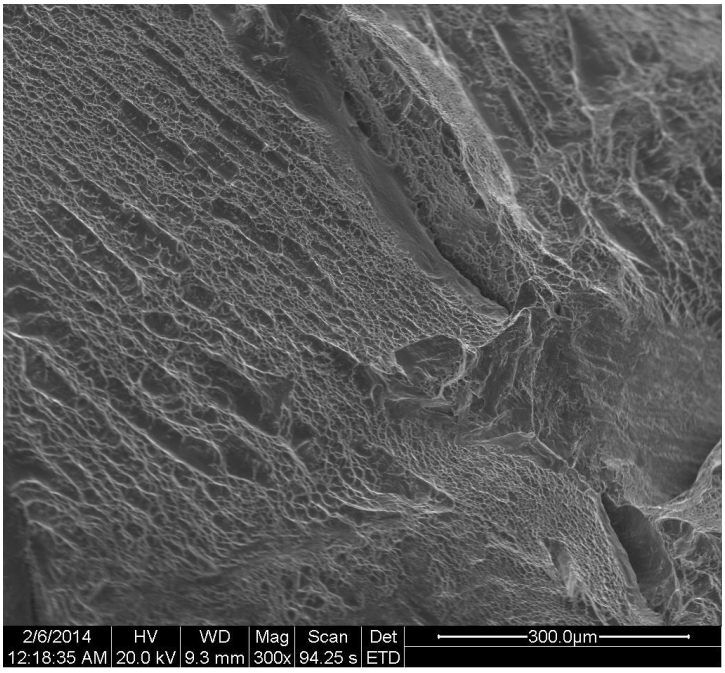

Location 6 showing a ductile failure mode.

Appendix K. SEM images of the fracture surfaces for region 2 in the x-direction corresponding to tensile Sample Y.

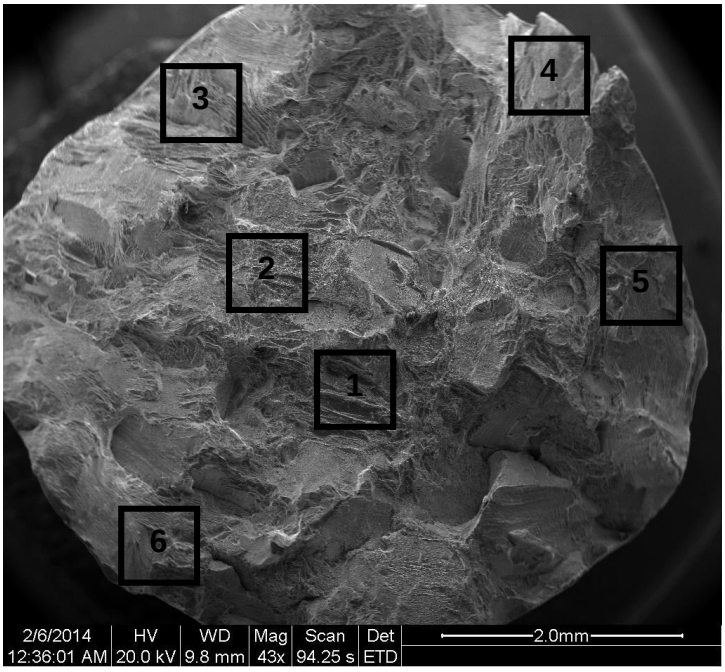

Entire fracture surface with locations of magnified images identified.

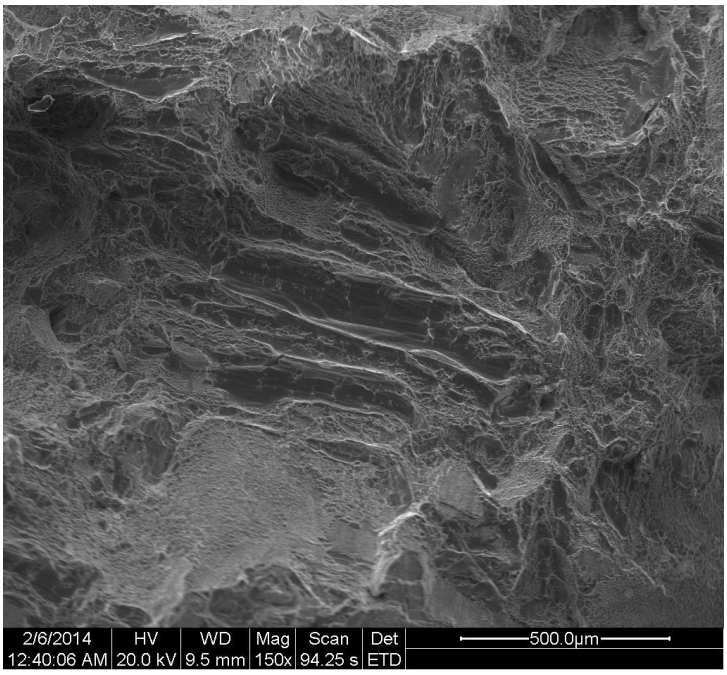

Location 1 which showing interlamellar decohesion.

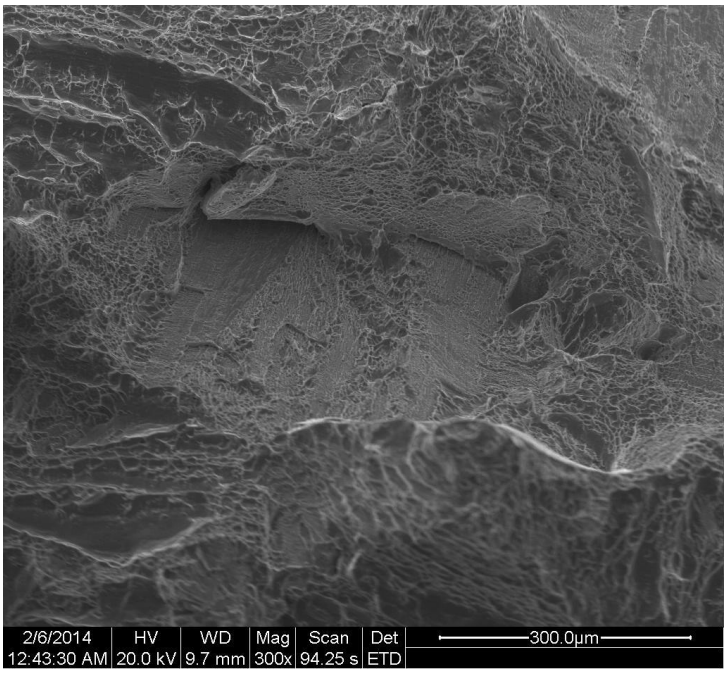

Location 2 showing trans-lamellar brittle failure mode.

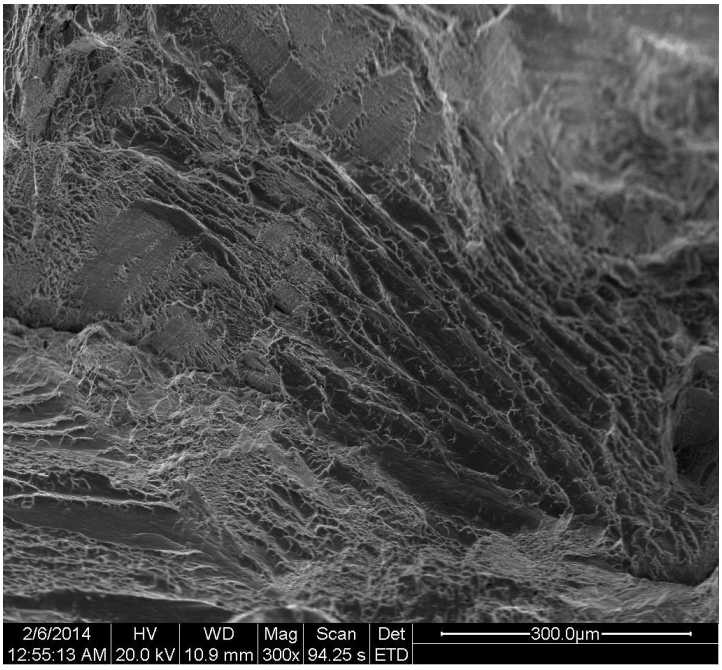

Location 3 showing interlamellar decohesion and trans-lamellar brittle failure mode.

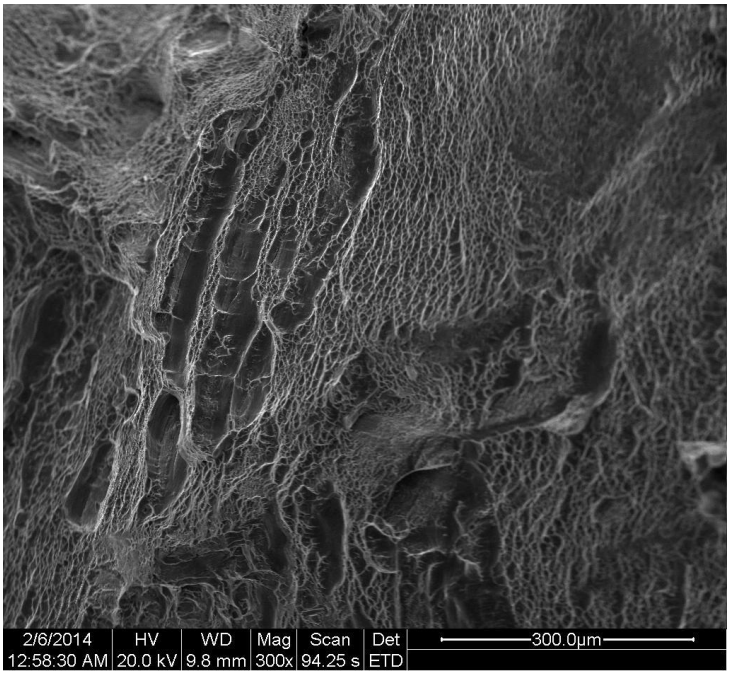

Location 4 showing interlamellar decohesion to the left with surrounding dimpled ductile failure.

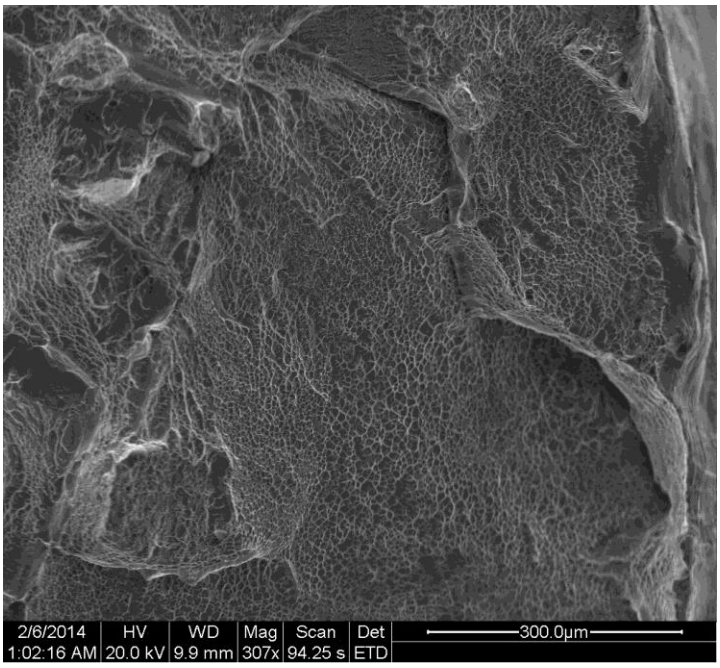

Location 5 showing dimpled ductile failure.

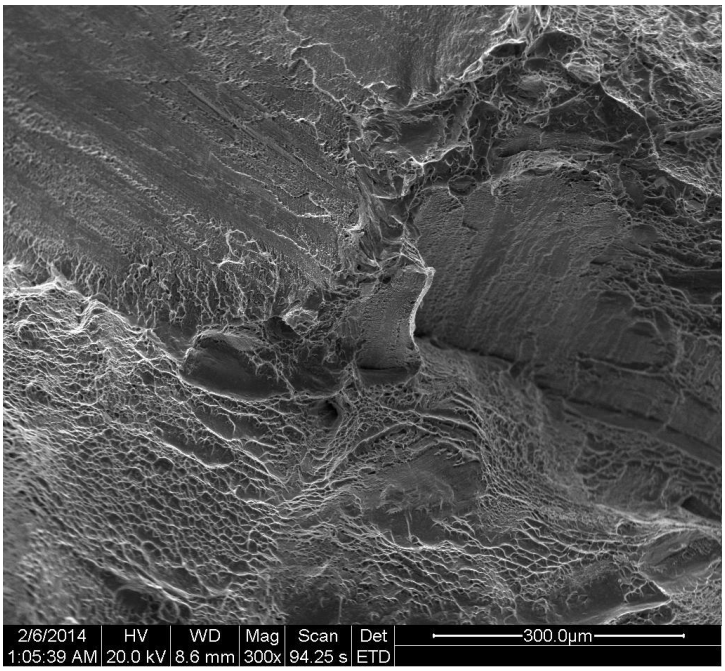

Location 6 showing trans-lamellar brittle failure in the upper left and dimpled ductile failure in lower left.

Appendix L. SEM images of the fracture surfaces for region 3 in the x-direction corresponding to tensile Sample X.

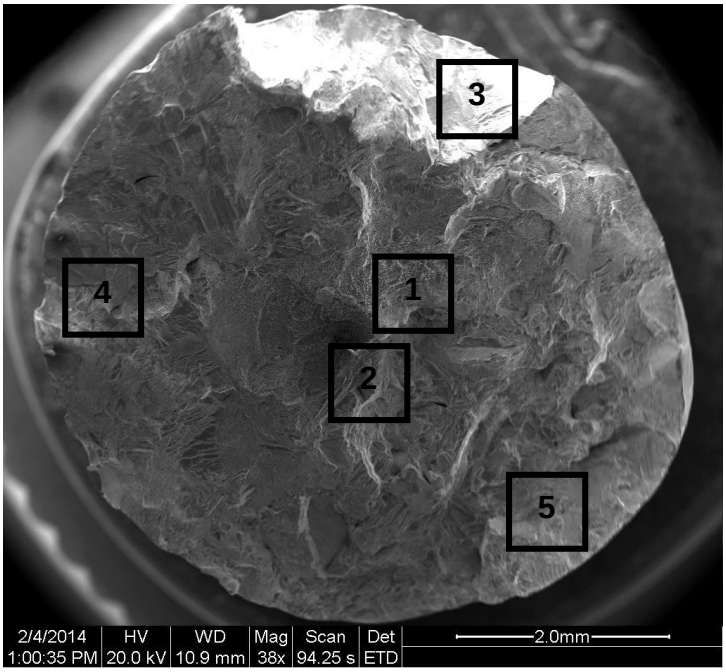

Entire fracture surface with locations of magnified images identified.

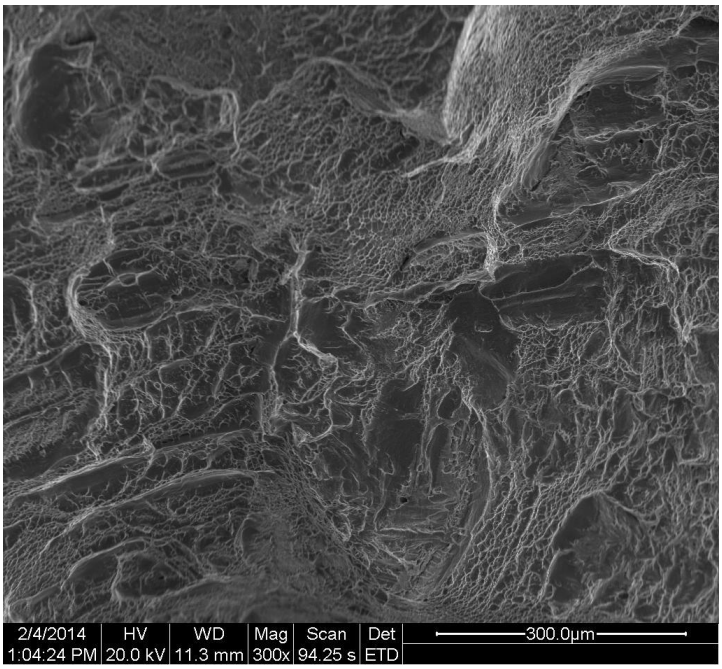

Location 1 showing dimpled surface corresponding to ductile failure.

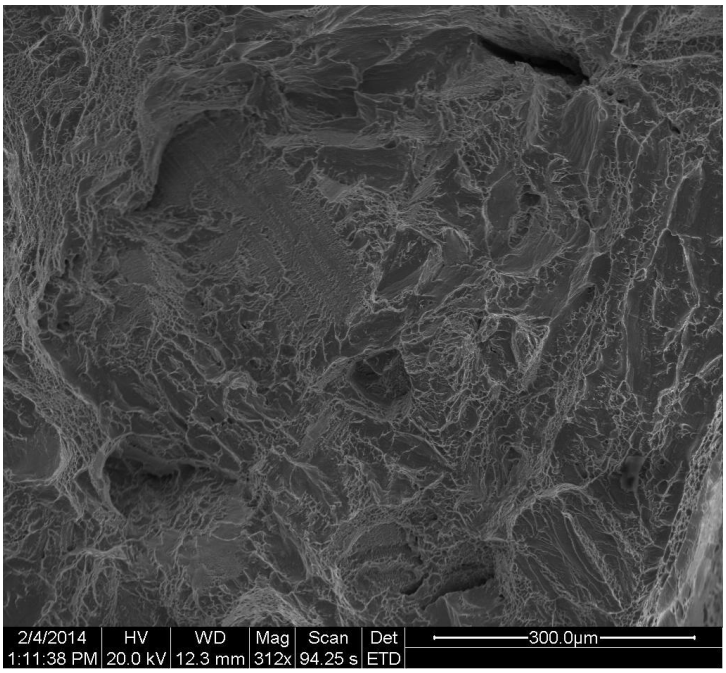

Location 2 showing trans-lamellar brittle failure with some potential interlamellar decohesion and dimpled ductile failure in surrounding areas.

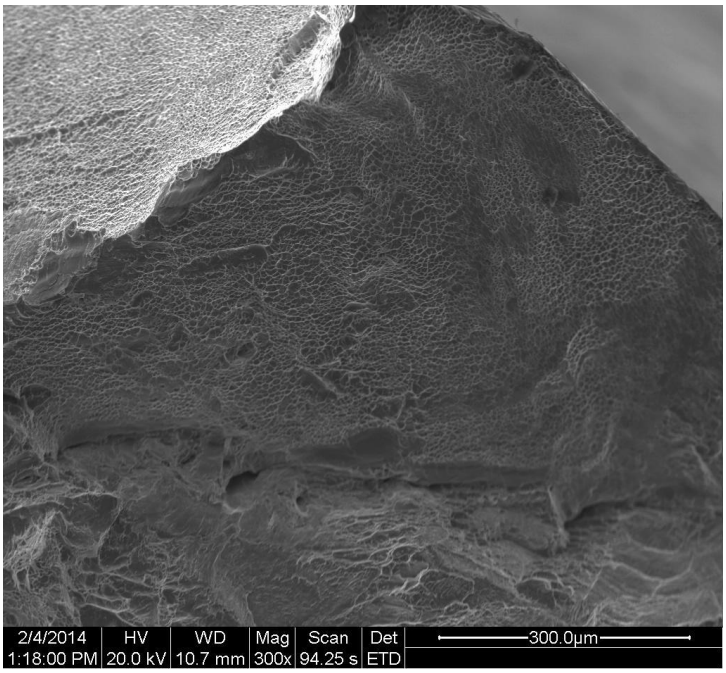

Location 3 showing dimpled surface corresponding to ductile failure with potential intergranular failure in upper left.

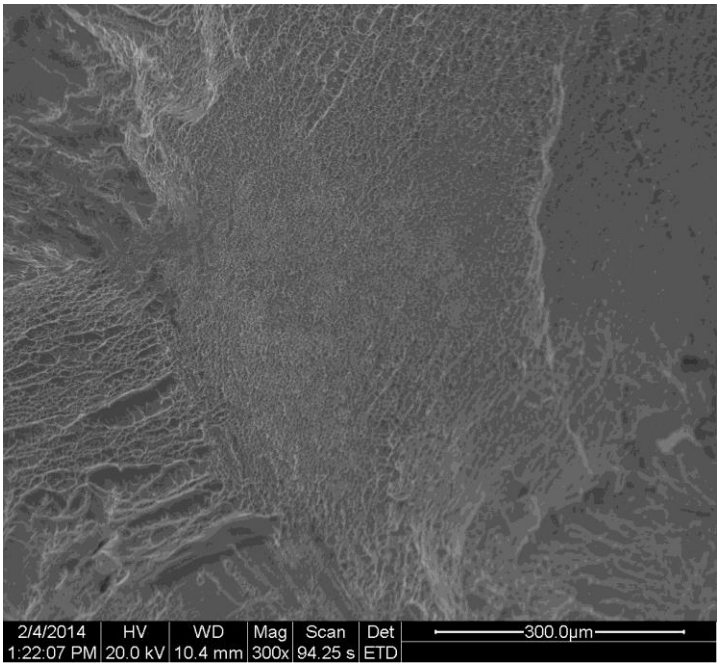

Location 4 showing trans-lamellar brittle failure surrounded by ductile failure.

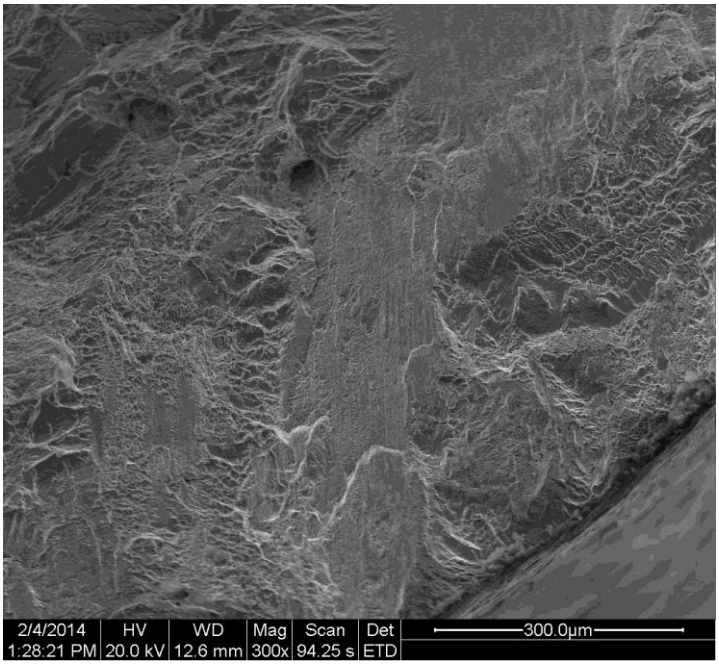

Location 5 showing trans-lamellar brittle failure surrounded by ductile failure.

Appendix M. SEM images of the fracture surfaces for region 1A in the y-direction corresponding to tensile Sample I.

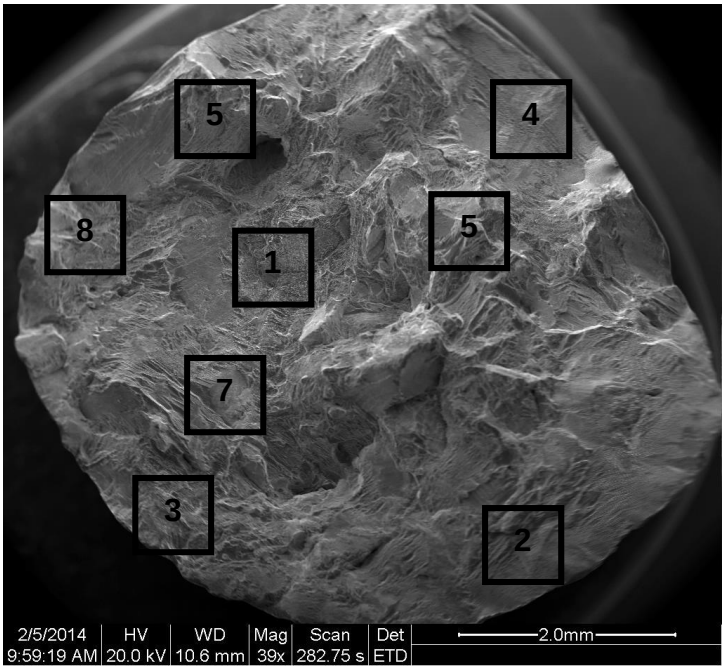

Image of the entire fracture surface with locations of magnified images identified.

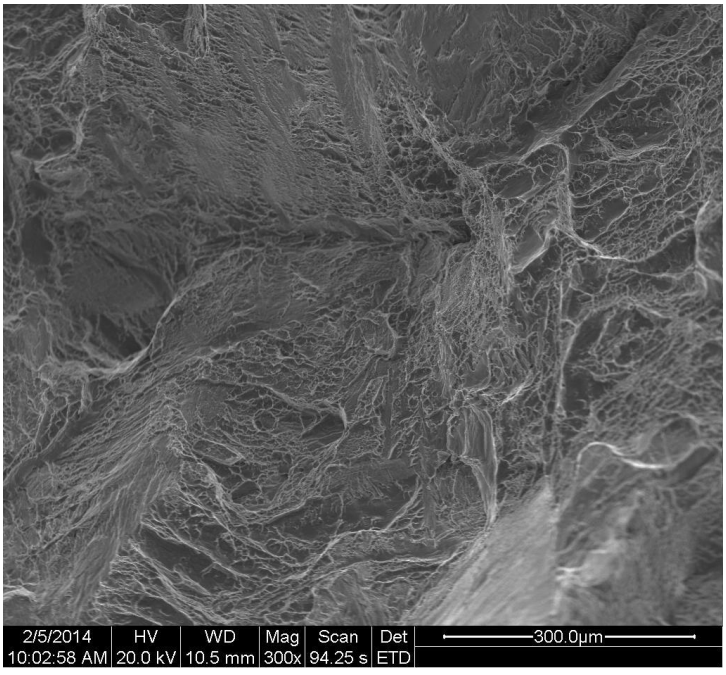

Location 1 showing primarily ductile failure.

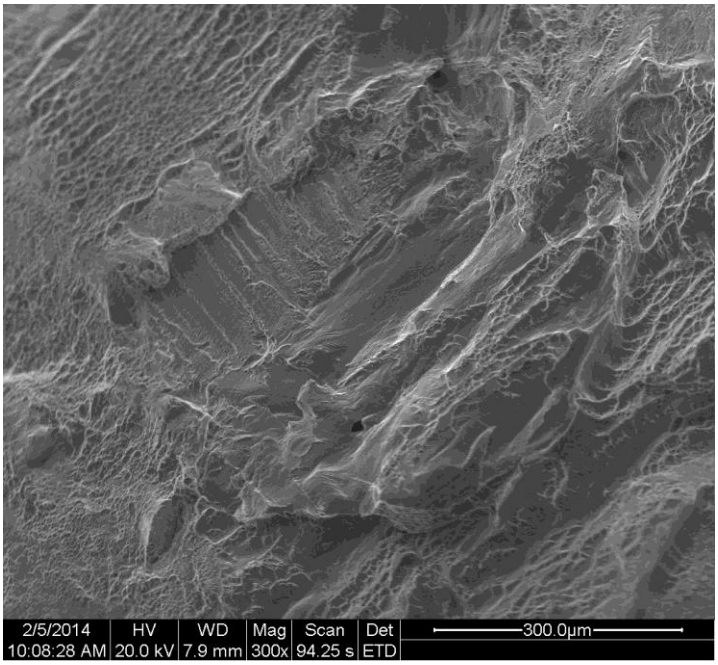

Location 2 showing trans-lamellar failure intercepting a region of interlamellar decohesion in the center of the image surrounded by ductile failure.

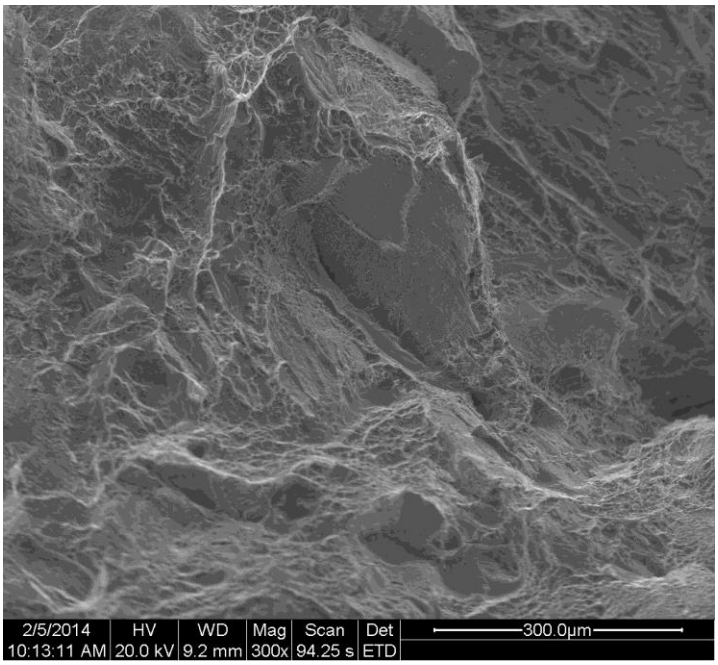

Location 3 showing ductile failure with a region in the center of brittle failure.

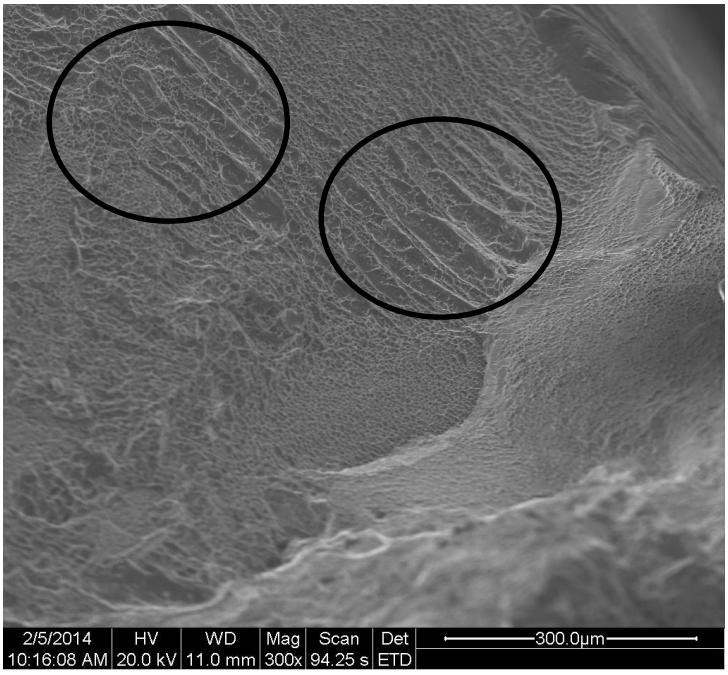

Location 4 showing interlamellar decohesion (circled areas) surrounded by ductile failure.

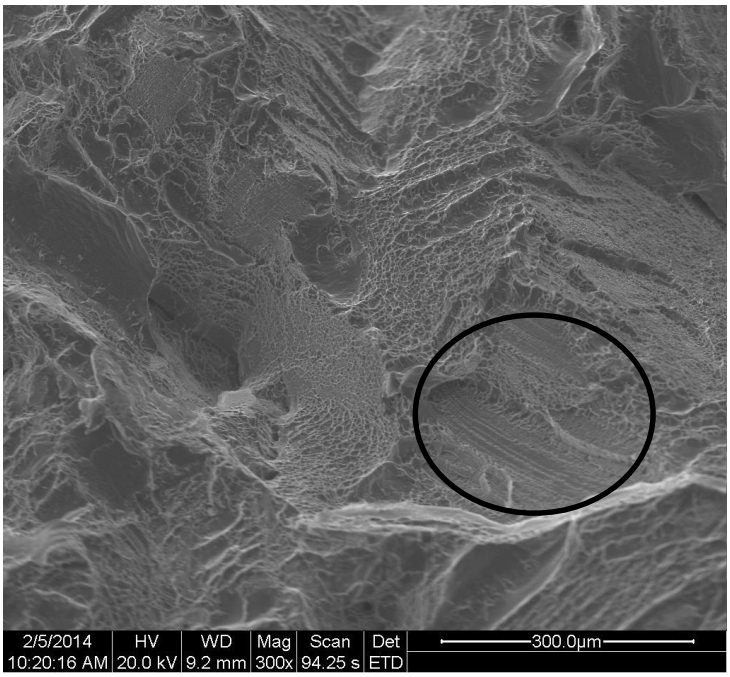

Location 5 showing trans-lamellar failure (circled area) with some brittle and surrounding ductile failure.

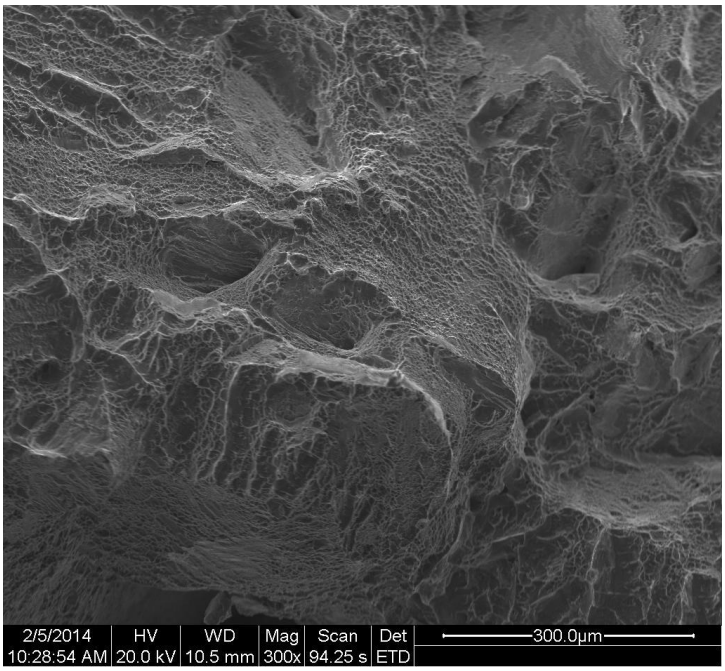

Location 6 showing primarily ductile failure.

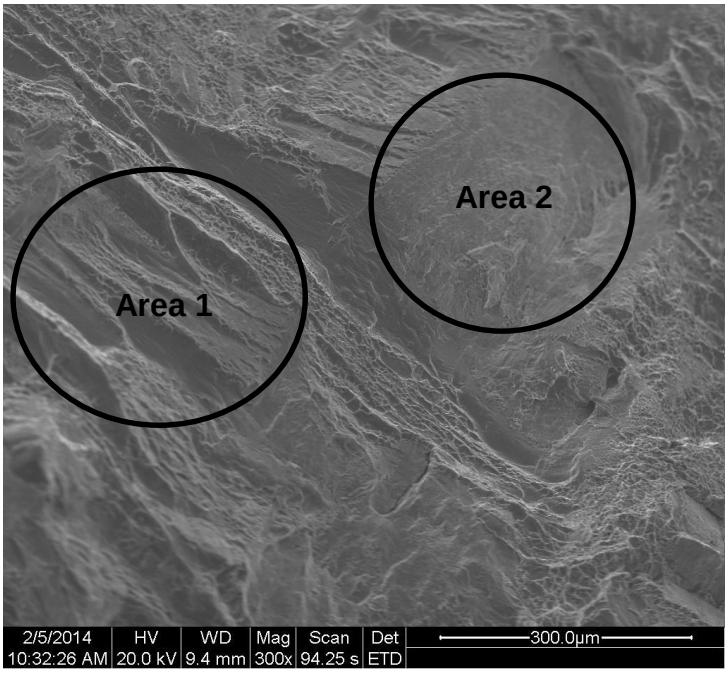

Location 7 showing interlamellar decohesion (circled area 1) and a brittle failure region (circled area 2).

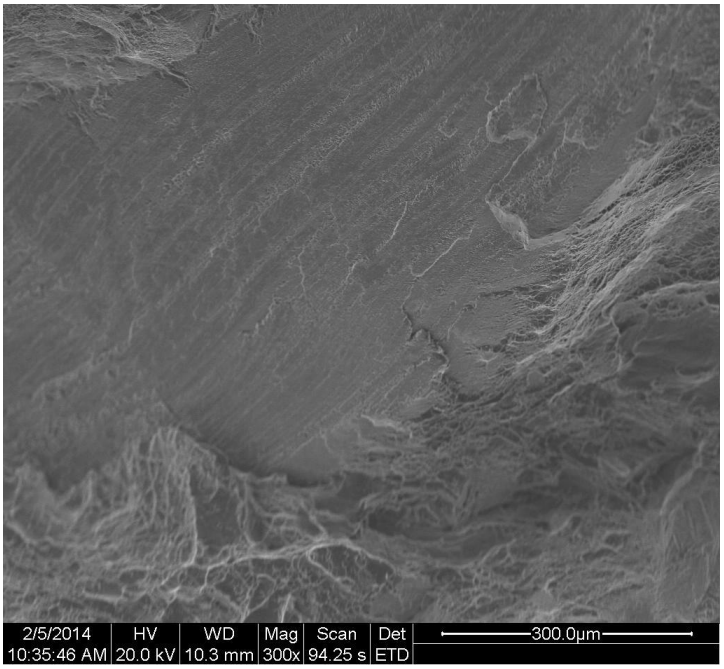

Location 8 showing trans-lamellar failure surrounded by ductile failure.

Appendix N. SEM images of the fracture surfaces for region 1A in the z-direction corresponding to tensile Sample F.

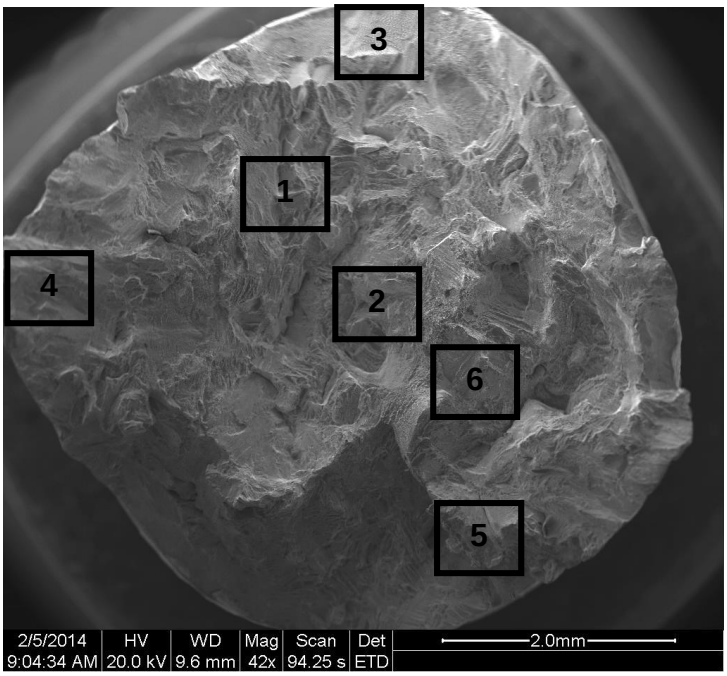

Entire fracture surface with locations of magnified images outlined.

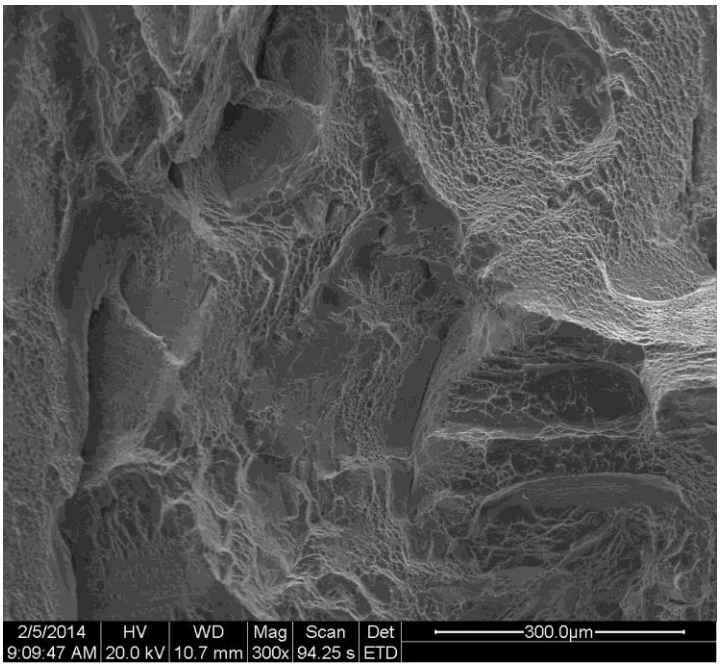

Location 1 showing primarily ductile failure.

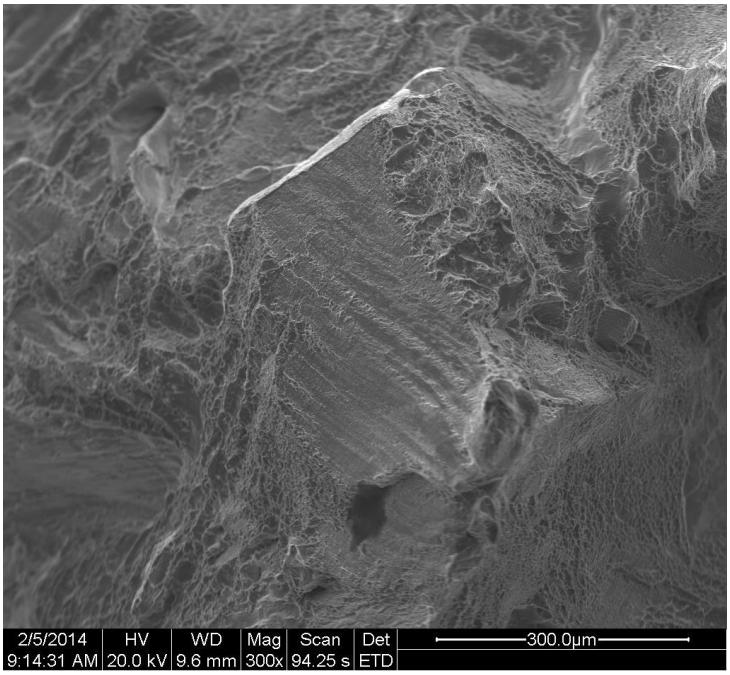

Location 2 showing trans-lamellar failure in center surrounded by ductile failure.

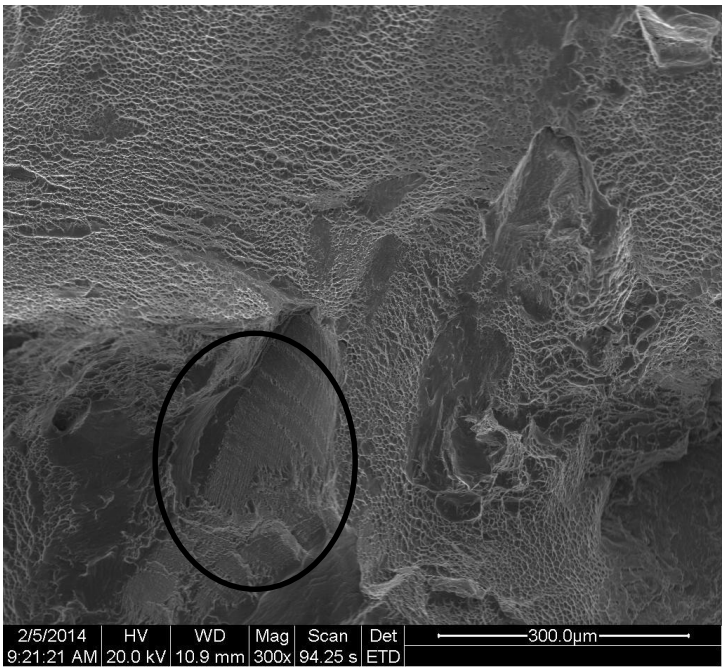

Location 3 showing primarily ductile failure with outlined brittle failure area.

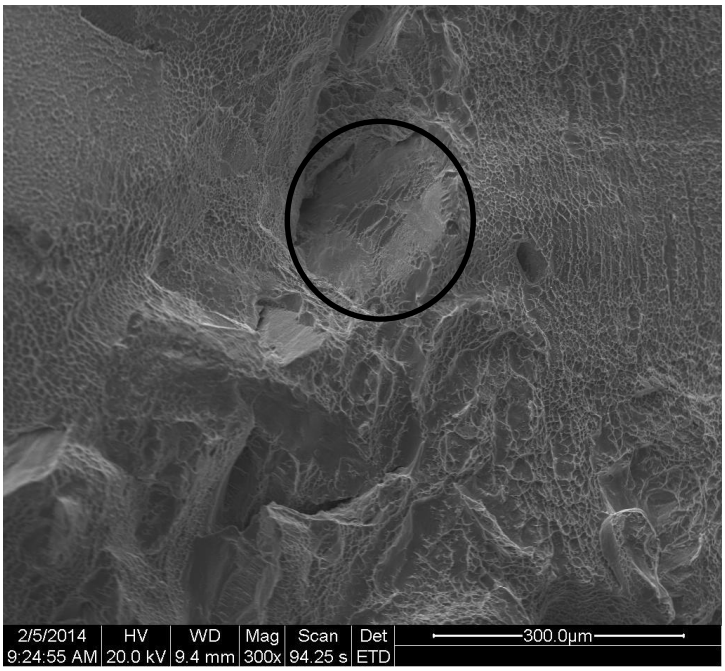

Location 4 showing primarily ductile failure with an outlined area of brittle failure.

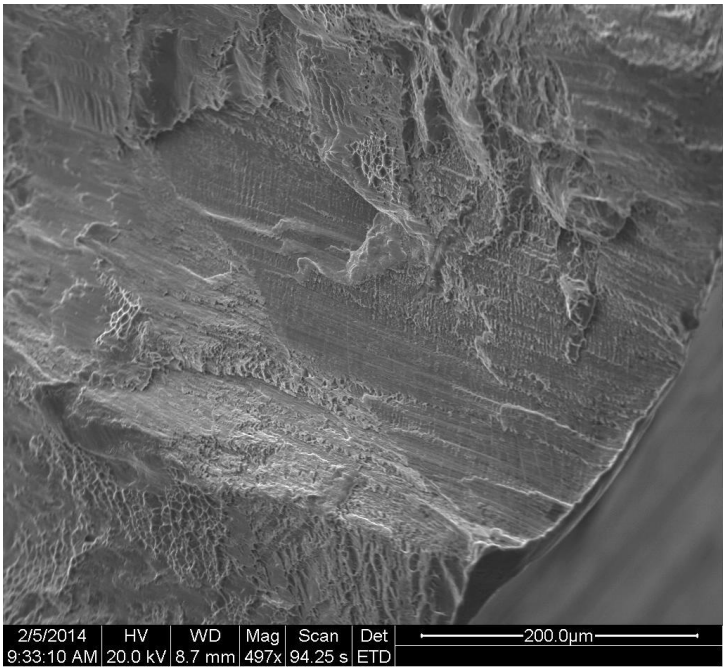

Location 5 showing trans-lamellar brittle failure along the edge of the sample.

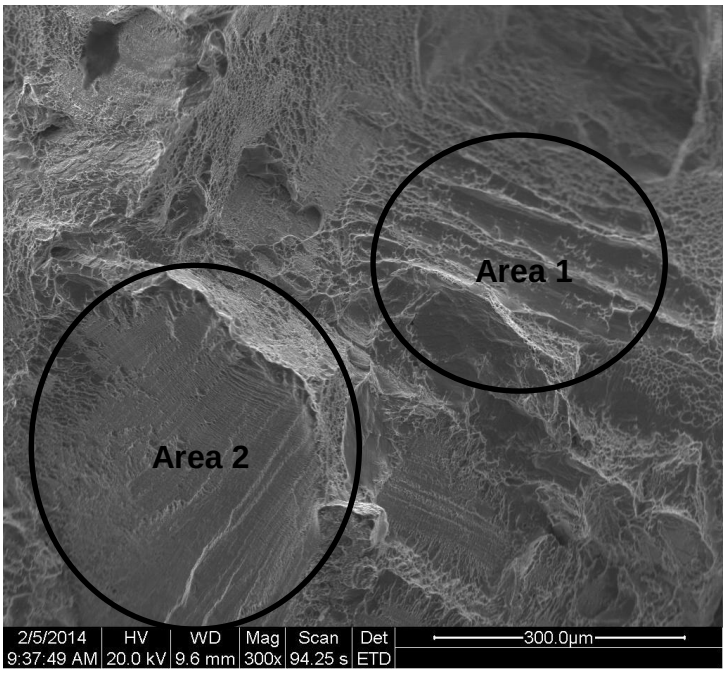

Location 6 showing interlamellar decohesion in area 1 and trans-lamellar brittle failure in area 2 with surrounding ductile failure.